Elucidating mammalian cellular responses to the uptake of nanoparticles (NPs), pathogens, and lipoproteins (similarities and differences)

A Dissertation Presented for the
Doctor of Philosophy
Degree
The University of Tennessee, Knoxville

Monireh Asoudeh
August 2022

DEDICATION

To my MAMAN,

And

To the passengers of PS752 and their moms.

ACKNOWLEDGEMENTS

We would like to thank Taylor Gebhart for assistance with flow cytometry experiments. She was supported on NIH R25ES02897603. We thank Dr. Eric Boder for the use of his flow cytometer.

ABSTRACT

Soft poly-ethylene-glycol (PEG)-based soft nanoparticles (NPs) including cylindrical (CNPs) micelles, spherical (SNPs) micelles, and lipid bilayer vesicles (LNPs) are thought to be treated as foreign objects by mammalian phagocytes. If this hypothesis is true, NPs should trigger a pro-inflammatory, autophagic phenotype that is similar to the one seen when macrophages phagocytose pathogens or when macrophage surface expressed proteins bind pathogen surface factors such as lipopolysaccharide (LPS). Here, we show that macrophage responses to the above NPs are almost completely unique from those triggered by group A *streptococcus* (GAS) pathogens (JRS4 cells) and LPS. Instead, macrophages treat these soft NPs more like high-density lipoprotein (HDL) and low-density lipoprotein (LDL). RNA sequencing of macrophage transcripts after hHDL, hLDL, JRS4 cell, LPS, and LNP incubation showed three diverse response clusters triggered by JRS4 cells, LPS, and hHDL-hLDL-LNP-PBS.

Of these reagents, LNPs triggered the fewest post-incubation transcript changes from macrophages to which PBS was added (control). LNPs did not increased the transcription of factors associated with foreign object identification including Fc and complement receptors. LNPs did not increase transcripts whose translated proteins are involved in phagocytosis, autophagy, lysosome biogenesis, or inflammation. LNPs did not increase Tfeb transcripts, which is a master regulator of lysosome biogenesis and a necessary component of autophagy. To further determine the effects of these NPs on cells, we performed fluorescence microscopy and flow cytometry experiments. CNPs, SNPs, and LNPs lowered macrophage autophagosome levels that were raised by the canonical challenges: starvation, rapamycin, and LPS. CNPs, SNPs, and LNPs lowered reaction oxygen species (ROS) levels, did not increase lysosome acidification, and the reduced the secretion of pro-inflammatory cytokines compared to basal conditions and LPS addition to macrophage cultures. CNPs and SNPs triggered low lysosome acidification and LNPs did not increase Tfeb levels, the master regulator of lysosome biogenesis and a necessary component of autophagy. Thus, the terminology that macrophages “clear” NPs, which has been used over many decades, is most likely misleading. Our findings challenge the hypothesis that the main uptake mechanism of soft PEG-NPs by M1-polarized murine macrophages *in vitro* is phagocytosis.

TABLE OF CONTENTS

LIST OF TABLES

LIST OF FIGURES

CHAPTER 1

THE ROLE OF AUTOPHAGY IN CANCER CHEMOTHERAPY DRUG RESISTANCE

This chapter is based on the published paper:
Asoudeh, M.; Dalhaimer, P. D.; The role of autophagy in cancer chemotherapy drug resistance. Scientific Letters. **2022**, Volume I (1), https://doi.org/10.48797/sl.2022.10.

Introduction

Tumor cells can become resistant to chemotherapy drugs [1]. At the gross anatomy scale, resistance is due mainly to the limited amount of drug that can be administered to a patient because of toxicity [2]. Thus, cells deep in tumors are usually exposed to less-than-lethal doses of drug that do not kill them. By being exposed to low doses of a chemical, the surviving cells become resistant through a variety of mechanisms. A key question is how this resistance occurs on the cellular and molecular levels. Answers to this question can be found, in part, in the cellular response mechanism autophagy. Autophagy is a conserved process that engulfs and degrades either seemingly random areas of the cytosol or targeted proteins and organelles [3]. The material to be broken down is engulfed in a double membrane structure that matures from the ER as an omegasome, grows into a phagophore, which then elongates into an autophagosome [4]. The autophagosome surrounds its cargo and then merges with a lysosome to form an autolysosome [5]. The contents of the autolysosome are degraded, and their fundamental moieties are reused [6] A comprehensive guide to the molecular mechanisms of autophagy has been recently published [7].

Autophagy plays at least two roles in cancer progression and cancer chemotherapy drug resistance. First, it keeps eukaryotic cells alive in times of nutrient deprivation. Since cancer cells need reagents for unregulated growth, autophagy helps them thrive when nutrients are scarce. Second, certain chemotherapy drugs cause the generation of reactive oxygen species (ROS). ROS in turn triggers autophagy. This also helps keep cancer cells alive. The goal of this review is to highlight the effects of a subset of cancer chemotherapy treatments on ROS and autophagy that were reported in recent years. More than one-third of the references are from studies within the last five years. We focus mainly on the mechanisms by which chemotherapy drugs alter the states of

proteins involved in the ROS-autophagy axis and provide a glimpse of the possibilities of co-treatments of anti-cancer and anti-autophagy agents.

Autophagy

Initiation of autophagy involves the formation of two protein complexes, the serine/threonine kinase ULK1 complex and the class III PI 3-kinase complex 1 (PI3KC3-C1) (Fig. 1.1) [7,8]. Under nutrient deprivation, phosphoinositide 3-kinase class 1 (PI3K1) turns on a signaling cascade involving protein kinase B (Akt) that inhibits mTOR and ultimately activates ULK1-mediated ULK1/ATG13/FIP200 dephosphorylation [9,10]. ULK1/ATG13/FIP200 complex cooperates with Beclin-1/PI3KC3/Vps34 and promotes phagophore nucleation. Activation of Beclin-1/PI3KC3 leads to hydrogen peroxide (H_2O_2) accumulation in mitochondria because of stress conditions and nutrition deprivation, ultimately leading to the generation of ROS [11]. ROS further induces autophagy through several pathways [11]. These include AMPK activation, which leads to the activation of the ULK1/ATG13/FIP200 complex.

The term autophagy encompasses a broad class of cellular responses. One classification strategy is for autophagy to be described as selective or non-selective. In the former, organelles and pathogens are directly targeted for degradation. In this form of autophagy, cargo adaptor proteins Sequestosome 1 (SQSTM1)/p62, neighbor of BRCA1 gene 1 (NBR1), or B-cell lymphoma 2 (Bcl-2)/adenovirus E1B 19-kDa-interacting protein 3 longform (NIX/BNIP3L) bind both the cargo and ATG8 family proteins such as LC3 and GABARAP, which are on the phagophore [12–15]. In the latter, volumes of the cytosol are engulfed and recycled. We focus on the subsets of autophagy that have been found to be important in cancer cells, with ROS-induced autophagy at the forefront. It is mechanistically unclear if ROS generates selective, non-selective, or both types of autophagy [16].

Reactive Oxygen Species (ROS)

ROS are unstable, partially reduced oxygen derivatives, which are byproducts of metabolic processes. They are continually being generated during normal metabolic processes [17]. They include hydrogen peroxide (H_2O_2), superoxide anion (O_2^-), hypochlorous acid (HClO), singlet

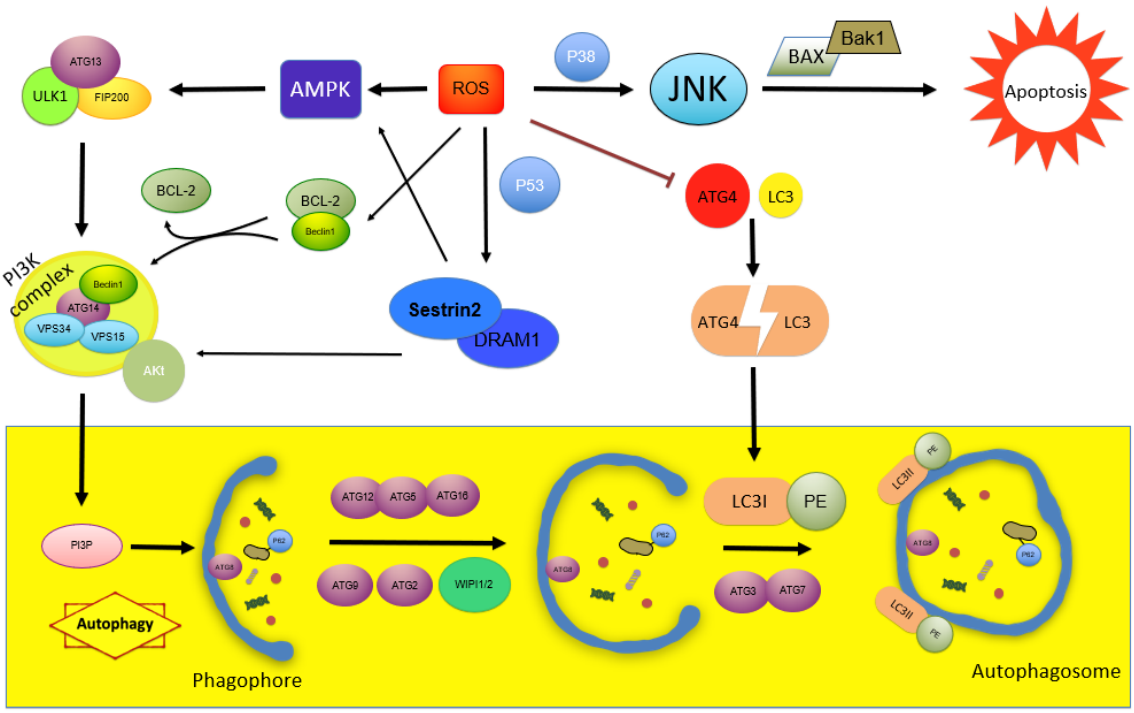

Figure 1.1. Proteins involved in autophagy initiation, phagophore formation, elongation and autophagosome formation. Autophagy and ROS levels are positively correlated.

oxygen ($^1O_2$), and hydroxyl radical (·OH) [18]. ROS-producing enzymes include NADPH oxidases, cyclooxygenases (COX), and lipoxygenases (LOX). ROS are generated from oxygen mostly in mitochondria during oxidative phosphorylation [19,20]. Peroxisomes generate superoxide and H_2O_2, contributing to ROS production. Chemotherapy drugs also contribute to ROS production, as discussed below.

ROS Regulates Autophagy

The main downstream autophagic effectors of ROS are ATG4 (at Cys-81) AMP-activated protein kinase (AMPK), ULK1/ATG1 (through AMPK), and the transcription factor NF-kB, which leads to the expression of Beclin-1 and SQSTM1/p62 [11,21–26]. ATG4 oxidized by ROS at specific cysteine residues is unable to delipidate LC3 [27,28]. Since lipidated LC3 is part of the autophagosome, ROS interaction with ATG4 leads to the sustained presence of autophagosomes [21]. Because mitochondria produce ROS, autophagy of mitochondria, a process called mitophagy, is crucial for regulating ROS levels. Mitophagy initiation involves either the ubiquitin-mediated PINK1-Parkin pathway or the receptor-mediated FUNDC1/BNIP3/NIX pathway[29]. In the former, PINK1 accumulates in the outer mitochondrial membrane [30]. A phosphorylation cascade involving PINK1 and Parkin activates Parkin's ubiquitin ligase activity [31]. Parkin then ubiquitylates outer mitochondrial membrane proteins Mfn1, Mfn2, VDAC, and MIRO1 [32]. Ubiquitinated proteins are then recognized by ATG8-family junction proteins SQSTM1/P62, OPTN, NDP52, TAX1BP1, and NBR1. Interestingly, PINK1-PRKN-dependent mitophagy requires GABARAP, not LC3 [33,34]. The phagophore then nucleates around the damaged mitochondria and autophagy is initiated. In the latter case, the mitochondrial receptor proteins FUNDC1, BNIP3, NIX, FKBP8, Bcl2L13, Ambra1, PHB2, and NLRX1 contain a conserved LC3-interacting receptor domain that can bind LC3 and thus be engulfed in a developing autophagosome [35–43].

ROS in Cancer Cells

Cancer cells have high ROS levels [44]. This is due mainly to augmented cell proliferation, differentiation, protein synthesis, glucose metabolism, and inflammation [45]. Increased

metabolism in cancer cells results in respiratory dysfunction and electron leakage from mitochondria [46]. In fact, cancer cells often have dysfunctional mitochondria. ROS levels can further increase by oncogene activation, or cytokine/growth factor signaling [28,47]. During ROS-induced tumor cell progression, ROS activates the Wnt signaling pathway. Wnt activation leads to the epithelial-mesenchymal transition [48]. It also upregulates the transcription factor c-Myc [49]. Overexpression of c-Myc is a hallmark of cervical carcinomas, leukemias, lymphomas, colon, and testicular cancer [50,51]. In turn, c-Myc overexpression can generate additional ROS [52]. With this background in autophagy and ROS, we now focus on the mechanisms by which chemotherapy drugs trigger additional ROS production, which in turn triggers pro-survival autophagy in cancer cells.

Autophagy plays different roles in cancer cells depending on the stage of tumor progression [53]. Autophagy can help reduce the probability of DNA mutations by suppressing ROS in the early stages of oxidative cell stress [54]. This occurs mainly through mitophagy. In primary tumor cells, autophagy can cause p53-dependent apoptosis, thus preventing accumulation of oncogenic p62 protein aggregates and metastasis [55]. p53 plays pro- and anti-autophagic roles depending on its localization in cells [56]. p53 is usually localized to the cytosol. Cytosolic p53 suppresses autophagosome formation by interacting with FIP200, which leads to inhibition of ULK1/Atg13/FIP200 complex [56]. When p53 translocates to the nucleus, it initiates autophagy. In the nucleus, p53 activates autophagy inducers, including DRAM1 and Sestrin2 [57]. In these cells, downregulation of BCL-2/BCL-xl induces pro-apoptotic autophagy [58]. At this point in cancer progression, when cells are adapting to stress (e.g., nutrient deprivation, hypoxia, metabolic stress, and chemotherapy), autophagy reduces both DNA and ROS damage, and removes damaged organelles [59]. In metastasis, autophagy helps migrating cells overcome hypoxia, nutrient deprivation, and autophagic gene mutation that leads to chemotherapy resistance [55]. Thus, depending on the stage of the cancer, with more advanced cancers needing more nutrients, cancer cells should naturally trigger ROS production [60].

The Effects of Chemotherapy on ROS Production

Chemotherapy can cause ROS generation by disrupting and/or by inhibiting the cellular antioxidant system [61–67]. In the former, chemotherapy drugs can destabilize mitochondrial membranes, disrupting the mitochondrial electron transport chain. This leads to electron leakage, which elevates ROS production [61–63]. Thus, mitophagy could play a central role in chemotherapy drug resistance. In the latter, chemotherapy agents can cause the depletion of antioxidants such as glutathione (GSH) and the superoxide dismutase (SOD) enzyme [65,66].

Since autophagy can sustain cell viability, it is important to determine if there are functional overlaps or interactions with autophagy gene products and the anti-apoptotic proteins that cancer cells use for survival [68]. BCL-2 family members are a prominent class of anti-apoptotic genes [69]. During stress conditions, Beclin-1 interacts with BCL-2/xl/w/MCL-1, thereby activating autophagy via the interaction of Beclin-1 with Vps15 and Vps34 [70]. (Figure 1.2) This complex promotes phagophore nucleation [69]. Thus, we see that anti-apoptotic genes work with autophagy genes to maintain cell viability. However, BCL-2 proteins can also be apoptotic. BCL-2, BCL-xl, BCL-w, and MCL-1 inhibit survival autophagy when BCL-2 interacts with Beclin-1. This complex blocks the action of Bax/Bak1 [69]. Activated Bax/Bak1 complex causes mitochondrial membrane permeabilization and rupture by interacting with ceramide channel-forming sphingolipid or form putative cytochrome c release channels on the outer membrane of mitochondria to induce permeabilization [71].

Certain Chemotherapy Drugs Cause Autophagy

The main link between cancer chemotherapy drug resistance and autophagy is that drugs trigger ROS production, which triggers autophagy, keeping certain cancer cells viable. Table 1.1 summarized drugs that are involved in chemotherapy treatments that trigger autophagic pathways.

***Piperlongumine*.** Piperlongumine is used as an anti-cancer drug for lung, breast, prostate, and gastric cancers. Piperlongumine causes p38 and JNK phosphorylation via a ROS-dependent pathway. This leads to increased expression of Bax and Beclin-1 [72,73]. It also inhibits Akt/mTOR phosphorylation, triggering autophagy. Piperlongumine activation of p38 inhibits ATG5 and the formation of autophagosomes (Figure 1.3). In piperlongumine-treated androgen-independent

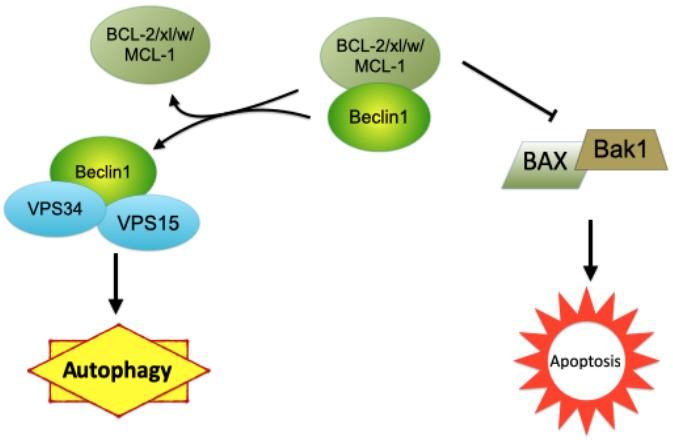

Figure 1.2. Different functions of BCL-2 family members. Beclin1 dissociation from BCL-2, BCL-xl, BCL-w, MCL-1 during the stress conditions causes phagophore nucleation and triggers autophagy. While, Pro-apoptotic BCL-2 (Bax and Bak1) causes mitochondrial membrane rupture. Cell survival genes coordinate with autophagic genes to promote viability.

Table 1.1. Drugs and their effect on autophagy. MM: multiple myeloma; HCC: hepatocellular carcinoma cancer; HER2: Human epidermal growth factor receptor 2; ROS: reactive oxidative species; Caspases: cysteine-dependent aspartate-directed proteases; DOX: Doxorubicin; PI3K1: phosphoinositide 3-kinase class 1; mTOR: mechanistic target of rapamycin [serine/threonine kinase]; Akt: A serine/threonine kinase; AMPK: adenosine monophosphate-activated kinase;

Authors	**Drugs/Proteins**	**Disease/Cell line**	**Effect on autophagy**	**Pathway**
Makhov *et al.*[74]	Piperlongumine	prostate cancer (786-O and PC-3)	Generating ROS	mTOR inhibition signaling via Akt phosphorylation
Wang *et al.*[73]	Piperlongumine	leukemia(U937)	Promoting ROS	p38 and JNK phosphorylation Bax and Beclin1 upregulation
Rodríguez-Hernández *et al.*[75]	Sorafenib	HCC (HepG2 cells)	Reducing the caspase-9 activity	AMPK signaling
Shen *et al.*[76]	Cisplatin	NSCLC	Autophagy activation by targeting ATG7	downregulated miRNA cells and PI3K complex
Zhang *et al.*[77]	Bortezomib	MM cells (MM1.R)	MARCKS suppression	Initiating Beclin1/Bcl-xL complex
Xiao *et al.*[78]	Trim14	Gastric cancer cells (SGC)	Promoting autophagy by FGFR inhibition	PI3K/mTOR/AMPK complex
Condello *et al.*[79]	DHA/ epirubicin	breast cancer (MDA and MCF-7)	Autophagy induction by blocking Beclin1/Bcl-2 complex	mTOR autophagic signaling
Hu *et al.*[80]	DHA/ DOX	breast cancer (MDA and MCF-7)	Enhancing DOX localization in the nucleus, generating ROS	AKt/mTOR signaling

Table 1.1 Continued

Authors	**Drugs/Proteins**	**Disease/Cell line**	**Effect on autophagy**	**Pathway**
Inokuchi-Shimizu *et al.*[81]	Paclitaxel (PTX)	Ovarian, esophageal, breast, lung, Kaposi's sarcoma, cervical, and pancreatic cancers	Inhibits autophagy, but co-treatment of breast cancer cells with the autophagy blocker CQ improves PTX resistance.	LC3-II and SQSTM1 signaling
Loibl *et al.*[82]	Trastuzumab emtansine	HER2-positive breast cancer	Promoting autophagy	Caspase-3/7 activation and AKt/mTOR signaling
Barceló *et al.*[83]	Vemurafenib/ mibefradil	MM cells (Vem-R and Vem-S)	Promoting autophagy	Activation of PI3K/protein kinase B pathway

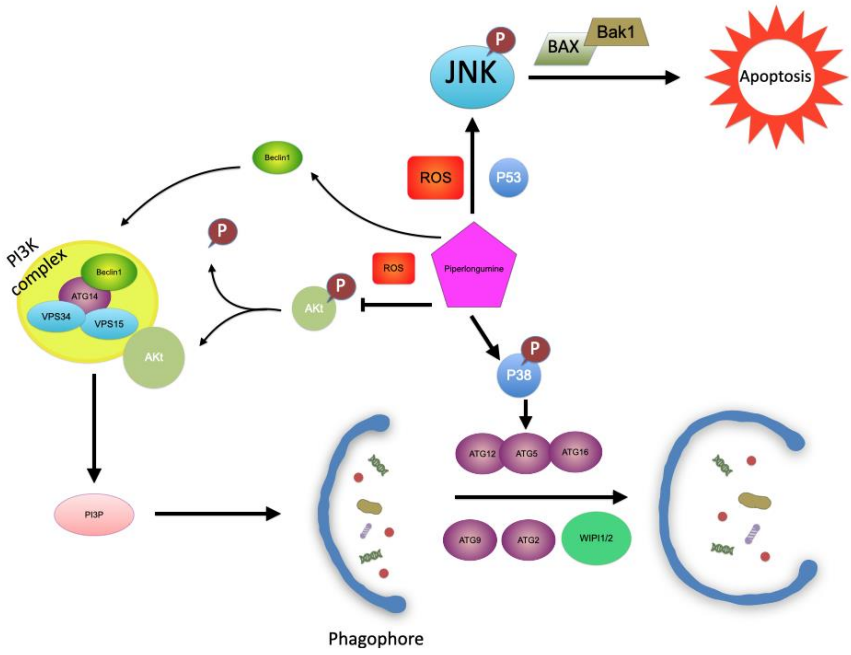

Figure 1.3. Role of piperlongumine in the autophagic pathway. Piperlongumine activates p38 phosphorylation leading to autophagosome formation. It also triggers autophagy via ROS promotion and Akt/mTOR inhibition. Piperlongumine also phosphorylates JNK leading to the triggering of apoptosis by Bax and Beclin-1. Piperlongumine triggers a combination of autophagic and apoptotic pathways.

human PC-3 prostate cancer cells and renal carcinoma 786-O cells, stimulation of ROS inhibits the phosphorylation of Akt [74].

Sorafenib. Sorafenib inhibits protein kinases including VEGFR, PDGFR, and RAF [84]. Rodríguez-Hernández et al. have shown that a low dose of sorafenib, a drug to treat advanced hepatocellular carcinoma (HCC), increased autophagy in HepG2 liver cells *in vitro* [75,85] The survival role of autophagy has been seen in lower doses of sorafenib through activation of caspase-9 [75]. Caspase-9 is activated by adenosine uptake into mammalian cells followed by conversion to AMP, and ultimately AMPK activation 86]. In contrast, higher doses of sorafenib induced cell death through caspase-3 pathway by inhibiting BCL-2 family proteins [85]. (Figure 1.4) FOXO3a is an important transcriptional factor which is regulating stress responses such as hypoxia and nutrition depravation in the cells. Phosphorylation of FOXO3a occurs under starvation condition via PI3K-AKT signaling pathway [87]. mTOR is upregulated by sustained sorafenib and AKT activation therefore, it leads to autophagy induction and cell apoptosis [88]. FOXO3a knockout inhibits hypoxic induced autophagy so to eliminate the sorafenib resistance FOXO3a plays a pivotal role in HCC cells [89].

miRNAs and lncRNAs. MicroRNAs (miRNAs) are non-coding RNAs that regulate gene expression, cell proliferation, and apoptosis [90]. miRNAs are involved in the initiation, progression, and drug resistance of HCC [91]. Similarly, miR-212 downregulates lethal autophagy through the Akt/PTEN pathway in sorafenib-resistant cells [92]. Xie et al. have confirmed the downregulation of the AKT/PTEN/NF-kB signaling pathway by miR-132, which blocks resistance by doxorubicin (DOX) in HCC cells [93,94]. miR-132 targets PIK3 regulatory subunit 3 (PIK3R3) and inhibits autophagy and drug resistance in HCC cells [95]. Also, miR-223 overexpression induced non-lethal autophagy in cisplatin-resistant cells; therefore, miR-223 inhibition enhanced cisplatin efficacy in vivo [96]. In another example of HCC treatment, it was shown that cisplatin-induced downregulation of miR-199a-5p increased drug resistance by activating AGT7, another autophagy associated gene that interacts with LC3 [89]. (Figure 1.5) miR-22 increases the sensitivity of osteosarcoma cells to cisplatin [97]. An miR-22 mimic that was transfected into osteosarcoma cells downregulated ATG5, beclin1, and LC3 [98]. Thus, miR-22 may improve cisplatin sensitivity by inhibiting autophagy. This is an example where the combination of anti-cancer drugs and autophagy modulators may improve chemotherapy treatment outcomes.

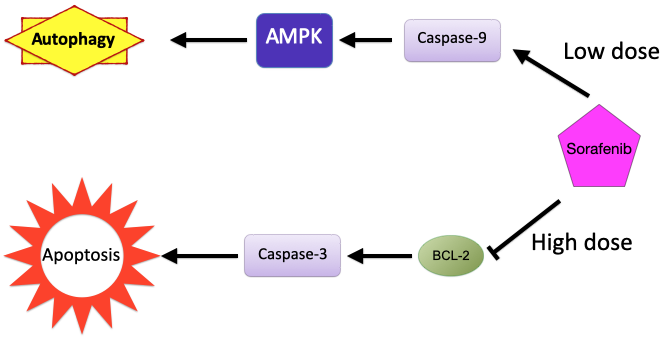

Figure 1.4. Role of sorafenib in autophagic pathway. The extent of autophagy and apoptosis by sorafenib are dose-dependent.

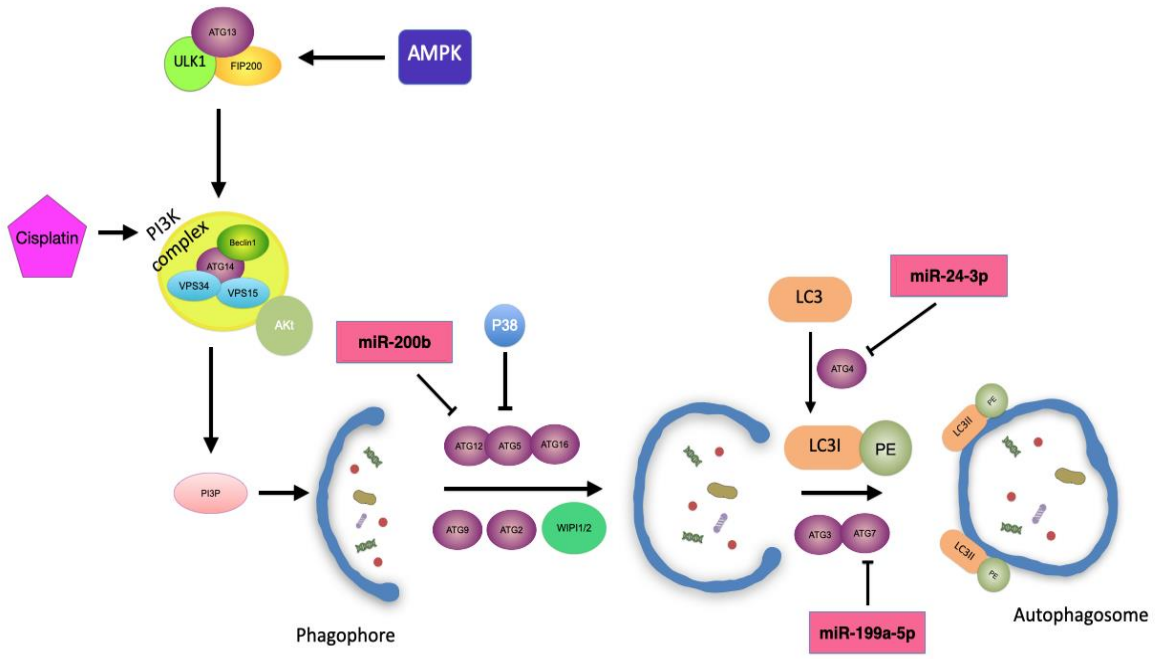

Figure 1.5. Inhibiting non-lethal autophagy by miRs to overcome drug resistance in cisplatin-treated cells. miR-200b, miR-24-3p, and miR-199a-5p respectively inhibit atg12, atg4, and atg7 in different stages of autophagy. The role of METTL3 in autophagy induction in sorafenib resistance cells. By depletion of this RNA, it is possible to overcome drug resistance in NSCLC cells.

Long non-coding RNAs (lncRNA) LUCAT1 contributes to cisplatin resistance by regulating the miR-514a-3p/ULK1 axis in human non-small cell lung cancer [76]. LUCAT1 was upregulated in cisplatin-resistant cancer cells. ULK1 was determined to be the target gene of miR-514a-3p. LUCAT1 positively regulated ULK1 expression by targeting miR-514a-3p. Gene ontology analysis of lung cancer cells revealed that autophagy plays a protective role against cisplatin [99]. That study showed that autophagy is more active in cisplatin-resistant small cell lung cancer cells, that autophagy protects cisplatin-resistant small cell lung cancer cells, and that anti-malaria drugs, which increase the pH of lysosomes, enhance cisplatin effectiveness. miR-17 binds ATG7 mRNA and negatively regulates ATG7 expression [100]. High expression of ATG7 leads to chemotherapy resistance [101]. Temozolomide, a brain cancer treatment, showed the most resistance in T98G cells of glioblastoma cell line [102]. Inhibition of miR-17 combined with temozolomide decreases the drug resistance in T98G cells via autophagic pathway underlying ATG7 regulation [103].
In human lung adenocarcinoma cells, miR-24-3p was found to regulate cisplatin resistance in small-cell lung cancer by targeting ATG4 and finally, miR-200b participated in autophagy regulation through ATG12 signaling [97,104]. (Figure 1.5) MiR-133a also plays a prominent role in tumorigenesis, progression, autophagy, and drug-resistance in various malignancies [105]. It could incorporate with DOX and cisplatin to improve the drug efficiency in breast cancer cell line MCF-7 and Hep-2v cells, respectively [106,107]. miR-133a-3p can promote proliferation and autophagy in gastric cancer cell lines by binding the 3'-UTR of forkhead protein 3 (FOXP3) [108].

***Bortezomib and Carfilzomib*.** Bortezomib and carfilzomib – two drugs that are used for the treatment of multiple myeloma (MM) – activate AMPK which promotes prosurvival autophagy [74]. (Figure 1.6) Similarly, Zhang and colleagues showed that bortezomib suppressed myristoylated alanine-rich C kinase substrate (MARCKS) causing p53 upregulation, which released the autophagy initiating Beclin1/Vps34 complex from BCL-2 family proteins [109]. They also showed that the interaction between Beclin1 and Bcl-xl is weakened in MARCKS-silenced cells. The reduced Beclin1/Bcl-xL interaction suggest a mechanism whereby MARCKS suppression induces autophagy [99]. Combining the drugs mentioned above, bortezomib and carfilzomib, with MARCKS knocked-down cells, led to increased MARCKS suppression.

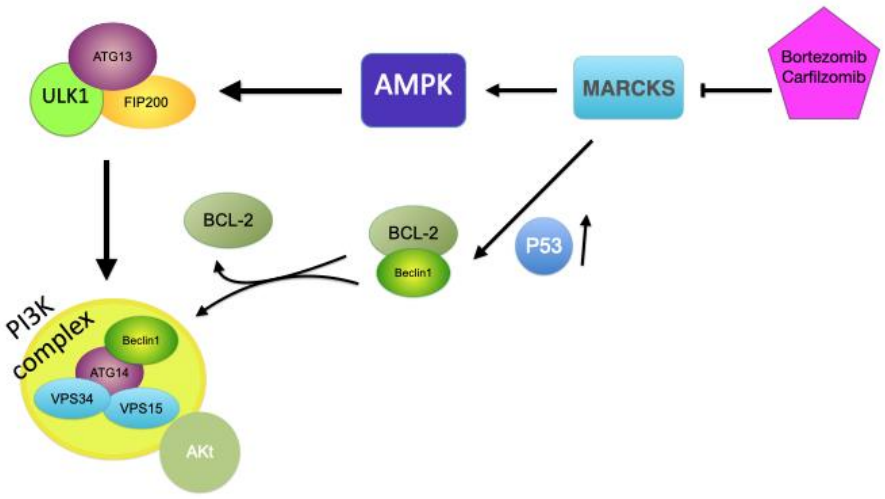

Figure 1.6. Role of bortezomib and carfilzomib in autophagic pathway. These drugs trigger autophagy by activating AMPK pathway and increasing nuclear p53 via MARCKS suppression.

Therefore, the triggering of lethal autophagy with MARCKs suppression seems to help to combat drug resistance in the MM cells [99]. (Figure 1.6)

Further studies on HCC have shown the regulation of autophagy by lncRNAs. In response to drug-resistance to DOX and sorafenib, LINC00160 (long intergenic non-coding RNA 00160) triggers autophagy by targeting PIK3 and ATG5 [110]. LINC00160 correlates with breast cancer survival and regulates the expression of PIK3R3, whose main function is ATG5 activation at the transcriptional level, and by binding to miR-132 inhibits cell viability and drug resistance in HCC cells [109]. (Figure 1.7) LINC600 Silencing suppresses non-lethal autophagy and cell proliferation by decreasing PIK3R3 and miR-132 promotion [111]. In terms of the key autophagy regulator, ATG7, lncRNA BLACAT is up-regulated in DDP-resistant non-small cell lung cancer (NSCLC) cells and acts as ceRNA in reducing miR-17 expression. This leads to increased expression of ATG7 and autophagy promotion [112]. LncRNA XIST also causes autophagy and drug resistance to chemotherapy by regulating ATG7 expression through miR-17 [113].

However, lncRNAs have different effects on liver cancer cells and are highly upregulated in HCC tissues and human HCC cell lines including HepG2, Hep3B, PLC, Huh7, and smmc7721 [111,114]. In a similar study on HCC and sorafenib, Lin and colleagues have represented autophagy suppression by an RNA complex. METTL3 is an RNA methyltransferase complex that inhibits autophagy under hypoxia environment through PI3k/AKT signaling pathway. METTL3-knockdown provides another solution to improve sorafenib drug-resistant in NSCLC via upregulation of LC3-II, ATG5, Beclin 1 and Vps34 and downregulation of BCL-2 [115,116]. (Figure 1.8)

Gemcitabine and Asparaginase. Gemcitabine is used to treat prostate cancers. Zhang and colleagues demonstrated that gemcitabine treatment in hormone-independent prostate cancer (HIPC) has a dose-dependent outcome on the protein level of high mobility group box 1 (HMGB1) [117]. HMGB1 upregulates of Beclin1/2 complex by dissolving it from Bcl-2 to initiate and regulate autophagy in the cytosol. Nuclear localization of HMGB1 activates heat shock protein β-1 (HSPB1) expression and autophagy. HMGB1-Overexpression or -knockdown affects HSPB1 level but did not have any effect on Beclin1 level. This leads to the postulate that gemcitabine sensitivity is due to HSPB1-initiated autophagy. Although the exact pathway of Beclin1 autophagy induction is still unclear [92]. (Figure 1.9).

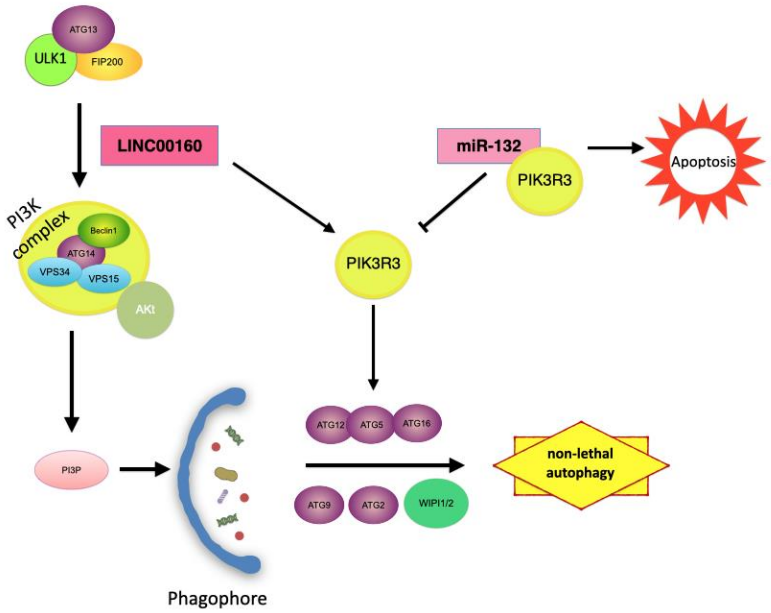

Figure 1.7. LINC00160 upregulates PIK3R3 while miR-132 is downregulated. Silencing of LINC160 suppresses autophagy by decreasing PIK3R3 and miR-132 promotion in Dox and sorafenib-resistance cells to overcome drug resistance.

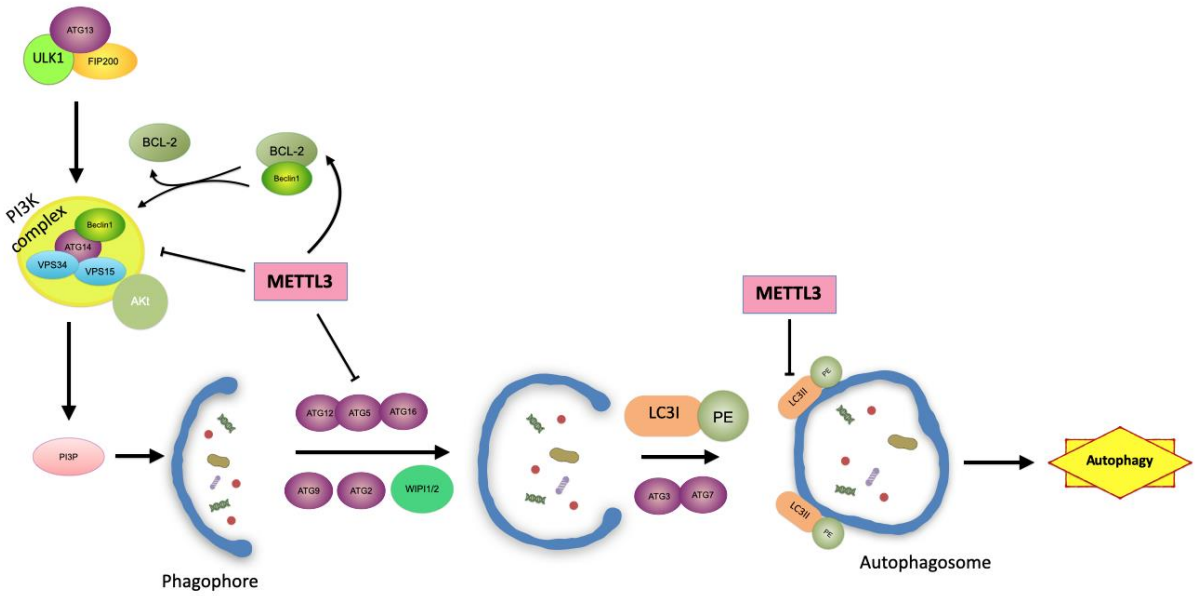

Figure 1.8. The role of METTL3 in autophagy induction in sorafenib resistance cells. Depletion of METTL3 in hypoxia conditions activates the autophagic pathway in HCC cells.

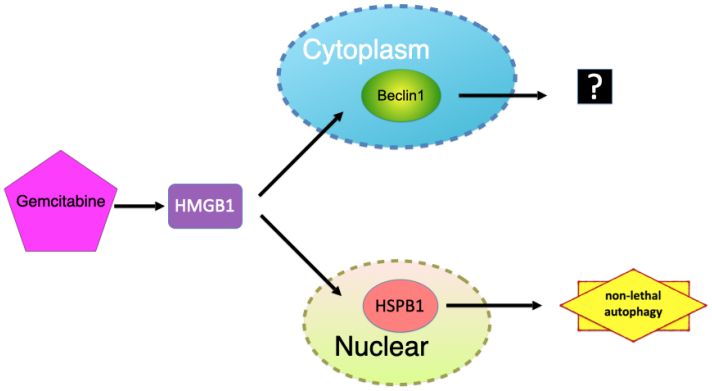

Figure 1.9. Role of gemcitabine in autophagic pathway. HMGB1 regulate non-lethal autophagy in the cytosol. Nuclear localization of HMGB1 expresses HSPB1 and induce autophagy.

Asparaginase is a common drug in the treatment of nature kill / T-cell lymphoma. As the name suggests, asparaginase kills these target cells by depriving them of L-asparagine [118]. Patients with higher levels of the non-messenger RNA factor BCYRN1 had markedly lower progression-free survival than patients with lower levels [119]. The authors found that asparaginase increased degradation of p53 through ubiquitination. This resulted in the increase of autophagy via the PI3K/AKT/mTOR and p53/mTOR pathways ultimately leading to asparaginase resistance. In this case, drug resistance was reversed by drug-induced autophagy inhibition in a xenograph model.

Trim14, a protein that has been expressed in gastric cancer (GC) cells, has promoted autophagy and increased the proliferation of chemotherapy resistance. The autophagic pathway that has been involved here is consist of PI3K/mTOR/AMPK complex. As it was mentioned before, the activation of AMPK reversibly regulates the activation of mTOR [78].

In advanced stages of GC, human fibroblast growth factor receptor (FGFR) protein inhibition has been reported to activate autophagy and improve therapeutic strategies [110]. FGFR activates mitogen-activated protein kinase (MAPK), and PI3K/AKT complex [120,121]. Peng et al. have shown that the FGFR inhibitor is connected with autophagy by targeting the AMPK/mTOR signaling pathway in GC cells [110]. Previous studies have shown the role of TGF-β-activated kinase 1 (TAK1) in autophagy induction via AMPK/mTOR signaling pathway [81,122,123]. In sum, with the combination of EFGR and TAK1 inhibitors, chemotherapy resistance could potentially be overcome [94].

Cancer stem cells and autophagy

Cancer is in large part a stem cell disease. Recently, mechanistic links among cancer stem cell factors and autophagy have been uncovered. In the context of our discussion of GC and colorectal cancer, it was recently determined that Beclin-1 is partially responsible for chemoresistance, stemness, and the epithelial-mesenchymal transition [124]. In that work, the sex-determining region Y-box2 (SOX2), a master regulator of embryonic and induced pluripotent stem cells, increases the expression of Beclin-1. This increases autophagy and activated a malignant phenotype. Furthermore, xenograph mouse models showed that SOX2 inhibition reduced autophagy and abated tumor growth and decreased chemotherapy resistance *in vivo*. These results confirm those of a previous study suggesting that SOX2 plays a crucial role in maintaining GC stem cell

properties [125]. Certainly, more links between stemness and autophagy will be uncovered that will hopefully be able to be exploited as drug targets.

Targeting autophagy to overcome drug resistance

Combining chemotherapy drugs with autophagy inhibitors can optimize the drug concentration, accelerate binding with the targets and/or transporters, and inhibit autophagy leading to cell apoptosis and eventually more efficient anticancer treatment. Table 1.2 provides a list of complement enhancers to improve the drug resistance in cancer. Ramirez and colleagues saw an increase in ATGs, SQSTM1, Beclin-1, and ULK1 after 5-fluorouracil (5-FU) treatment of human colon cancer cell line HCT-116 in vitro [126]. But when they added chloroquine (CQ), an autophagy suppressor, LC3-II and SQSTM1 levels increased indicating that autophagy was blocked at autophagosome formation. It should always be noted that autophagy is a dynamic process and can be halted at certain gateway points [3]. Incomplete autophagy and autophagosomes accumulation can cause oxidative stress and lead to organelles dysfunction and, ultimately, cell death [79,127]. Indeed, adding CQ to 5-FU increases cell apoptosis [126].

In the following, more examples of multidrug resistance and autophagy are discussed. In some recent studies on cancer treatment by dihydroartemisinin (DHA), apoptosis has been noticed widely in autophagy induction and tumor cells. For example, in breast cancer, a combination of DHA and epirubicin, another breast cancer drug, improved the treatment due to higher drug concentration and prolonged drug interference to the cells through the mTOR autophagic signaling pathway [79,128].

DHA interacts with Bcl-2, therefore it blocks Beclin1/Bcl-2 complex. Beclin1 activates PI3K complex to promote autophagy. On the other hand, DHA suppresses binding Bcl-2 with Bax, resulting Bax association with the mitochondria, to activate apoptosis cascade via the mitochondria pathway. Epirubicin intercalates DNA strands, resulting in apoptosis of cancer cells. Moreover, DHA enhances the uptake of epirubicin due to the distribution of the cell membrane to DHA [80]. Similarly, in colon cancer, DHA+DOX enhanced the localization of DOX in the nucleus, followed by autophagy enhancement and, finally, cancer cell apoptosis [110]. Other than Bax, DHA contributes with other cell mechanisms, such as inhibition of NF-κB, generation of active oxygen

Table 1.2: The effect of drug enhancer co-treatment with chemotherapy on autophagy. MARCKS: myristoylated alanine-rich C kinase substrate; LINC00160 :long intergenic non-coding RNA 00160; METTL3: methyltransferase like 3; HMGB1: High mobility group box 1; TTCC: T-type calcium channel; TRAIL: Tumor necrosis factor-related apoptosis-inducing ligand; MM: multiple myeloma; HCC: hepatocellular carcinoma cancer; VPS: vacuolar protein sorting; Akt: A serine/threonine kinase; PTEN: phosphatase and tensin homolog; NF-κB: nuclear factor of kappa light polypeptide gene enhancer in B-cells; PI3K: phosphoinositide 3-kinase; HSPB1: Heat shock protein β-1; SQSTM1: sequestosome 1; ULK1: unc-51 like autophagy activating kinase 1; AMPK: adenosine monophosphate-acticated kinase; BCL-2: B-cell lymphoma 2; Caspases: cysteine-dependent aspartate-directed proteases

Authors	**Drugs**	**Drug Enhancers**	**Cell lines**	**Pathway**
Zhang *et al.*[109]	Bortezomib	Carfilzomib	MM cells(MM1.R)	MARCKS knocked-down Upregulating P53, initiating Beclin1/Vps34 complex
Ucar *et al.*[92]	Sorafenib	miR-212	HCC (HCCLM3-SR)	Akt/PTEN signaling
Xie *et al.*[93]	Dox	miR-132	HCC (MHCC97 cells)	Downregulating AKT/PTEN/NF-kB signaling pathway
Peng *et al.*[135]	Dox and Sorafenib	LINC00160 Suppression	HCC	Targeting PIK3 and ATG5
Lin *et al.*[115]	Sorafenib	METTL3	HCC (HepG2)	PI3k/AKT signaling pathway
Zhang *et al.*[128]	Gemcitabine	HMGB1	HIPC cells	Beclin1 and 2 complex and HSPB1 expression
Ramirez *et al.*[126]	5-fu	CQ	HCT-116 colon cancer	Increasing in ATGs/SQSTM1/Beclin1/ULK1; and LC3- II/SQSTM1
Inokuchi-Shimizu *et al.*[81]	Paclitaxel	CQ	human lung adenocarcinoma (A549/T) cells ovarian carcinoma (A2780/T) cells	Increasing LC3-II and SQSTM1 levels
Barceló *et al.*[83]	Vemurafenib	TTCC and BRAF inhibitor	MM cells (Vem-R and Vem-S)	Activation of PI3K/protein kinase B pathway
Zinnah *et al.*[136]	Sertraline	TRAIL	lung A549 cells	Downregulation of AMPK and BCL-2, increase caspase-3 activity.

radicals, autophagy regulation, and apoptosis induction [129–131]. Downregulation of NF-κB promotes ROS and suppresses mTOR signaling leads to autophagy induction [132]. In an in vivo study on rat ventricular cardiomyocytes, DOX-induced autophagy was proven through GATA4 pathway. In response to DOX treatment, GATA4 protein is depleted, which results in Bcl2 inhibition and ATG5, ATG7, ATG12, and Beclin 1 upregulation. (Figure 1.10) Ultimately, it leads to autophagy activation that contributes to cardiomyocyte death [133]. The drug combination also resulted in downregulation of Bcl-xl [132]. Recent strategies for overcoming autophagy-based resistance to DOX include the co-delivery of DOX with mirror siRNA that knocked down ATG7 [134]. Another study has shown that alteration of paclitaxel (PTX) with CQ caused autophagy inhibition in lung adenocarcinoma cells and ovarian carcinoma cells [106].

In a different approach to breast cancer, Liu and colleagues precisely demonstrated the notable result on Trastuzumab emtansine (T-DM1) autophagy induction in a type of breast cancer cells [134]. Human epidermal growth factor receptor 2 (HER2)-positive breast cancer patients who have progressed after prior treating with trastuzumab and taxane received T-DM1, an antibody-drug conjugate (ADC) of trastuzumab [82]. T-DM1 has trigger autophagy inhibition and cell apoptosis through the Caspase-3/7 activation pathway and shows therapeutic improvement. They also revealed a molecular pathway of T-DM1, which first T-DM1 reduces p-mTOR-S2448 expression in cells. Then, mTOR and Akt regulators are dephosphorylated and trigger autophagy [116].

Hormone therapy has also reported for HCC treatment underlying autophagy [137]. Thyroid hormone is involved PTEN-induced kinase1 pathway and triggers selective mitophagy, autophagy of mitochondria [138]. Therefore, it can be an option for liver cancer treatment while further investigations are required.

Another chemotherapy-resistant disease is malignant Melanoma that is affected by autophagy activation. Vemurafenib tends to reduce the standard type of this tumor, and melanomas harbor *BRAF* gene mutation kinase inhibitors. However, these tumors repeatedly face drug resistance through chronic Vemurafenib-induced autophagy [83]. It has been observed in a study on mutant melanoma cells that it is possible to overcome the resistance development by blocking autophagy. Barcelo et al. have proposed an autophagy blocker complex to treat melanomas. This complex consists of a biomarker, T-type calcium channel (TTCC), and BRAF inhibitor. The results have

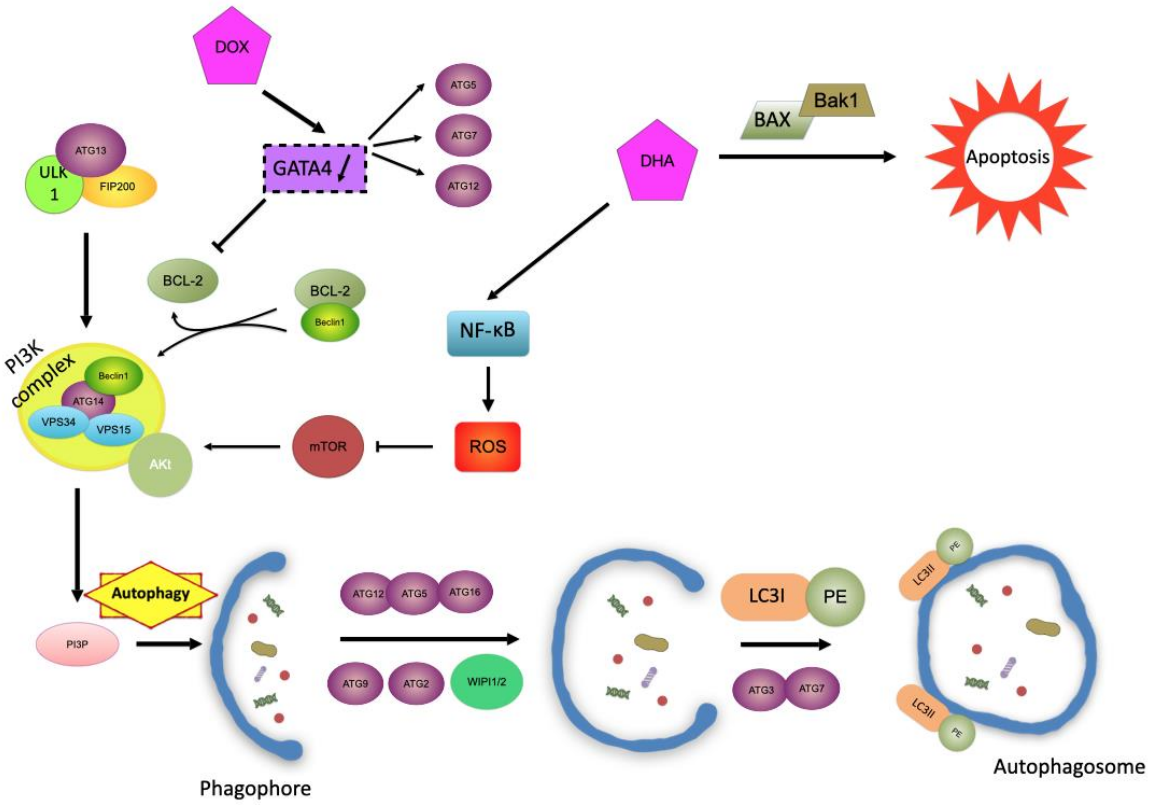

Figure 1.10. Role of DHA and DOX in autophagic pathway. Combination of these drugs enhances autophagy by downregulation of Bcl-xl.

shown a successful progression in post-therapeutic levels with mibefradil, the chemicals to block TTCCs [138].

Oleanolic acid, a chemical found in food and plants, is used in the treatment of leukemia, breast, lung, and liver cancer [139]. Oleanolic acid can inhibit the phosphorylation of PI3K in leukemia cells through the Akt/PI3K/mTOR signaling pathway and ROS pathway, or it dephosphorylates mTOR in prostate cancer cells [140–142]. Zhou et al. also revealed the autophagy inhibition role of Oleanolic acid in HCC cells. Their results confirm that Oleanolic acid has induced autophagy through the Akt/mTOR pathway by downregulating the Beclin2/Beclin1 ratio followed by mitochondrial dysfunction and eventually cell apoptosis [143].

Tumor necrosis factor-related apoptosis-inducing ligand (TRAIL) enhances cancer cell apoptosis via binding with death receptors and caspase cascade activation. Cancer cells are often resistant to TRAIL due to their insufficient expression of death receptors (DR4/DR5), excessive expression of decoy receptors, or genetic and epigenetic modification of TRAIL receptors [136,144]. In an in vitro study of lung A549 cells, it has shown that small doses of sertraline in combination with TRAIL notably enhances apoptosis [81]. Sertraline is an antidepressant drug that has proved anti-tumor activities against cancers [145]. Sertraline mediates apoptosis through the inhibition of autophagy via the downregulation of AMPK phosphorylation and activation of DR5 in TRAIL-resistant lung A549 cells. Besides, sertraline was demonstrated to decrease the expression of BCL-2 and increase caspase-3 activity [146].

As an example of lethal autophagy enhancer, irinotecan (IRI) has an anti-tumor activity for second-line treatment of advanced gastric cancer. IRI promotes MAPK signaling proteins p-JNK and p-p38 associated with ROS and induces lethal autophagy [111]. Furthermore, after IRI treatment in MGC803 and SGC7901 cells, two gastric cancer cell lines, it has been observed that ROS generation promotes autophagosome formation by phosphorylating BCL-2 and disrupting the BCL-2/Beclin 1 complex [147].

Current clinical trials

There are currently nine clinical trials of cancer chemotherapy drugs that have an autophagy aspect. Eight of the nine chemotherapy treatments group an anti-cancer drug with hydroxychloroquine. Thus, the approach is to block autophagy by inhibiting the merger of the

autophagosome with the lysosome. This will lead to the accumulation of autophagosomes in any cell that takes up hydroxychloroquine. It will be interesting to see how these combination therapies affect the normal autophagic process in healthy cells which is so crucial to organism-wide homeostasis.

Conclusions

Treating malignant cells with chemotherapy drugs can result in the increase in ROS generation, which leads to autophagy and cancer cell survival. This is one of many defenses cancer cells trigger to maintain viability and to proliferate. Combination therapies that utilize cytotoxic anti-cancer drugs along with autophagy inhibitors may increase positive outcomes for patients. But as always, targeting mostly cancer cells and avoiding healthy tissues is a major obstacle. Off-target autophagy inhibition could trigger several side effects including increased susceptibility to infection, increased fatty acid accumulation, and cellular senescence. Recently, immunotherapy such as check point strategies have shown success in the clinic. PD-1 is a prominent target in these strategies. Reduction of PD-1 increases autophagy. Therefore, check point therapies may also benefit from co-administration of autophagy-reducing agents.

CHAPTER 2

SOFT, POLY-ETHYLENE-GLYCOL-BASED (PEG-BASED) NANOPARTICLES (NPS) REDUCE AUTOPHAGOSOME SIGNAL, ROS, AND DO NOT ACIDIFY PHAGO-LYSOSOMES IN MACROPHAGES

Introduction

Soft poly-ethylene-glycol (PEG) nanoparticles (NPs) that are intravenously administered to mammals localize mostly to macrophages in the liver. Paradoxically, liver macrophages are also intriguing targets for NPs because they are at the hub of immunity and metabolism, two prominent drivers of mammalian health, which are intertwined with autophagy [148,149,150]. Therefore, understanding how macrophages process NPs is of keen interest to the field of nanomedicine. Yet it is unclear how macrophages respond to NPs. It is widely assumed that macrophages "clear" NPs because they are foreign objects. This could occur via the deposition, or opsonization, of foreign-body indicators on the NP, such as complement and immunoglobulin [151,152].

Fc and complement receptors on the surfaces of immune response cells such as macrophages and neutrophils would recognize these opsonized factors, bind them, and internalize the NP via phagocytosis where it would ultimately be enzymatically degraded in the lysosome. If so, these factors should increase in number. One of the most crucial is the transcription factor EB (Tfeb), which is a master regulator of lysosome biogenesis and expression of autophagic genes [153–155]. Thus, Tfeb levels would be expected to increase if any object is being trafficked to the lysosome for degradation. This would include pathogens and possibly NPs. An additional part of this story is that pathogens have evolved to escape the endo-phagosome [156]. Autophagy is triggered to capture these cytosolic pathogens, engulf them, and deliver them to lysosomes. Since NPs that carry nucleic acids are now designed to escape endo-phagosomes, for example pfizer sars-cov-2 mrna vaccine, the autophagy pathway becomes crucial to understand in the context of soft NPs.

Though the hypothesis of serum proteins depositing on NPs leading to clearance by phagocytes is widely accepted, open questions remain. Indeed, the most prominent corona factors on LNPs are not immunoglobulins or complement but apolipoproteins ApoA-I, ApoB-100, ApoC-III, and ApoE [157,158]. These apolipoproteins are structural components of chylomicrons, HDL, LDL, and VLDL. It is possible that apolipoproteins that bind NPs take the NP to the

apolipoprotein/lipoprotein receptor on the cell surface. Since macrophages have high numbers of lipoprotein receptors [159], NPs could be guided to these cells through this mechanism. Yet, it is unclear how the NP would enter the cell if it binds lipoprotein receptors on the cell surface. hHDL particles are postulated to remain bound to the macrophage surface whereas hLDL particles are postulated to be endocytosed and processed in the lysosome. Unfortunately, the binding affinity and rate constants of apolipoproteins for LNPs are largely unknown.

Recently, an additional NP uptake mechanism emerged. PEG was found in the cholesterol binding pocket of endosomal LIMP-2 [160]. LIMP-2 is in the CD36 superfamily of proteins along with the major high-density lipoprotein receptor, SR-BI. These proteins function as lipoprotein receptors and cholesterol and fatty acid transporters. PEG NP micelles bind SR-BI and are internalized, at least partially, by macrophage SR-BI [161]. It is unclear which additional proteins may or may not assist in the NP internalization mechanism. Thus, PEG itself can bind receptors of lipoproteins. It is currently unclear which of these pathways result in NP uptake by macrophages. It could certainly be a combination of these pathways.

It is further hypothesized that NPs taken up by macrophages are processed by autophagy [162,163]. This phenomenon is mostly seen with hard NPs that have high aspect ratios [156]. If the NP stays in the endo-phago-lysosome pathway, it is unclear why autophagy would be needed. But if NPs localize to and are processed by lysosomes, Tfeb should increase. Tfeb increase should lead to autophagy as mentioned above. This could be the link between NPs that do not escape endo-phagosomes and their triggering of autophagy. Again, NPs that are designed to escape endo-phagosomes will most likely trigger a different form of autophagy.

Cells use autophagy to regulate a variety of processes including response to pathogens. The signature autophagic event is the formation of a double membraned autophagosome [164]. The autophagosome engulfs areas of the cytosol in macroautophagy or specific targets like invading pathogens in xenophagy [156]. Autophagosomes merge with the lysosome and the contents of the former are degraded. Many pathogens trigger selective autophagy through p62/SQSTM1, which binds the pathogen and delivers it to a forming autophagosome, the phagophore [165]. The components of pathogens such as the gram-negative endotoxin, LPS, also contribute to autophagy initiation. The binding of LPS, to toll-like receptor 4 (Tlr4) results in Traf6 both ubiquitinating Becn1 and activating Ulk1 [166,167]. Both actions trigger autophagy [168]. LPS-induced autophagy

is Mapk/p38 and Ticam1/Trif dependent but does not involve the Tlr4 binding partner MyD88 [169]. MyD88 is a widely studied factor that is downstream if Tlr4. Other connections between TLRs and autophagy include the recruitment of Atg16l1 to the plasma membrane at the site of pathogen entry [170,171]. LPS induces interleukin-1 expression through ROS generation [172]. Tnf and Il1α induce autophagy as do IFNγ, IFNα, and IL6.

In the context of NPs, most is known about autophagy triggered by hard NPs such as silica, carbon nanotubes, gold and silver metals, and fibers [173]. We point the reader to a recent review of NP-induced autophagy [174]. Semi-soft cross-linked polystyrene (PS) nanoparticles particles activate Tfeb [153]. Open questions remain about the autophagic response to soft PEG NPs. It is unclear if soft PEG NPs trigger selective autophagy, canonical autophagy, or if they increase autophagy at all [175,176]. We aim to answer this question. Further, if the macrophage response to PEG NPs is similar to the response to pathogens and LPS, one would expect innate immunity to play a role in PEG NP processing. Yet, PEG-phosphatidylserine liposomes reduced LPS-elevated Tnfα mRNA levels in RAW 264.7 macrophages [177]. This result is interesting because there could be parallels between the uptake of soft NPs of certain chemistries – like phosphatidylserine – and efferocytosis, which is a natural macrophage process of clearing apoptotic cells. Efferocytosis appears to help macrophages remain viable [178]. We explore the concept of NPs increasing macrophage proliferation below.

Our goal was to understand how sustained incubation of soft PEG-based NPs with macrophages over 24-hours affected how the NPs entered macrophages, how macrophages processed the NPs once they were taken up. To achieve these goals, we incubated IFNγ-polarized RAW264.7 murine macrophages (here after, macrophages) with human high-density lipoprotein (hHDL), human low-density lipoprotein (hLDL), group A *streptococcus* pathogens (JRS4 cells), LPS, PEG (MW 6000), PEG-based cylindrical micelles (CNPs), PEG-based spherical micelles (SNPs), and PEGylated lipid nanoparticles (LNPs). hHDL and hLDL were used as controls to test similarities in macrophage response among lipoproteins and soft PEG-NPs. JRS4 cells were used as a positive control for a phagocytosis-, inflammatory-, and autophagy-triggering pathogen. LPS was used as a positive control for autophagy and inflammation. We incubated macrophages with hHDL, hLDL, JRS4 cells, LPS, PEG (MW 6000), PEG-PBD cylindrical micelle NPs (CNPs), and PEG-PBD spherical micelle NPs (SNPs) macrophages and determined the extent of autophagosome

formation, lysosome formation and function, ROS production, cell proliferation, and cytokine secretion. We chose 24 hours as our analysis timepoint for all reagents, except JRS4 cells (3 hours [156]), because most PEG NPs that are administered to mice have a $t_{1/2}$ of ~24 hours post injection.

Results

We wished to determine the effects of PEG-based cylindrical micelle NPs (CNPs), PEG-based spherical micelle NPs (SNPs), and PEGylated lipid vesicle NPs (LNPs) on M1-polarized RAW264.7 murine macrophages (hereafter, macrophages) over 24-hours of continual interaction *in vitro*. These are the timescales over which macrophages in a mouse are exposed to circulating NPs post tail-vein injection. The CNPs and SNPs used in this study had a PEG exterior and a polybutadiene (PBD) interior (Fig. 2.1A). The LNPs used in this study were a 56:38:5 molar ratio of hydrogenated soy phosphatidylcholine (HSPC), cholesterol and N-(carbonyl-methoxypolyethylene glycol 2000)-1,2-distearoyl-sn-glycero-3-phosphoethanolamine sodium salt (MPEG-DSPE) (Fig. 2.1B). These lipids form the bilayer vesicle of the anti-cancer drug DOXIL. Schematic diagrams of CNPs, SNPs, and LNPs are shown in Fig. 2.1C. All three NPs are stable in PBS and in standard macrophage cell culture media: DMEM + 10% FBS (Fig. 2.1D).

We used group A *streptococcus* pathogens (JRS4 cells) as a positive control for phagocytosis, selective autophagy, and inflammation [156]. A significant fraction of macrophages took up JRS4 cells stained with the DNA dye TOTO™-3 iodide 642/660 after 3 hours of incubation (Fig. 2.1E). We chose this shorter time because we did not want the cells to undergo apoptosis. We used human HDL (hHDL) and human LDL (hLDL) as positive controls for macrophage lipoprotein uptake. We used LPS as a positive control for an inflammatory response.

Macrophages took up hHDL, hLDL, CNPs, SNPs, and LNPs that were each carrying the same near-infrared (NIR) fluorescent dye over 24 hours incubations (Fig. 2.2A). We used flow cytometry to determine the quantity of hHDL, hLDL, CNPs, SNPs, and LNPs in the supernatant during the incubation with the macrophages. Our goal was to have enough of these reagents in the cell culture media over the duration of the 24 hours so that the cells could continually take them up. In each incubation, there was signal for the lipoprotein and NPs at the 24-hour time point (Fig. 2.2B-F). Note that CNPs had the most persistent presence in the cell culture media over the 24-hours (Fig. 2.2G).

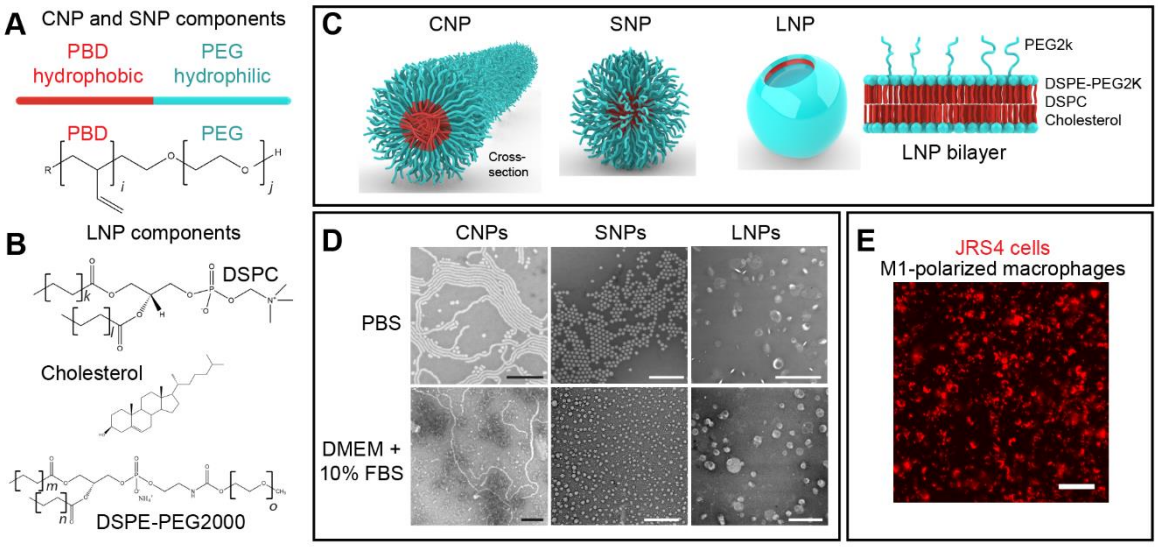

Figure 2.1. Properties of the nanoparticles (NPs) used in this study. (A) Chemistries of the components of the CNP and SNP micelles. For the CNPs: i = 46, j = 56. For the SNPs: i = 69, j = 132. **(B)** An LNP is comprised of HSPC/CHOL/PEG2000-DSPE (56.2 : 38.5 : 5.3 mol:mol). For the LNPs: k = 8 and l = 8, m = 8 and n = 8, and o = 45. **(C)** Schematic drawings of the three NPs used in this study. Drawings are simplified: a one-micron-long CNP has ~1M copolymers, a 50 nm SNP has ~30k copolymers, and a 100 nm LNP has ~85k lipids. **(D)** Electron micrographs of the CNPs, SNPs, and LNP used in this study. CNPs, SNPs, and LNP were incubated in PBS (top panels) or in DMEM + 10% FBS media that had been incubated with macrophages for 3 hours (bottom panels). Scale bars are 500 nm. **(E)** Fluorescence microscopy images of M1-polarized RAW264.7 murine macrophages after 3h incubations with JRS4 cells carrying a red DNA dye (TOTO). Scale bar is 50 microns.

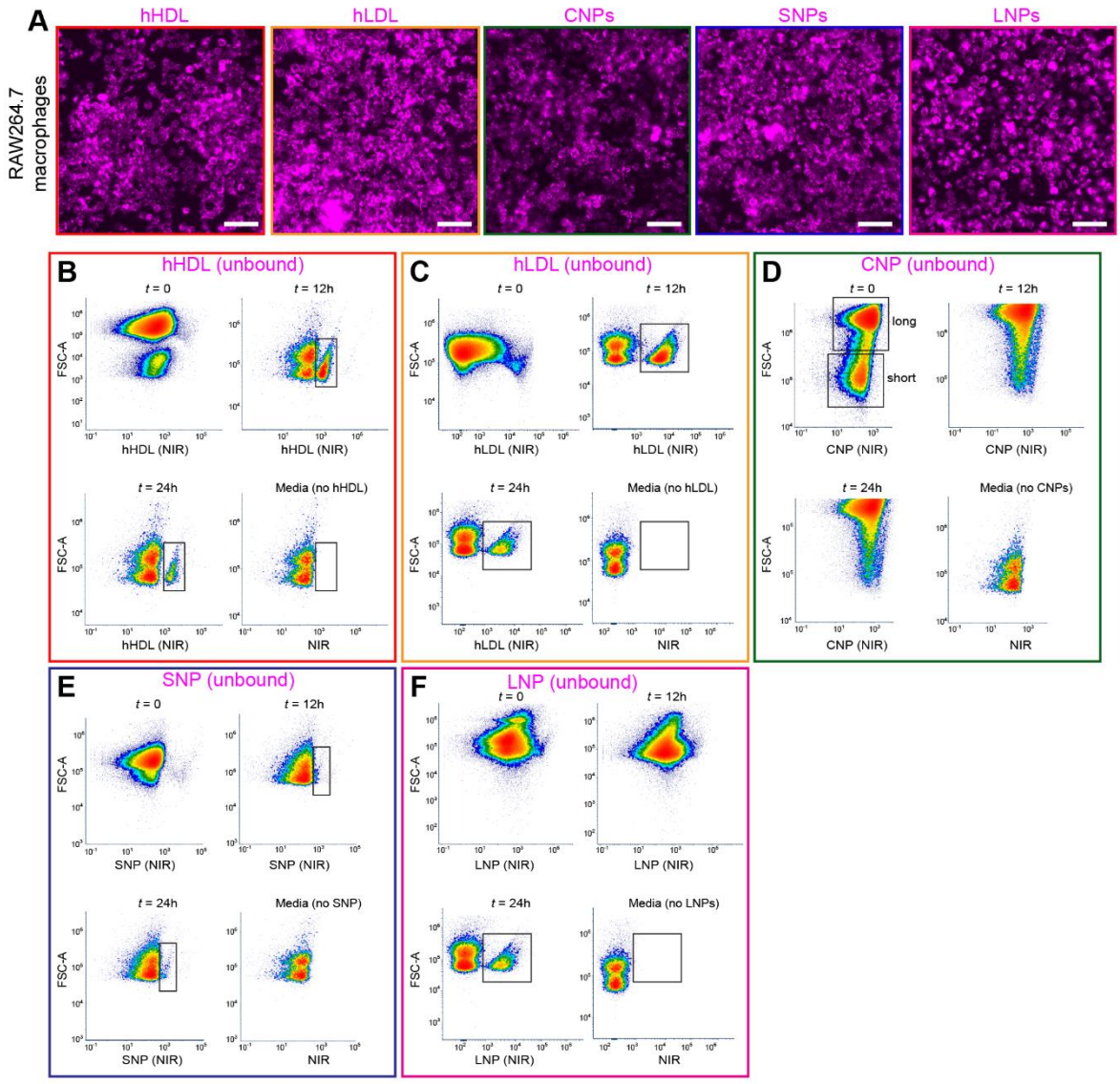

Figure 2.2. Internalization of the particles in macrophages. (A) Fluorescence microscopy images of IFNγ-polarized RAW264.7 murine macrophages after 24h incubations with the indicated lipoproteins and NPs carrying near-infrared (NIR) dye. Scale bars are 50 microns. **(B-F)** Plots of the forward scatter and fluorescence intensity (NIR channel) of the cell culture media over the time course of lipoprotein and NP incubation with macrophages. The data points represent lipoprotein and NPs that were not taken up by macrophages. A maximum of 100 ml of cell culture media was analyzed for each flow cytometry experiment.

hHDL, hLDL, CNPs, SNPs, and LNPs lower autophagosome levels in murine macrophages

It is widely held that NPs trigger autophagy in mammalian cells post internalization. To further explore the effects of LNPs on macrophage autophagy, we used fluorescence microscopy and flow cytometry analysis to measure autophagosome levels. We started with hHDL, hLDL, and JRS4 cells as controls. We incubated hHDL carrying NIR dye with macrophages for 24 hours, washed the cells with PBS, and stained them with an autophagosome dye (CYTO-ID). The autophagosome signal dropped 60% compared to PBS controls as measured by flow cytometry of CYTO-ID (Fig. 2.3A-C). We then used starvation (DMEM without 10% FBS), the mTOR inhibitor rapamycin (RAPA 250 nM), and LPS (250 ng/ml) to trigger autophagy. Starvation inhibits mTOR, which in turn activates autophagy. Amino acid deprivation - which can be caused by pathogens - is the strongest trigger of starvation-induced autophagy [179]. Rapamycin forms a complex with FK506-binding protein (FKBP12), which blocks mTOC1's kinase activity [180]. Since active mTOR inhibits autophagy, rapamycin triggers autophagy by this effect. LPS triggers autophagy that defends the cell against invading pathogens. Each of these challenges caused the CYTO-ID signal to increase (Fig. 2.3A-C).

To determine the effects of HDL on these challenges we performed co-incubation experiments of each of the above challenges with hHDL. hHDL lowered the CYTO-ID signal that was raised by each challenge. This shows that HDL has either anti-autophagosome formation properties or increases the flux of the autophagosome-lysosome merger. The second possibility is unlikely since hHDL did not increase the expression of the lysosome biogenesis factor Tfeb (Q-value = 0.98 > 0.05), although it was significantly increased by hLDL (+20.6; Q-value = $4e^{-5}$), which agrees with the finding that LDL is processed through lysosomes [181]. We performed the same CYTO-ID-labeled autophagosome experiments with hLDL in place of hHDL and observed similar reductions in CYTO-ID signals. However, hLDL was not as effective at lowering CYTO-ID signal versus hHDL (Fig. 2.3D-F). We used JRS4 cells as a positive control for selective autophagy. Indeed, three-hour incubations of JRS4 cells labeled with the TOTO DNA dye increased the CYTO-ID signal in macrophages by 60% (Fig. 2.4A-B).

To determine the effects of our NPs on autophagosome abundance, we separately incubated PEG, CNPs, SNPs, and LNPs with macrophages for 24 hours in four different culture conditions: 1)

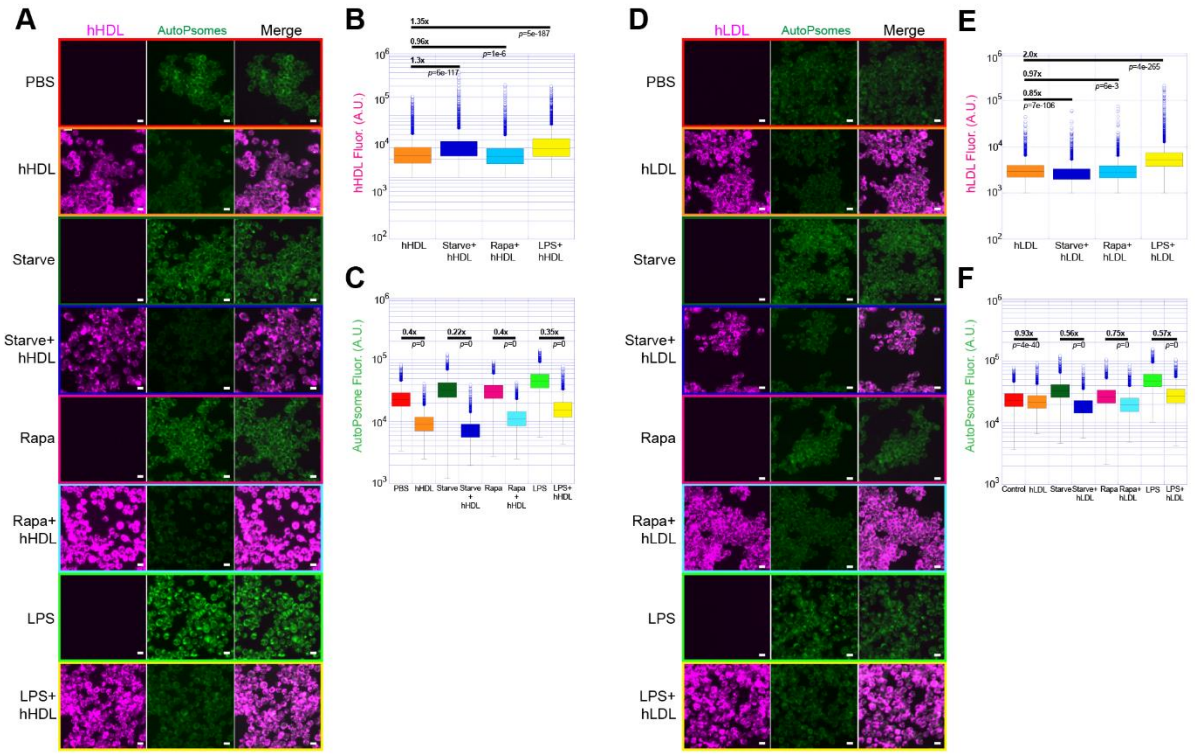

Figure 2.3. hHDL and hLDL reduce autophagosome signals in macrophages. (A) Fluorescence micrographs of macrophages that have been incubated with the indicated reagents for 24 hours subsequently stained with CYTO-ID to visualize autophagosomes. **(B)** Plot of the intensity of the hHDL (NIR) signal of the cells depicted in (A) measured by flow cytometry. **(C)** Plot of the intensity of the autophagosome signal of the cells depicted in (A) measured by flow cytometry. **(D)** Fluorescence micrographs of macrophages that have been incubated with the indicated reagents for 24 hours. **(E)** Plot of the intensity of the hHDL (NIR) signal of the cells depicted in (D) measured by flow cytometry. **(F)** Plot of the intensity of the autophagosome signal of the cells depicted in (D) measured by flow cytometry. N = 5000 x 3 (triplicate) for flow cytometry data. p-values were calculated using Microsoft Excel's t.test() function. Scale bars are 10 microns.

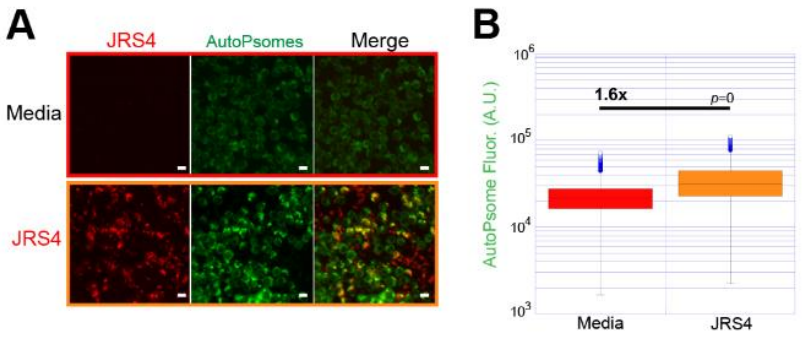

Figure 2.4. JRS4 increases autophagosome signals in macrophages. (A) Fluorescence micrographs of macrophages that have been incubated with the JRS4 for 3 hours subsequently stained with CYTO-ID to visualize autophagosomes. **(B)** Plots of the fluorescence intensity of the macrophages shown in (A) measured by flow cytometry. *N* = 5000 x 3 (triplicate) for flow cytometry data. *p*-values were calculated using Microsoft Excel's t.test() function. Scale bars are 10 microns.

normal (DMEM + 10% FBS), 2) starve (DMEM), 3) RAPA (250 nM rapamycin + DMEM + 10% FBS), and 4) LPS (250 ng/ml LPS + DMEM + 10% FBS). We washed the cells in PBS and identified NPs by NIR dye. We identified autophagosomes with CYTO-ID using fluorescence microscopy and flow cytometry as in the experiments involving hHDL, hLDL, and JRS4 cells. Macrophage NIR signal (a measure of NIR uptake) followed an increasing trend from CNP < SNP < LNP (Fig. 2.5A-H). CNPs have the highest entropic energy because they are polymers; therefore, entropy is maximized when they are diffusing in the media above the macrophages. SNPs should not have a large entropic component in the bulk; therefore, the energetic cost of binding macrophages should be minimal. It has recently been shown that both CNPs and SNPs interact with SR-BI and LIMP-2 [[161]]. The LNP entry mechanism is postulated to be heavily influenced by its protein corona, which has components of lipoproteins [[157,158]]. However, note that LNP signal in macrophages is highest in starvation conditions where the protein corona should come only from proteins excreted by the macrophages. Therefore, it is puzzling why macrophages should take up LNPs in such high quantities in starvation (DMEM only) conditions.

In DMEM + 10% FBS conditions, PEG had little effect on autophagosome signal; CNPs, SNPs, and LNPs all reduced autophagosome signal by ~25% (Fig. 2.5A,I). In starved conditions, PEG, CNPs, SNPs, and LNPs reduced autophagosome signals by 30%, 30%, 50%, and 40% (Fig. 2.5B,J). PEG increased the macrophage autophagosome signal by 30% when co-incubated with rapamycin; CNPs, SNPs, and LNP reduced the autophagosome signal by 20%, 52%, and 50% (Fig. 2.5C,K). For LPS co-incubation, the changes were PEG (0%), CNPs (45%), SNPs (46%), and LNP (40%) (Fig. 2.5D,L). P-value less than 0.05 (equal to zero in most cases) means the data of those experiments is statistically significant. These results show that CNP, SNP, and LNP but not PEG itself, lower autophagosome levels as measured by CYTO-ID.

To further determine if our PEG and PEG NP reagents affected the autophagic process, we compared the number of macrophages before and 24 hours after PEG, CNP, SNP, and LNP addition with chloroquine (CQ) as a control for blocking autophagosome-lysosome fusion and halting cell division [[182]]. None of our reagents hampered macrophage division, whereas chloroquine stopped cell growth (Fig. 2.6A,B). This shows, in part, that PEG and PEG NPs do not block autophagosome-to-lysosome fusion. It also shows that PEG and PEG NPs do not interfere with cell division or cause proliferation-hampering toxicity in macrophages *in vitro*. This agrees

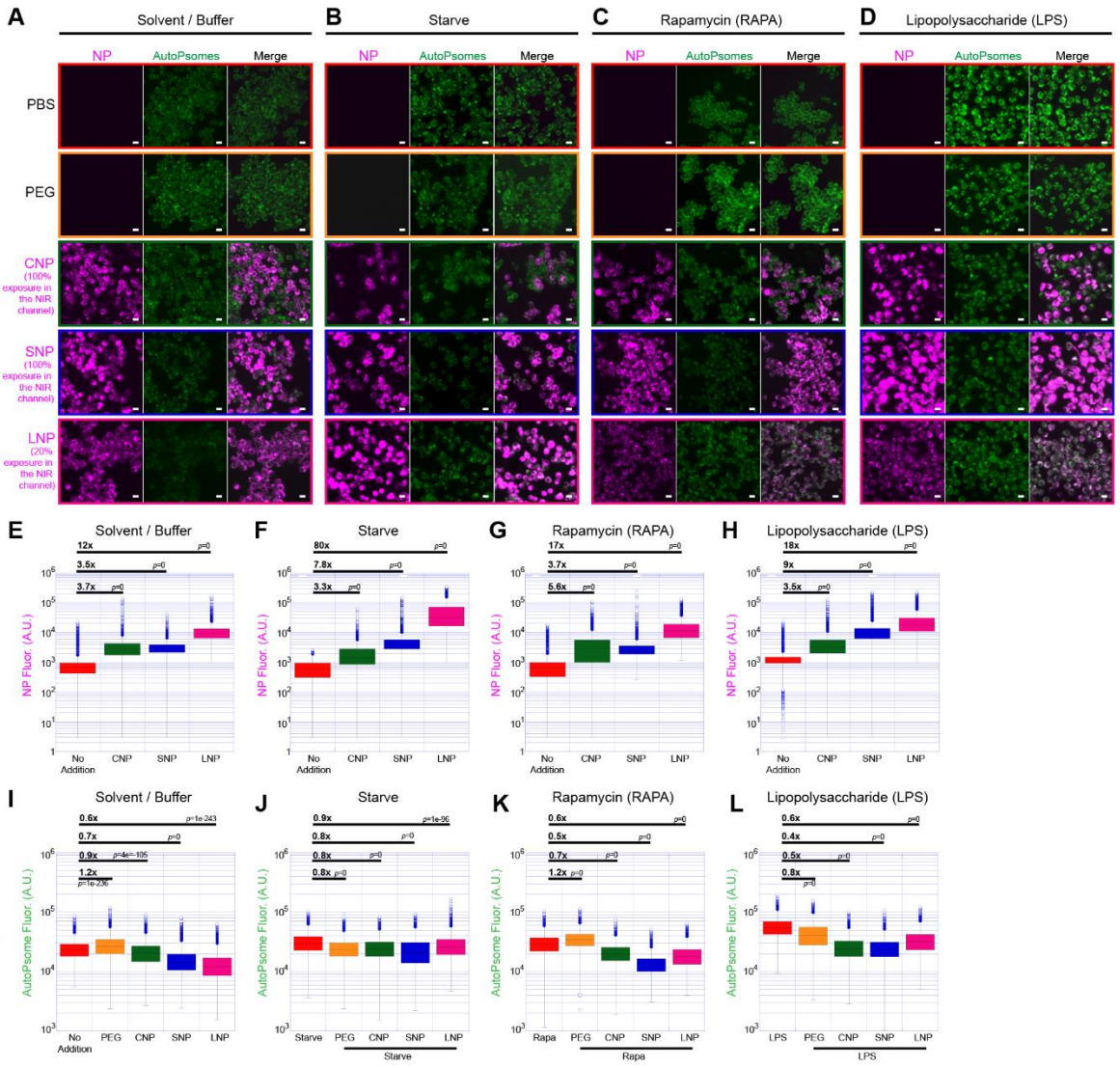

Figure 2.5. CNPs, SNPs, and LNP lower autophagosome signal, whereas PEG itself has little effect. (A-D) Fluorescence micrographs of macrophages that have been incubated with the indicated reagents for 24 hours and subsequently stained with CYTO-ID to visualized autophagosomes. Scale bars are 10 microns**. (E-H)** Plots of the intensity of the NIR signal of the macrophages depicted in (A-D) measured by flow cytometry. **(I-L)** Plots of the intensity of the autophagosome signal of the cells depicted in (A-D) measured by flow cytometry. N = 5000 x 3 (triplicate) for flow cytometry data in (E-L). *p*-values were calculated using Microsoft Excel's t.test() function.

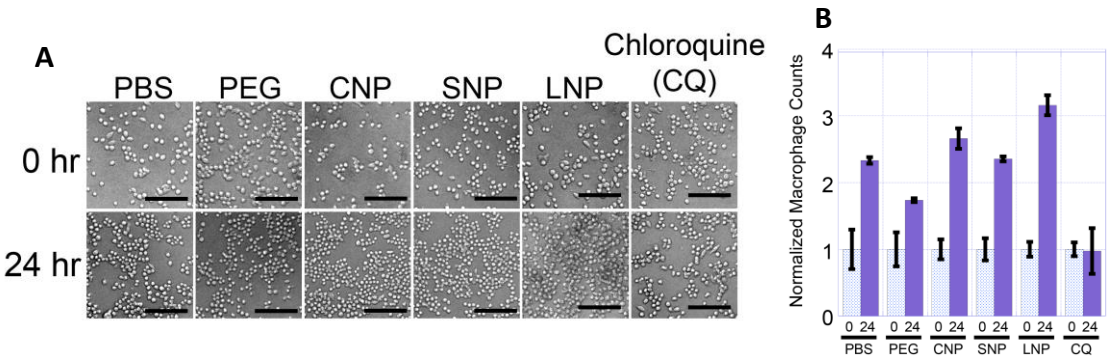

Figure 2.6. PEG, CNPs, SNPs, and LNP did not hamper macrophage division. (A) Phase contrast micrographs of macrophages before and after being incubated with the indicated reagents for 24 hours. **(B)** Plot of the normalized number of macrophages depicted in (A). The number of macrophages in four separate quadrants of 0.86 mm^2 were averaged to obtain the numbers in (B). Scale bars in (A) are 50 microns.

hHDL, hLDL, PEG, CNPs, SNPs, and LNP lower ROS levels but do not consistently resolve ROS levels that are increased by starvation, rapamycin, and LPS

ROS production is used by phagocytes to directly damage pathogens [185] and also to induce autophagy to engulf the pathogen in an autophagosome [186]. ROS generation is also triggered by the uptake of many hard NPs such as nanotubes [173]. Less is known about the effects of soft NPs on ROS generation. To determine the effects of our lipoproteins and NPs on ROS production, we incubated hHDL, hLDL, PEG, CNPs, SNPs, and LNP with our macrophages for 24 hours and subsequently stained the cells with a proprietary ROS dye. Each of these additions caused a decrease in ROS dye signal with SNPs having the strongest effect (Fig. 2.7A,B). We repeated these experiments and either starved, added rapamycin, or added LPS to the macrophages at the beginning of these 24-hour co-incubations. Only hLDL and SNPs lowered the ROS signal in starved macrophages. None of the other lipoproteins or NPs had a reducing effect on ROS signal in the starvation, rapamycin, or LPS experiments. Rapamycin is unique among autophagy-triggering reagents (mTOR inhibition) because it has ROS-lowering effects [187]. Activation of Nox2 leads to the production of ROS. This can occur through LC3-associated phagocytosis (LAP) [188]. In LAP, Rubicon stabilizes NOX2 to produce ROS.

JRS4 cells increased the macrophage ROS signal by 60% after a 3-hour incubation **(**Fig. 2.8A,B**)**. Nox2 levels increased slightly as measured by western blot (Fig. 2.8C,D). We analyzed known ROS regulator mRNA transcripts in our macrophages [189]. Of the major genes associated with ROS, the cold shock domain containing E1 protein, Csde1, increased to varying degrees across all five reagent additions (not shown). Csde1 knockdowns increase ROS levels [190]. Thus, higher Csde1 values should inhibit ROS. LPS treatment increased Nos2 and Prdx5 levels. Nos2 interacts with p62/Sqstm1 in macrophages and is degraded in lysosomes [191]. This is a mechanism by which autophagy controls nitrous oxide production during inflammation. JRS4 cells increased Stat6 and hLDL increased Xdh levels. LNPs had no effect on these transcript levels. The STRING database shows no connectivity of *Csde1*, *Nos2*, or *Xdh*. However, *Prdx2* interacts strongly with *Cybb*, *Cyba*, *Ncf1*, *Noxo1*, and *Rac2*.

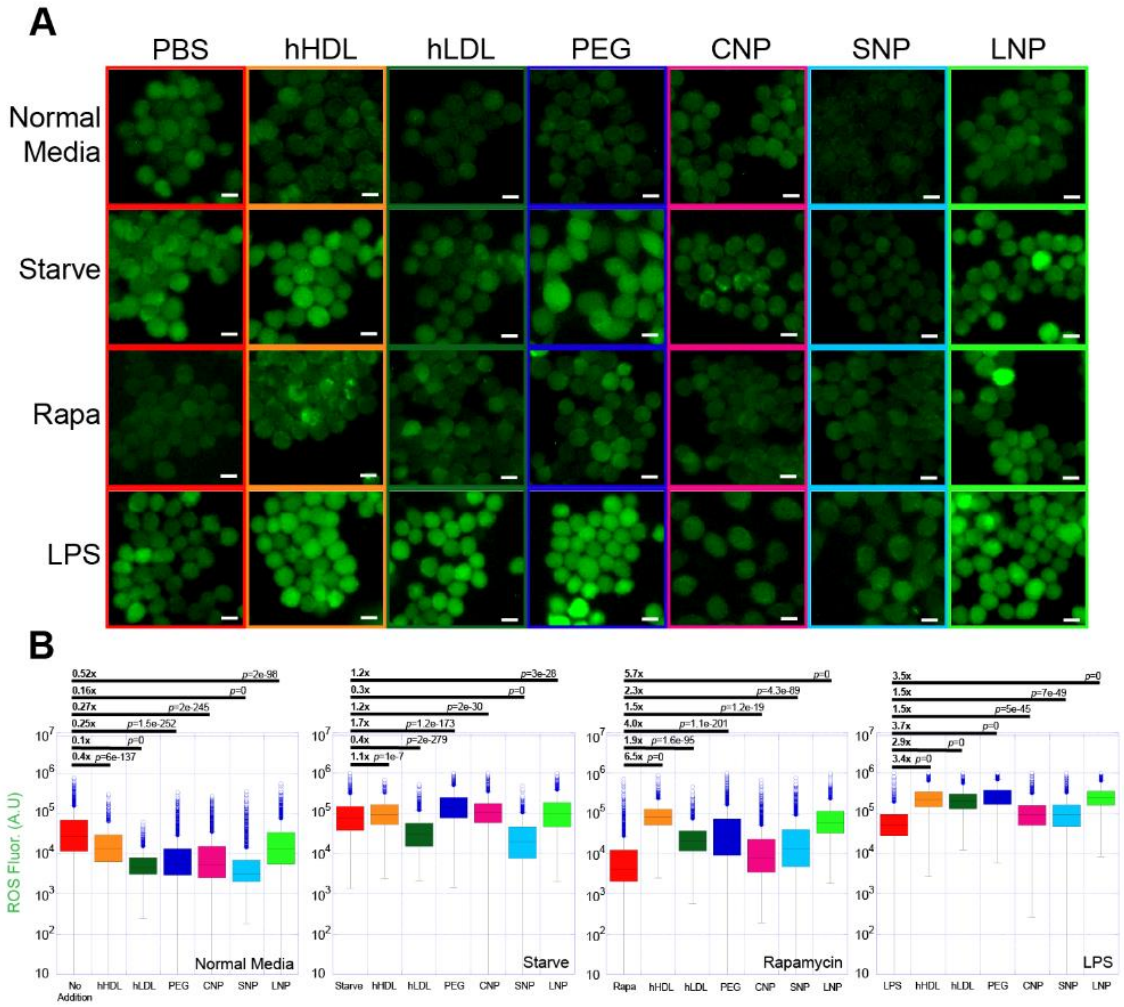

Figure 2.7. hHDL, hLDL, PEG, CNP, SNP, and LNP reduce ROS levels but cannot restore basal ROS levels after rapamycin or LPS challenge. (A) Fluorescence micrographs of macrophages that were incubated with the indicated reagents (without NIR dye) for 24 hours and then stained with a ROS dye. Scale bars are 10 microns. **(B)** Plots of the fluorescence intensity of the macrophages shown in (A) measured by flow cytometry.

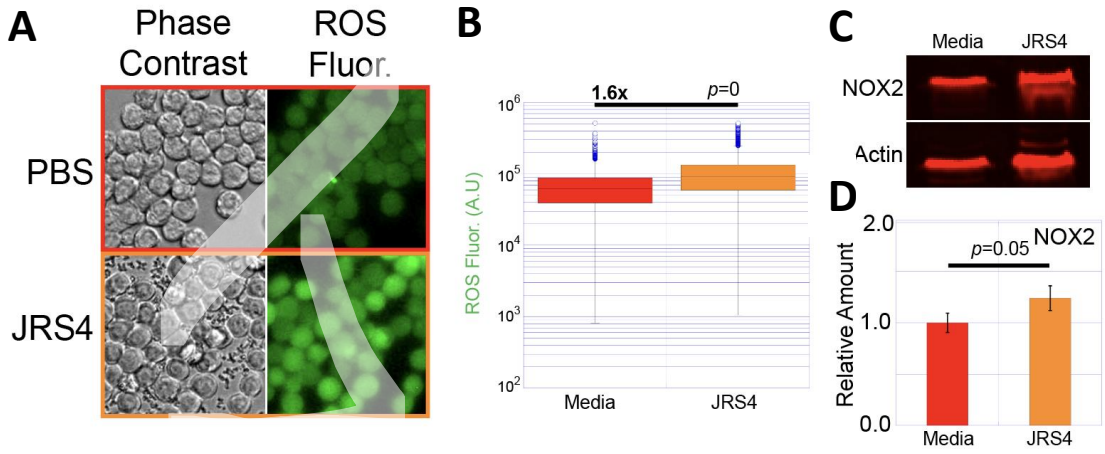

Figure 2.8. JRS4 increses basal ROS levels. (A) Phase contrast and fluorescence microscopy images of macrophages incubated first with JRS4 pathogens for 3 hours then ROS dye. Scale bars are 10 microns. **(B)** Plots of the fluorescence intensity of the macrophages shown in (B) measured by flow cytometry. **(C)** Western blots of NOX2 after JRS4 addition (3 hours) to macrophages. **(D)** Plot of the intensities of the bands in (C). *p*-values were calculated using Microsoft Excel's t.test() function. Western blots were run in triplicate.

hHDL, CNPs, SNPs, do not increase lysosomal pH in contrast to hLDL, LNPs, starvation, rapamycin, and LPS

It is unclear if soft PEG-based micelles like CNPs and SNPs or soft PEGylated liposomes like LNPs enter cells via the endosome-lysosome pathway although it is widely assumed that this is the entry mechanism. Phagocytosis is a subset of this endo-lysosome pathway. The working postulate is that most NPs are phagocytosed and then degraded in the lysosome. This excludes NPs that are designed to escape endosome such as ionizable liposomes [192]. We cultured our macrophages in DMEM + 10% FBS, DMEM, DMEM + 10% FBS + rapamycin, and DMEM + 10% FBS + LPS. We co-incubated the same macrophages with PBS, PEG, CNPS, SNPs, and LNPs with macrophages for 24 hours, washed the cells with PBS and stained with Lysotracker. Lysotracker signal stayed constant across all conditions, with the exception of an increase for PEG incubation in the LPS condition (Fig. 2.9A-H). This shows that these reagents have minimal effect on lysosome biogenesis – at the end of 24-hour incubations. To determine if our NPs increased lysosomal pH, we incubated macrophages with pHrodo dye, which fluoresces when the cellular pH is below ~6.5. Since phagosomes and lysosomes have low pH values, pHrodo is essentially a marker of phagocytosis and lysosome activity [193]. We performed 24-hour incubations of PEG, CNPs, SNPs, LNPs with macrophages. Positive controls for lysosome activation were hLDL (via LDLR-mediated endocytosis and Niemann-Pick-mediated processing of LDL contents), starvation (lysosome activation through autophagy), and rapamycin (lysosome activation through autophagy). The NP negative control for lysosome activation was hHDL, since hHDL does not seem to enter macrophages via endocytosis although this is somewhat controversial. hLDL and rapamycin increased pHRodo signal, whereas hHDL and SNPs lowered pHRodo signal (Fig. 2.10A,B). PEG, CNPs, and starvation conditions had little effect on pHRodo signal compared to PBS. We mined our mRNA data for transcripts involved in cellular uptake, phagocytosis, and lysosome function. In agreement with our fluorescence microscopy and flow cytometry data, only JRS4 cells and LPS had impact on factors involved in these pathways (not shown). Interestingly, hHDL increased *Apoe* and *Trl7* transcripts; hLDL increased *Apoe*, *Rab12*, and *Tfeb* transcripts; and LNPs increased *Sirpα* and *Tlr3* transcripts (not shown). *Tlr7-/-* mice are protected from *Apoe*$^{-/-}$ atherosclerosis, but HDL levels stayed the same in these mice [194]. Thus, it is unclear if HDLs

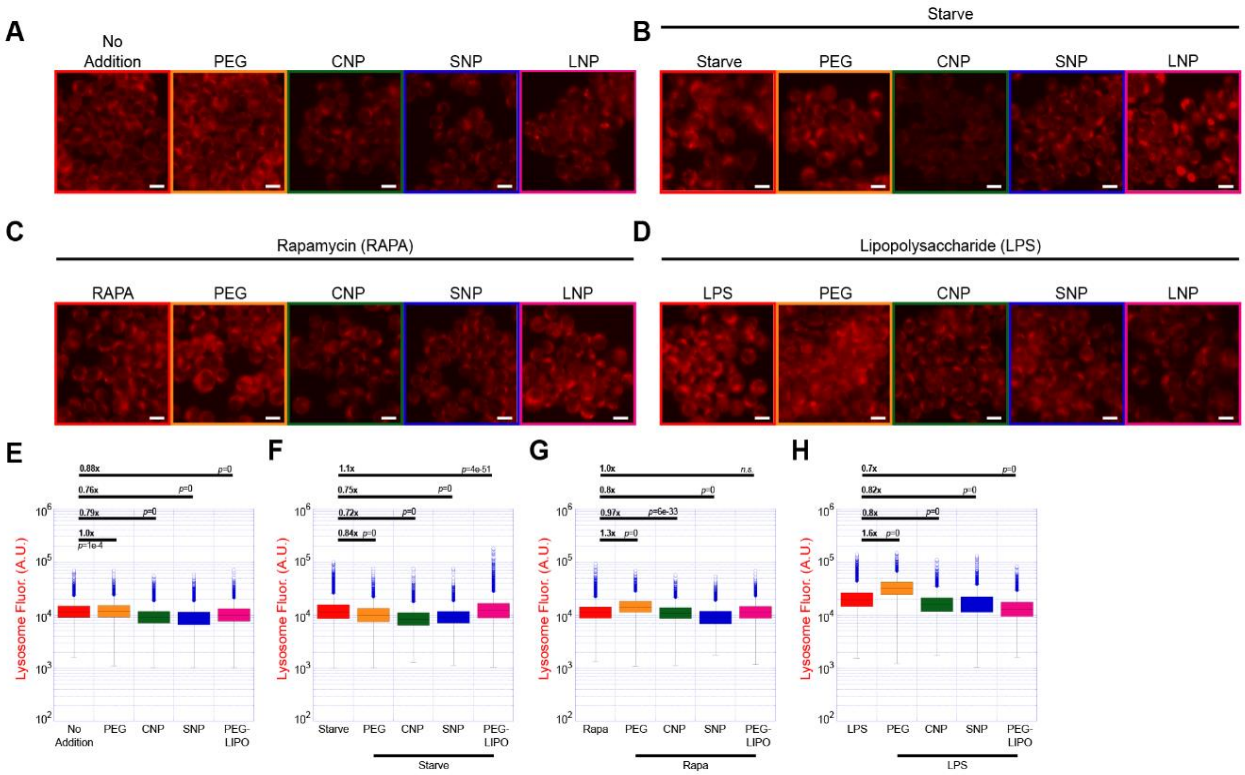

Figure 2.9. CNPs, SNPs, and LNPs have a minimal effect on lysosome signal. (A-D) Fluorescence micrographs of macrophages that were incubated with the indicated reagents for 24 hours, then stained with Lysotracker. **(E-H)** Plots of Lysotracker intensity of the macrophages in (A-D) as measured by flow cytometry. Scale bars are 10 microns. *N* = 5000 x 3 (triplicate) for flow cytometry data.

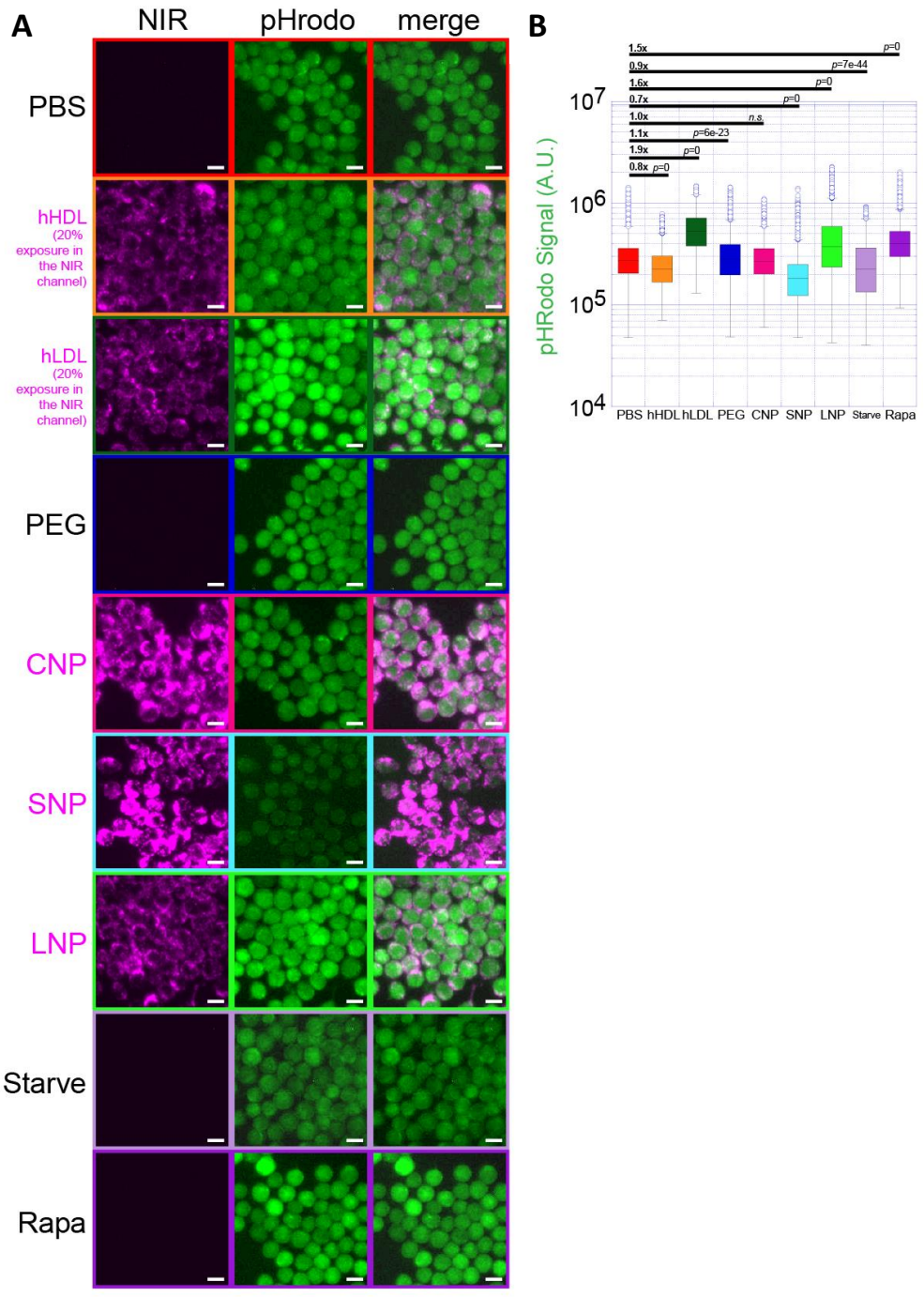

Figure 2.10. CNPs, SNPs, and LNPs have a minimal effect on cellular pH. (A) Fluorescence micrographs of macrophages that were incubated with the indicated reagents for 24 hours, then stained with pHrodo dye. **(B)** Plot of the pHrodo intensity of the macrophages in (A) as measured by flow cytometry. Scale bars are 10 microns. *N* = 5000 x 3 (triplicate)

protective role by inhibiting the protein degradation that is triggered by hard TiO_2 NPs [196]. These results suggest that hLDL and LNPs are potentially processed by lysosomes, and that hHDL, PEG, SNPs, and CNPs are not.

CNPs, SNPs, and LNPs reduce the secretion of cytokines by macrophages

We collected the media from each well of macrophages after 24-hour incubations of CNPs, SNPs, LNPs, LPS, and PBS and determined the levels of 32 cytokines by ELISA (Eve Technologies). Cytokine levels were normalized by the number of cells in each culture well. Cytokine levels in the CNP, SNP, LNP, and LPS experiments were normalized by the levels in the PBS control. Surprisingly, CNPs, SNPs, and LNPs either reduced or did not increase the abundance of most cytokines in the media after 24 hours (Fig. 2.11A-AF). Of the three NPs, LNPs had the largest cytokine reduction effects, including GM-CSF, IL-3, IL-6, IL-12p70, LIF, MCP-1, and VEGF. LPS greatly increased the secretion of G-CSF, GM-CSF, IL-6, LIF, MCP-1, MIP-2, and RANTES/CCL5. These results show that PEG NPs are capable of lowering macrophage cytokine secretion and do not trigger a cytokine secretion reaction that is similar to that triggered by LPS. JRS4 cells and LPS caused wide-spread increases in pro-inflammatory factor transcripts (not shown). On the other hand, hHDL, hLDL, and LNPs triggered either no change or reduced change in $\log_2$(FC) values. The notable exception was the increase in Il1rl1 by hLDL. This member of the Tlr family does not induce an inflammatory response through activation of Nfκb, but does activate MAP kinases. The reduction of inflammation by hHDL is to be expected [197,198]. Mechanistically, *SCARBI*$^{-/-}$ (the gene that codes for SR-BI) mice are hypersensitive to LPS [199]. LPS-induced cytokine expression in these animals was dependent on Nfκb, JNK, and p38. PEG and PEG-NPs bind SR-BI [160,161]. Therefore, a potential mechanism for inflammation inhibition by CNPs, SNPs, and LNPs is their PEG-driven interaction with SR-BI.

We used flow cytometry to determine the quantity of hHDL, hLDL, CNPs, SNPs, and LNPs in the supernatant during the incubation with the macrophages. Our goal was to have enough of these reagents in the cell culture media over the duration of the 24 hours so that the cells could continually take them up. In each incubation, there was signal for the lipoprotein and NPs at the 24-hour time point (Fig. 2.2B-F). The profiles of the lipoproteins and NPs in the supernatant (not

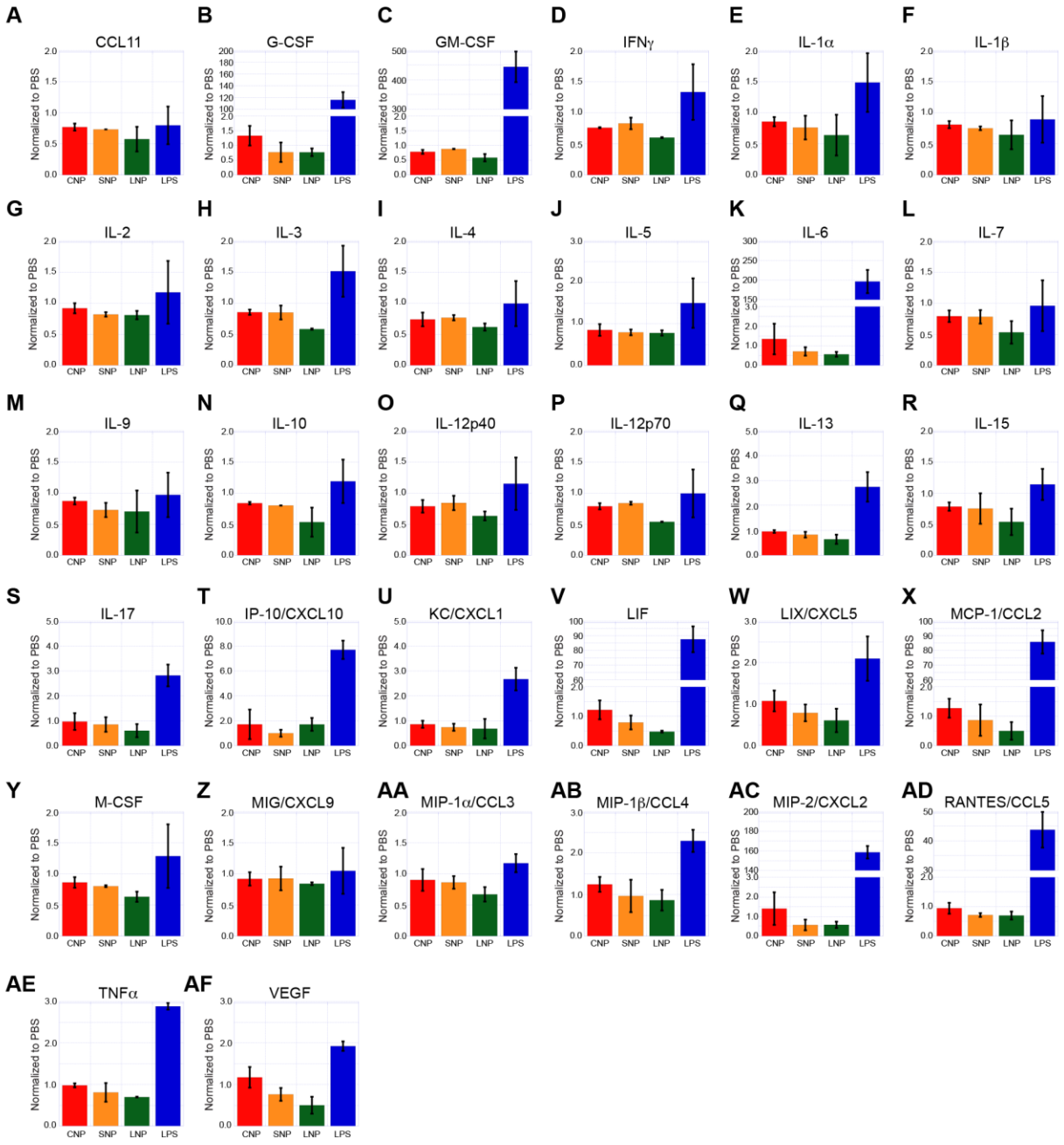

Figure 2.11. CNPs, SNPs, and LNP either lower or do not increase cytokines secreted by macrophages. (A-AF) Plots of cytokine levels in the media of macrophages that were incubated with either CNPs, SNPs, LNP, LPS, or PBS (control) for 24 hours. Cytokine levels were normalized by cell count. Then, normalized cytokine levels for CNPs, SNPs, LNPs, and LPS were divided by cytokine levels for PBS. Each column represents three separate experiments

cytometry events had a signal greater than plain media (Fig. 2.2B,C). Short CNPs were taken up first by macrophages (Fig. 2.2D). This is expected because of the high entropy of long CNPs. SNPs were the smallest NPs used in this study, thus it was challenging to differentiate them from the background. LNP signatures most resembled those of hHDL and hLDL as expected (Fig. 2.2F). These results agree with the differences in macrophage signal after 24 hours (Fig. 2.2G).

Discussion

Overview

NPs have been used primarily to kill cancer cells by delivering cytotoxic agents [200]. Currently NPs can successfully deliver nucleic acids to target cells (for example, [192]). Therefore, the goal is to keep the cells alive. Thus, it is now necessary to determine how the recipient cell is affected by the NPs. For decades, the word "cleared" and its synonyms have been used to describe the uptake of NPs - regardless of chemistry - by macrophages. Here we show that this phrasing is likely misleading because PEG-NP micelles (CNPs, SNPs) and PEGylated liposomes (LNPs) triggered macrophage responses that were very different from those triggered by phagocytosis-inducing pathogens - in this case, JRS4 cells. If NPs are "cleared" by macrophages as foreign bodies, one would also expect an increase in pro-inflammatory signaling. Again, PEG- and lipid-based NPs triggered a completely different response from LPS.

Flow cytometry and fluorescence microscopy

Under both control and autophagy-stimulated conditions, macrophages were treated with hHDL, hLDL, CNPs, SNPs, LNPs, and JRS4. The results showed that hHDL, hLDL, CNPs, SNPs, and LNPs lowered autophagosome levels against PBS, starvation, rapamycin, and LPS. JRS4 cells increased autophagosome abundance. PEG had minimal effect on autophagosome abundance. hHDL, hLDL, PEG, CNPs, SNPs, and LNPs lowered ROS in DMEM + 10% FBS macrophage culture conditions. However, only hLDL and SNPs lowered ROS levels raised by starvation. None of the reagents restored normal ROS levels when rapamycin or LPS were added. As expected JRS4 cells raised ROS levels. We detected no increase in agonist ROS-related transcripts after LNP addition. CNPs and SNPs had no effect and a lowering effect, respectively, on lysosome pH levels – a marker of lysosome activity. However, hLDL and LNPs both raised lysosome pH. CNPs, SNPs, and LNPs all either maintained low levels of secreted cytokines or reduced their levels in

the media as measured by ELISA. Bearing in mind that conceptual models can never be proved, only disproved, we show that CNPs, SNPs, and LNPs most likely do not trigger classic phagocytic or autophagic pathways. Instead, they reduce autophagy and inflammation, and promote proliferation [183].

Methods

Cell Culture

RAW264.7 macrophages were purchased from ATCC (#TIB-71) and cultured according to the manufacturer's instructions. Macrophages were polarized to an M1 phenotype by adding IFNγ. We used either DMEM + 10% FBS or DMEM (starve) as media for the macrophages for all experiments.

Lipoprotein, JRS4 cells, and nanoparticles

Human high-density lipoprotein (hHDL) and human low-density lipoprotein (hLDL) were obtained from Lee Biosolutions (#361-25, #360-10). Samples were diluted to 10 mg/ml in PBS before administration to macrophages. JRS4 cells were a gift from Dr. Michael Caparon (Washington University, St. Louis). They were cultured in Todd Hewitt broth (Millipore; #T1438). PEO_{56}-PBD_{46} diblock copolymers (filomicelles/CNPs) were synthesized according to the methods of Ref. [201]. PEO_{132}-PBD_{69} diblock copolymers (spheres/SNPs) were a gift from Dr. Frank S. Bates (Minnesota). NPs were formed at 10 mg/ml copolymer using film rehydration with phosphate buffered saline (PBS) as the aqueous buffer as described previously [202]. Nanoparticles were stained with near-infrared (NIR) dye (Thermo; #D12731) and dialyzed overnight into 1 liter of PBS at 4°C [202]. LNPs were obtained from Formumax Scientific Inc. (#F30204BD22) is a PEGylated liposome. They are the structural shell of the anti-cancer NP DOXIL [203].

Fluorescence microscopy and flow cytometry

Macrophages were cultured in 96-well plates to confluence. hHDL, hLDL, PEG, CNPs, SNPs, and LNPs were added at ~200 μg/ml; thus, the weight of material was consistent throughout the experiments. Rapamycin was added to a final concentration of 250 nM. LPS (Sigma; #L2630) was added to a final concentration of 250 ng/ml. After the incubation time, the macrophages were washed with PBS. They were then stained with the appropriate dye for 10 minutes. Washed again with PBS and imaged on a fluorescence microscope. After imaging, the cells were trypsinized (100

µl) for 5 minutes at 37°C. After incubation, the cells were removed from the well by gentle pipetting. They were then added to an equal volume of ice-cold 0.5% BSA in PBS. Samples were run in biological triplicate on an Accuri C6. Cells were gated based on their position in the FSC-A vs. SSC-A plot and subsequently by their position in the FSC-H vs. FSC-A plot. For pathogen vs. CYTO-ID and NP vs. CYTO-ID plots, all cells with signals less than background for either signal were eliminated. 5,000 data points representing macrophages in the final gate were randomly chosen by a Mersenne-Twister random number generator. This random selection was repeated for the other two samples. We used FIJI/ImageJ for image analysis and FlowJo for flow cytometry gating.

Dyes

JRS4 cells were identified with the DNA marker TOTO™-3 iodide 642/660 (Thermo; #T3604). Autophagosome levels were determined using a propriety green fluorescence kit CYTO-ID (Enzo; #ENZ-KIT175). Lysosomes were identified using Lysotracker (Thermo; #L7528). Macrophage pH levels were measured by the fluorescence signal of pHrodo (Thermo; #P35380). ROS were identified by a propietary dye (Sigma; #MAK143)

Statistics

P-values were determined using the Excel t.test() function.

CHAPTER 3

LIPID NANOPARTICLES TRIGGER mRNA TRANSCRIPTION THAT IS MORE SIMILAR TO THAT TRIGGERED BY LIPOPROTEIN THAN PATHOGENS AND ENDOTOXINS.

Introduction

As we were mentioned in the previous chapter, we were examining how macrophages internalized soft PEG-based NPS, the impacts on the cells over a period of 24 hours, and how NPs ingestion changed mRNA transcript regulation. We wished to determine the macrophage mRNA transcript levels of factors involved in autophagy after hHDL, hLDL, JRS4 cell, LPS, and LNP addition to test our fluorescence microscopy and flow cytometry results. Again, we used IFNγ-polarized RAW264.7 murine macrophages (hereinafter, macrophages) as our cell model and incubated them with human high-density lipoprotein (hHDL), human low-density lipoprotein (hLDL), group A *streptococcus* pathogens (JRS4 cells), LPS, PEG (MW 6000), PEG-based cylindrical micelles (CNPs), PEG-based spherical micelles (SNPs), and PEGylated lipid nanoparticles (LNPs). To investigate if lipoproteins and soft PEG-NPs had similar macrophage responses, hHDL and hLDL were utilized as controls. The pathogen that induced phagocytosis, inflammation, and autophagy was tested using JRS4 cells as a positive control. LPS was also used as a positive control for autophagy and inflammation. Of these reagents, we performed RNA sequencing on macrophages that were incubated with hHDL, hLDL, JRS4 cells, LPS, LNPs, and PBS (control). we chose 24 hours as the analysis timepoint for all reagents, with the exception of JRS4 cells (3 hours [(Nakagawa et al., 2004)]).

The mRNA transcripts of macrophages differed significantly after incubation with hHDL, hLDL, LNP, and PBS on the one hand and JRS4 cells and LPS on the other. JRS4 cells and LPS triggered substantial changes in transcripts responsible for pathogen binding and entry, phagocytosis, autophagy, and inflammation versus PBS controls. LNPs triggered the fewest transcriptome changes from PBS controls of the five treatments. In chapter two, from fluorescence microscopy and flow cytometry experiments, hHDL, hLDL, CNPs, SNPs, and LNPs lowered autophagosome levels against PBS, starvation, rapamycin, and LPS. JRS4 cells increased autophagosome abundance. PEG had minimal effect on autophagosome abundance. hHDL, hLDL, PEG, CNPs, SNPs, and LNPs lowered ROS in DMEM + 10% FBS macrophage culture conditions. However, only hLDL and SNPs lowered ROS levels raised by starvation. None of the reagents restored normal ROS levels when rapamycin or LPS were added. As expected JRS4 cells raised ROS levels. We detected no increase in agonist ROS-related transcripts after LNP addition. CNPs and SNPs had no effect and a lowering effect, respectively, on lysosome pH levels – a marker of lysosome activity. However, hLDL and LNPs both raised lysosome pH. CNPs, SNPs, and LNPs all either maintained low levels of secreted cytokines or reduced their levels in the media as measured by ELISA. mRNA transcripts of pro-inflammatory factors agreed with the ELISA results. By mining the mRNA transcriptome databases (ImmGen [204]) macrophages incubated with LNPs have similar profiles to mouse primary cells from lung and spleen but also to mouse stromal cells. Bearing in mind that conceptual models can never be proved, only disproved, we show that CNPs, SNPs, and LNPs most likely do not trigger classic phagocytic or autophagic pathways. Instead, they reduce autophagy and inflammation, and promote proliferation [183].

Results

We wanted to know how the mRNA transcripts of murine macrophages changed in response to PEG-based cylindrical micelle NPs (CNPs), PEG-based spherical micelle NPs (SNPs), and PEGylated lipid vesicle NPs (LNPs) during the course of a 24-hour continuous contact *in vitro*. The NPs were used in these experimets has the same characteristics as NPs in chapter two. The CNPs and SNPs have a PEG exterior and a polybutadiene (PBD) interior. The LNPs are a 56:38:5 molar ratio of hydrogenated soy phosphatidylcholine (HSPC), cholesterol and N-(carbonyl-methoxypolyethylene glycol 2000)-1,2-distearoyl-sn-glycero-3-phosphoethanolamine sodium salt (MPEG-DSPE).

LNPs trigger minimal yet unique mRNA transcript changes compared to hHDL and hLDL, and especially compared to JRS4 cells and LPS

To quantify the macrophage response to our NPs versus their response to lipoproteins, pathogens, and endotoxin, we incubated macrophages in DMEM + 10% FBS with the addition of either PBS (24h), hHDL (24h), hLDL (24h), JRS4 cells (3h) [^{156}], LPS (24h), or LNPs (24h). At the indicated times, we washed the cells with PBS, and extracted the mRNA. We chose LNP as a model NP for mRNA sequencing because it is more widely used in the clinic than CNPs or SNPs, which are still in developmental stages. mRNA fold change (FC) values were based from the transcript quantities of the PBS sample. JRS4 pathogens (2800^{+},2400^{-}) and LPS (2100^{+},1700^{-}) triggered the largest FC values where "+" refers to increased transcript numbers and "-" refers to decreased transcript numbers (Fig. 3.1A). LNPs triggered about 10-fold fewer changes (188^{+},155^{-}). hHDL (528^{+},375^{-})

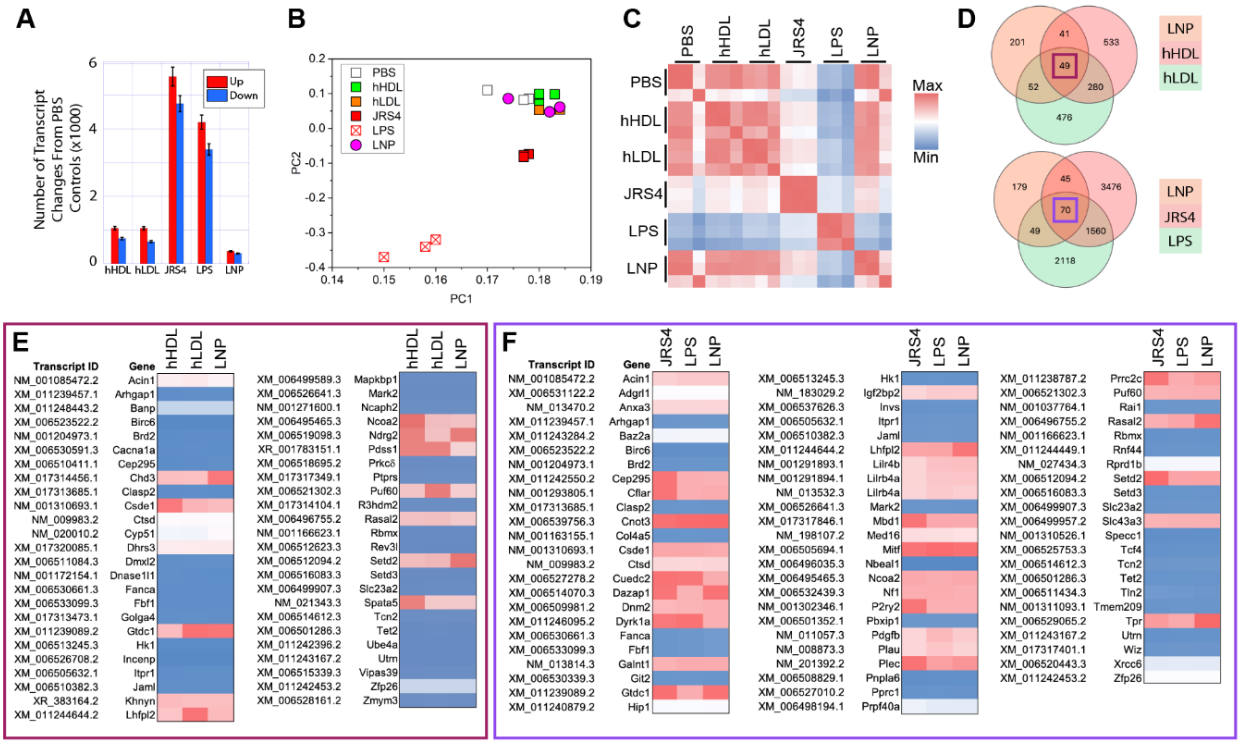

Figure 3.1. mRNA sequencing data show differences among macrophage transcripts that were incubated with PBS, hHDL, hLDL, JRS4 cells, LPS, and LNPs. (A) Plot of the number of macrophage transcripts that either increased (red) or decreased (blue) in a statistically valid manner (Q-value < 0.05) for each of the indicated treatments. Incubation times were 24h except for JRS4 (3h). **(B)** Principal component analysis of macrophage transcripts after being incubated with the indicated reagents. **(C)** Pearson coefficients of the macrophage transcripts after being incubated with the indicated reagents. **(D)** Venn diagrams comparing the similarities and differences of LNPs, hHDL, and hLDL (top) transcripts, and LNP, JRS4 cells, and LPS transcripts (bottom). **(E)** LNP, hHDL, and hLDL 49 shared transcripts. **(F)** LNP, JRS4, and LPS 70 shared transcripts. The matching macrophage transcripts after incubation with the other four reagents – hHDL, hLDL, JRS4 cells, LPS - are shown. The scale is from dark red (log_2(FC) = +25) to deep blue (log_2(FC) = -25).

and hLDL (527^{+},330^{-}) triggered almost identical statistically significant changes in transcript numbers.

Of the six conditions, principal component analysis (PCA) revealed that the transcripts of macrophages treated with LPS and JRS4 cells were significantly different from the other four treatments (Fig. 3.1B). This is a techniqe that reduces the dimentionality of the data sets which takes advantage of the fact that the images in these datasets share some characteristics. The PCA values for PBS, hHDL, hLDL, and LNPs formed a cluster away from the JRS4 and LPS clusters. Thus, the transcript changes triggered by PBS, hHDL, hLDL, and LNPs were relatively similar on the genome-wide mRNA scale. Pearson coefficients were highest among PBS, hHDL, hLDL, and LNPs (Fig. 3.1C). They were lower between PBS and JRS4 and lowest between PBS and LPS. Venn diagrams of hHDL, hLDL, JRS4, LPS, and LNPs mRNA signatures revealed that LNPs, hHDL, and hLDL shared 49 macrophage transcripts that differed from PBS, and LNPs, JRS4 cells, and LPS shared 70 macrophage transcripts that differed from PBS (Fig. 3.1D-F). Note the significant increase in the number of changed macrophage transcript levels after JRS4 and LPS addition in comparison to LNP, hHDL, and hLDL transcript changes. From these genome-wide data, we postulate that LNPs trigger transcript-level changes that are more in line with those triggered by lipoprotein than those triggered by pathogens and endotoxin.

We used bubble plots to visualize the changes in macrophage mRNA levels versus PBS controls in specific KEGG pathways.(Figure 3.2) hHDL triggered changes in steroid biosynthesis and sesquiterpenoid and triterpenoid synthesis; hLDL triggered changes in steroid biosynthesis cholesterol metabolism, NOD-like receptor signaling pathway, and unsaturated fatty acid biosynthesis; JRS4 cells triggered many changes in surface receptor pathways, the phagosome

Figure 3.2. KEGG enrichment pathways show differences among macrophage transcripts that were incubated with PBS, hHDL, hLDL, JRS4 cells, LPS, and LNPs. (A-E) Bubble plots of KEGG enrichment pathways of macrophage transcripts after being incubated with the indicated reagents.

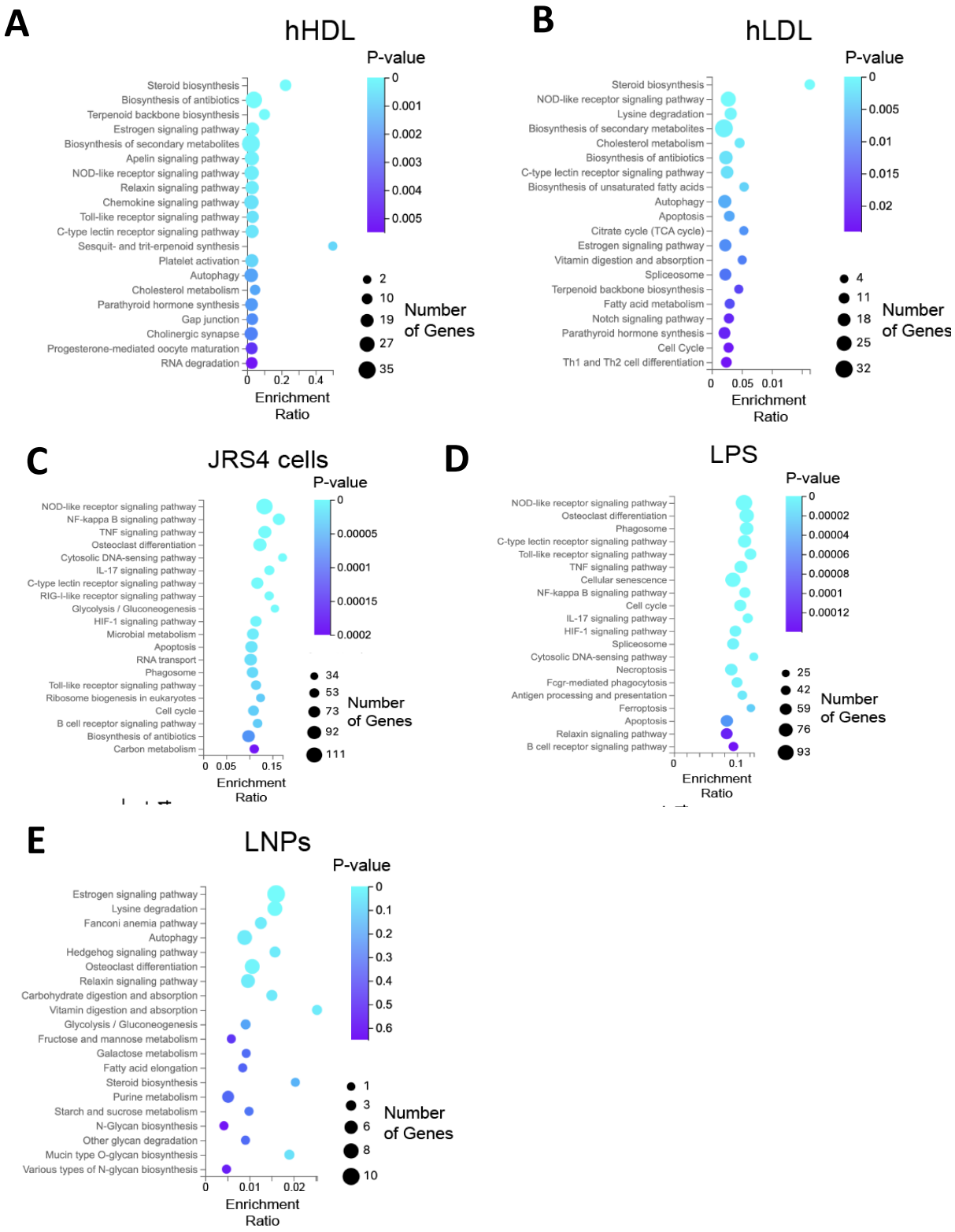
A
hHDL
P-value
Steroid biosynthesis
Biosynthesis of antibiotics
Terpenoid backbone biosynthesis
Estrogen signaling pathway
Biosynthesis of secondary metabolites
Apelin signaling pathway
NOD-like receptor signaling pathway
Relaxin signaling pathway
Chemokine signaling pathway
Toll-like receptor signaling pathway
C-type lectin receptor signaling pathway
Sesquit- and trit-erpenoid synthesis
Platelet activation
Autophagy
Cholesterol metabolism
Parathyroid hormone synthesis
Gap junction
Cholinergic synapse
Progesterone-mediated oocyte maturation
RNA degradation
0
0.2
0.4
Enrichment Ratio
0
0.001
0.002
0.003
0.004
0.005
2
10
19
27
35
Number of Genes
B
hLDL
P-value
Steroid biosynthesis
NOD-like receptor signaling pathway
Lysine degradation
Biosynthesis of secondary metabolites
Cholesterol metabolism
Biosynthesis of antibiotics
C-type lectin receptor signaling pathway
Biosynthesis of unsaturated fatty acids
Autophagy
Apoptosis
Citrate cycle (TCA cycle)
Estrogen signaling pathway
Vitamin digestion and absorption
Spliceosome
Terpenoid backbone biosynthesis
Fatty acid metabolism
Notch signaling pathway
Parathyroid hormone synthesis
Cell Cycle
Th1 and Th2 cell differentiation
0
0.05
0.01
Enrichment Ratio
0
0.005
0.01
0.015
0.02
4
11
18
25
32
Number of Genes
C
JRS4 cells
P-value
NOD-like receptor signaling pathway
NF-kappa B signaling pathway
TNF signaling pathway
Osteoclast differentiation
Cytosolic DNA-sensing pathway
IL-17 signaling pathway
C-type lectin receptor signaling pathway
RIG-I-like receptor signaling pathway
Glycolysis / Gluconeogenesis
HIF-1 signaling pathway
Microbial metabolism
Apoptosis
RNA transport
Phagosome
Toll-like receptor signaling pathway
Ribosome biogenesis in eukaryotes
Cell cycle
B cell receptor signaling pathway
Biosynthesis of antibiotics
Carbon metabolism
0
0.05
0.15
Enrichment Ratio
0
0.00005
0.0001
0.00015
0.0002
34
53
73
92
111
Number of Genes
D
LPS
P-value
NOD-like receptor signaling pathway
Osteoclast differentiation
Phagosome
C-type lectin receptor signaling pathway
Toll-like receptor signaling pathway
TNF signaling pathway
Cellular senescence
NF-kappa B signaling pathway
Cell cycle
IL-17 signaling pathway
HIF-1 signaling pathway
Spliceosome
Cytosolic DNA-sensing pathway
Necroptosis
Fcgr-mediated phagocytosis
Antigen processing and presentation
Ferroptosis
Apoptosis
Relaxin signaling pathway
B cell receptor signaling pathway
0
0.1
Enrichment Ratio
0
0.00002
0.00004
0.00006
0.00008
0.0001
0.00012
25
42
59
76
93
Number of Genes
E
LNPs
P-value
Estrogen signaling pathway
Lysine degradation
Fanconi anemia pathway
Autophagy
Hedgehog signaling pathway
Osteoclast differentiation
Relaxin signaling pathway
Carbohydrate digestion and absorption
Vitamin digestion and absorption
Glycolysis / Gluconeogenesis
Fructose and mannose metabolism
Galactose metabolism
Fatty acid elongation
Steroid biosynthesis
Purine metabolism
Starch and sucrose metabolism
N-Glycan biosynthesis
Other glycan degradation
Mucin type O-glycan biosynthesis
Various types of N-glycan biosynthesis
0
0.01
0.02
Enrichment Ratio
0
0.1
0.2
0.3
0.4
0.5
0.6
1
3
6
8
10
Number of Genes

pathway, microbial metabolism, glycolysis, and inflammation; LPS triggered changes in similar pathways as JRS4 cells, one interesting note being the significant impact on the DNA-sensing pathway even though LPS does not itself have DNA; LNPs triggered almost no significantly significant changes in these KEGG pathways since transcript levels changes had p-values > 0.05. Since autophagy is of special note, the transcript changes associated with autophagy (as identified by the somewhat narrow KEGG definition) were Atg9a (+20), Cflar (+21), Ctsd (*n.s.*), Itpr1 (-22), Pik3r2 (-25), Prkcδ (-22), and Supt20 (-21) with $\log_2$(FC) values in parentheses. Thus, we see that most of these autophagy-related transcripts decrease after LNP addition to macrophages. To understand LNP impact on macrophages we sorted all LNP transcripts by their $\log_2$(FC) values from PBS controls. Differences in the absolute value of the fold change (|FC|) that were less than 5.0 were not considered significant. Comparisons of $\log_2$(FC) values that had a Q-value > 0.05 were also not considered significant. We added the corresponding transcripts for the hHDL, hLDL, JRS4 cells, and LPS experiments to the plots (Fig. 3.3). Instead of discussing the transcripts that had the largest |FC| values here, we discuss these factors in the sections below specific to cellular processes important for NP uptake and processing.

We used tree maps to visualize the TPM values of the macrophage transcripts that were incubated in DMEM + 10% FBS and PBS versus those of the macrophages that were incubated in DMEM + 10% FBS and LNPs for 24 hours. The area of each rectangle corresponds to the TPM value for that transcript. The color of each rectangle corresponds to the $\log_2$(FC) value for that transcript where red indicates an increase and blue indicates a decrease. These TPM values provide insight into the quantity of each transcript. This information can be used in combination with the $\log_2$(FC)

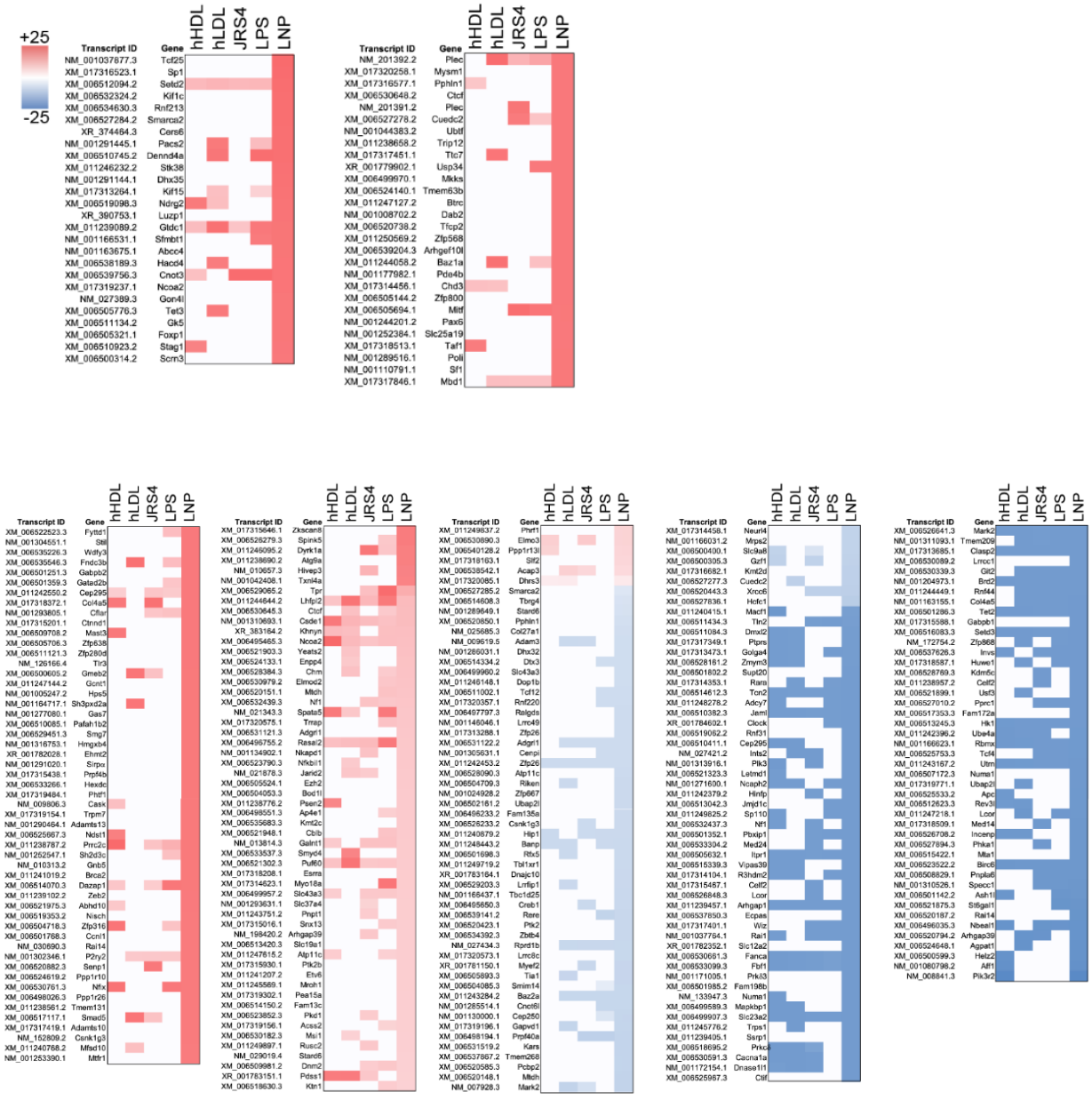

Figure 3.3. mRNA sequencing data show differences among macrophage transcripts that were incubated with PBS, hHDL, hLDL, JRS4 cells, LPS, and LNPs. Heat map of macrophage transcripts where |FC|>5 and Q-value < 0.05 after 24h for the LNP incubation. The matching macrophage transcripts after incubation with the other four reagents – hHDL, hLDL, JRS4 cells, LPS - are shown. The scale is from dark red (log_2(FC) = +25) to deep blue (log_2(FC) = -25).

data to understand the impact of transcript quantity and change. As a reference, the average β-actin TPM value across all samples was ~3000. Thus, we see that most of the TPM values of the genes whose transcripts were changed by LNPs are on a ~100-fold smaller size scale than highly expressed proteins. The amount of mRNA is an indicator, not a conclusive measure, of cell function. (The most important factor is the activity of the translated protein. Activity values are mostly unknown and challenging to quantify.) To further probe this feature of the transcriptomes, we plotted the TPM values of macrophage transcripts incubated in hHDL, hLDL, JRS4 cells, and LPS (Fig. 3.4D-G). Interestingly, transcripts responsible for cellular defense such as *Ccl3*, *Ccl4*, *Il6rα*, *Junb* [165], *Sqstm1*, *Tlr2*, *Tnf*, and *Trem2* had significant basal TPM levels (Fig. 3.4C). Spp1 is highly expressed in cancer cells; thus, its expression is probably due to RAW264.7 macrophages being an immortalized cell line. Large increases in transcript numbers come mostly from transcripts that have a ~0 TPM value in the PBS control. Exceptions in the change of large transcript sets are the striking increases in TPM values of pro-inflammatory genes in macrophages treated with JRS4 and LPS (Fig. 3.4F,G). Note that the TPM value of Ccl3 after LPS treatment is almost 10-fold higher than the β-actin TPM value (10500 vs. 3000). There are few blue squares because those transcripts have TPM values close to 0 after treatment.

Macrophage transcription networks after hHDL, hLDL, JRS4 cell, LPS, and LNP treatment show significant differences in hubs and connectivity

We determined the effects of hHDL, hLDL, JRS4, LPS, and LNP treatments on known signaling networks in the STRING database [205]. We entered all transcripts that had $\log_2(|FC|)$ values > 5 and Q-values < 0.05 into the STRING database. hHDL acted on proteins that are connected

Figure 3.4. Transcript per million (TPM) values of macrophages after incubation with PBS, hHDL, hLDL, JRS4 cells, LPS, and LNPs. (A-B) Tree maps of the TPM values of the macrophage genes shown in Fig. 3.3 for PBS and LNP. **(C-G)** Tree maps of the TPM values of the major macrophage genes for PBS, hHDL, hLDL, JRS4 cells, and LPS. The color code is the same as in Fig. 3.3 where red indicates an increase in $\log_2$(FC) and blue indicates a decrease in $\log_2$(FC).

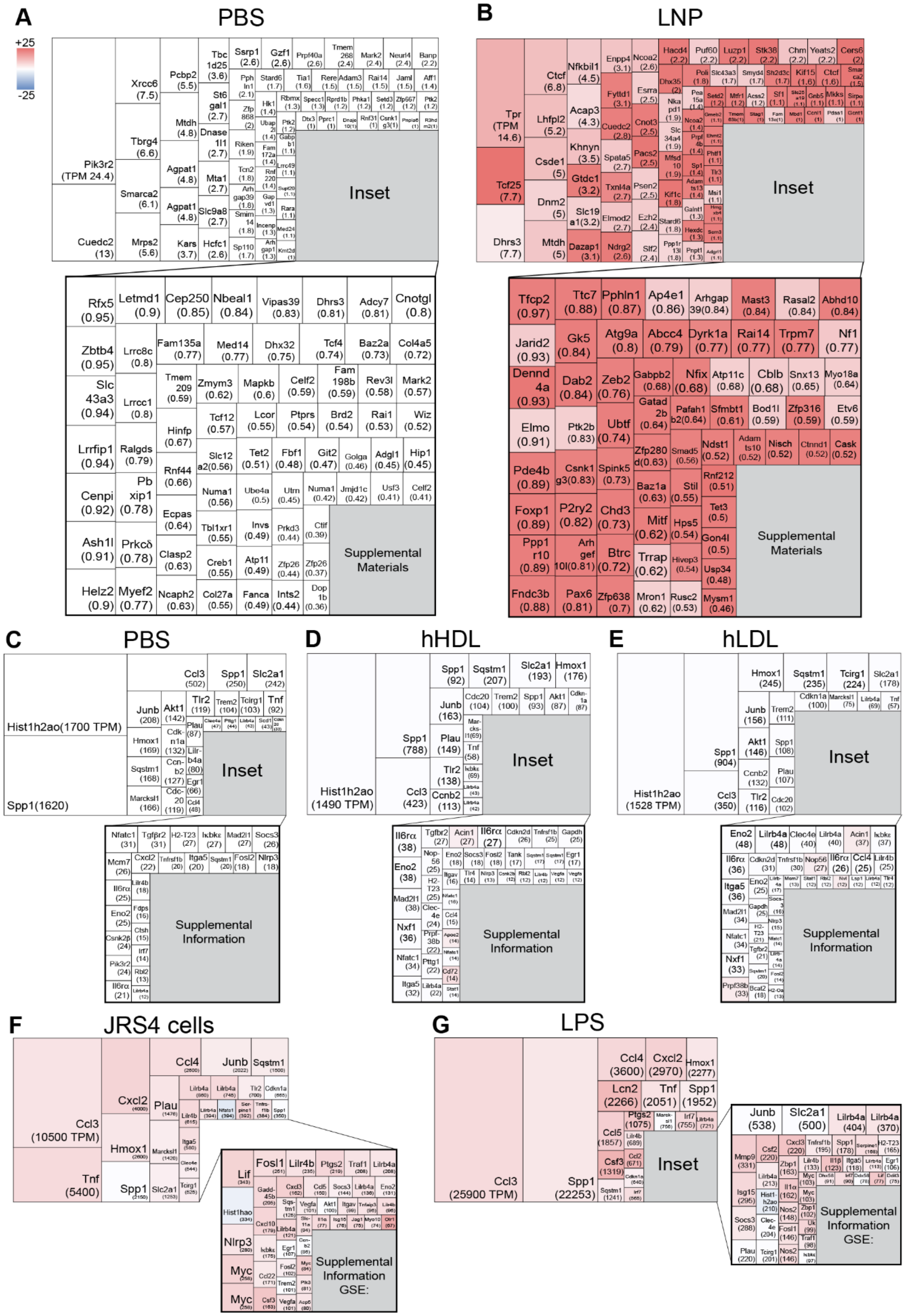
A
PBS
+25
-25
Pik3r2
(TPM 24.4)
Cuedc2
(13)
Xrcc6
(7.5)
Tbrg4
(6.6)
Smarca2
(6.1)
Mrps2
(5.6)
Inset
Supplemental
Materials
B
LNP
Tpr
(TPM
14.6)
Tcf25
(7.7)
Dhrs3
(7.7)
Ctcf
(6.8)
Inset
Supplemental
Materials
C
PBS
Hist1h2ao(1700 TPM)
Spp1(1620)
Inset
Supplemental
Information
D
hHDL
Hist1h2ao
(1490 TPM)
Spp1
(788)
Inset
Supplemental
Information
E
hLDL
Hist1h2ao
(1528 TPM)
Spp1
(904)
Inset
Supplemental
Information
F
JRS4 cells
Ccl3
(10500 TPM)
Tnf
(5400)
Cxcl2
Hmox1
Spp1
Supplemental
Information
GSE:
G
LPS
Ccl3
(25900 TPM)
Spp1
(22253)
Inset
Supplemental
Information
GSE:

through Akt3, Nras, Pik3r2, Pik3cd, Ptk2, and Rps6kb1/2 although a network-spanning pathway does not exist (Fig. 3.5A). The Akt family activates mTOR, thus inhibiting autophagy [206]. Indeed, HDL inhibits autophagy in experiments [197]. Nras is involved in cell proliferation. Pik3cd is a lipid kinase that plays widespread roles in cellular physiology including proliferation and migration. Ptk2 suppresses autophagy [207]. Rps6kb1 is activated by mTORC1 and inhibits IFNγ. In the hLDL STRING network, *Akt3* (+10.7), *Chm* (+9.6), *Crebbp* (+20.8), and *Ppp2r5c* (-7.8) were located at hubs (Fig. 3.5B). Akt3 elevation agrees with the finding that LDL inhibits autophagy [208]. Interestingly, Akt3 inhibits pinocytosis of LDL [209]. Chm interacts with Rab proteins, which have been shown to be important for LDL cholesterol recycling back to the plasma membrane [210]. Crebbp acts as a circadian transcriptional coactivator which enhances the activity of the circadian transcriptional activators Npas2-Arntl/Bmal1 and Clock-Arntl/Bmal1 heterodimers [211,212]. Ppp2r5c may play a role in DNA damage-induced inhibition of cell proliferation; it may also regulate the ERK signaling pathway through ERK dephosphorylation [213]. Thus, the reduction in its expression would encourage proliferation.

JRS4 cells and LPS trigger complex transcriptome network patterns. JRS4 uptake and processing triggered a macrophage network with significant clusters of immune regulation (Cd40, Ικbkβ, Il1α/β, Tnf, Crebbp), GTPase signaling transduction including the Jun-Dmp1 pathway and the Mapk cascade (Kras, Nras, Pik3cg, Prkcd, Rapgef1, Rgl1, Sos2), ribosome biogenesis (Aatf, Exosc10, Nat10, Nop56, Wdr75), chromatin organization and histone deacetylase binding (Baz2a, Chd4, Hist3h2a, Ncor2, Phf21a) factors (Fig. 3.5C). LPS triggered a macrophage network with significant clusters of nucleotide exchange and chemokine signaling (Arhgef12, Arhgef1, Abr, Arhgef39, Ect2, Fgd2, Arhgef11, Rhoc), cell cycle (Ccnb2, Cdc20, Espl1, Pttg1, Stag1, Stag2),

Figure 3.5. STRING database networks of macrophage transcripts after hHDL, hLDL and JRS4 cell addition. (A-C) Transcripts with |FC| > 5 vales from PBS controls and Q-values < 0.05 were entered into the STRING database. An interaction score of 0.9 was chosen. Transcripts were grouped into 10 k-means clusters.

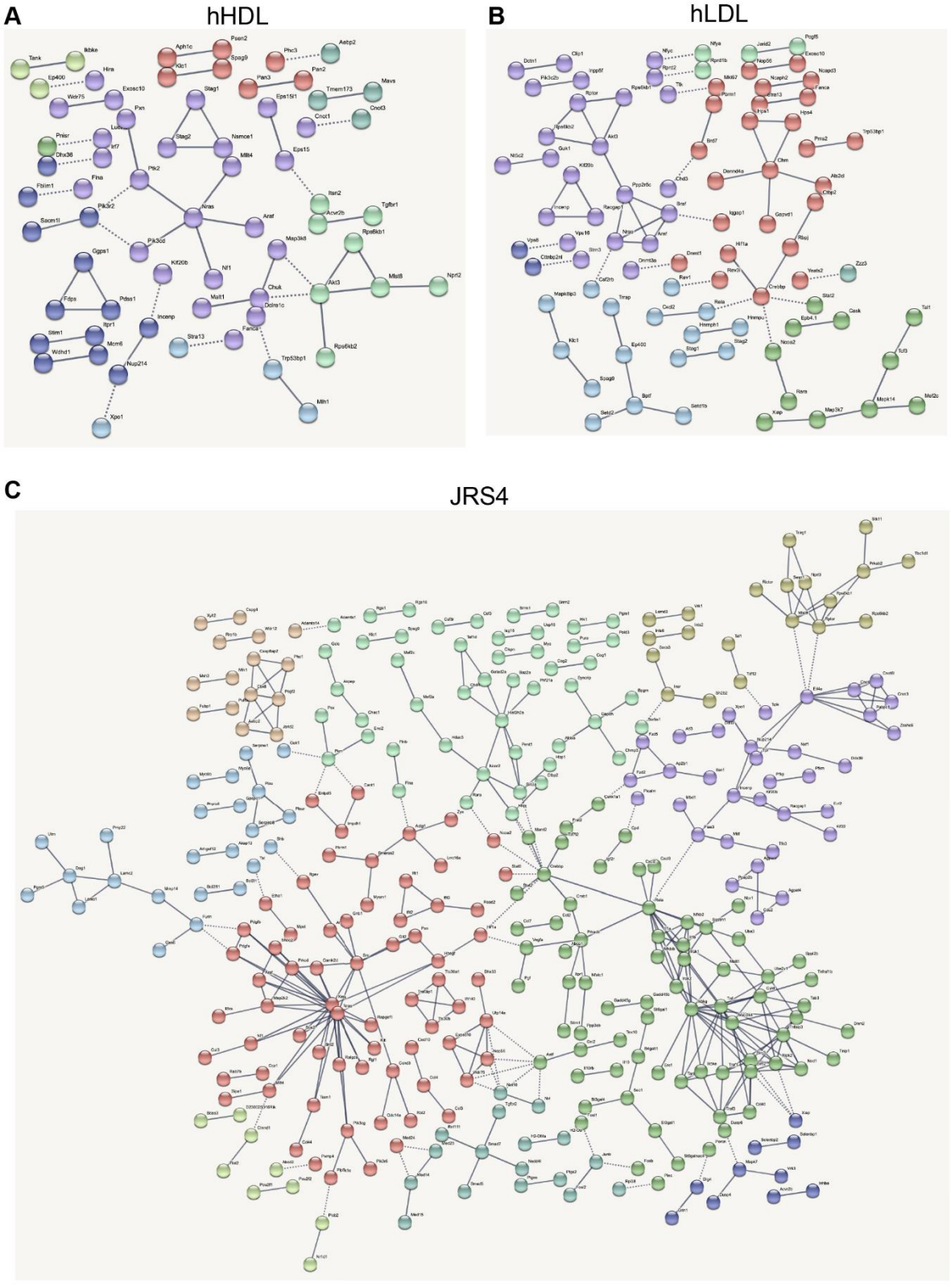
A
hHDL
B
hLDL
C
JRS4

and Akt-mTOR signaling and protein production (Akt1, Akt2, Mmp9, Rps6kb1, Rps6kb2, Src) factors (Fig. 3.6).

LNPs trigger a network with clusters of transcription regulation (Ehmt2, Gatad2b, Mta1, Smad5, Ubtf, Wiz, Zeb2), protein turnover and histone modification (Ash1l, Ezh2, Hcfc1, Huwe1, Jarid2, Kmt2c/d, Setd2, Supt20, Taf1, Trrap, Ubap2l), immunity (Adcy7, Cblb, Pde4b), and plasma membrane dynamics (Dnm2, Prkcζ) factors (Fig. 3.7). By increasing Cblb, LNPs should play an inhibitory role on BCR, TCR, and Fcγr1. Pik3r2 reduction would decrease the amount of the signaling lipid PIP3. This could have a number of effects on macrophage phenotype including modification of the signaling at the plasma membrane. These sequencing data show that macrophage response to LNPs is uniquely benign even through LNPs are 'foreign' objects and the amount of LNPs taken up by the macrophages is substantial over 24 hours (Fig. 2.2A).

hHDL, hLDL, CNPs, SNPs, and LNPs mRNA transcript changes related to autophagy

We wished to determine the macrophage mRNA transcript levels of factors involved in autophagy after hHDL, hLDL, JRS4 cell, LPS, and LNP addition to test our fluorescence microscopy and flow cytometry results. Instead of sorting the transcripts based on the KEGG classification of LNP data (Fig. 3.2A-E), we present mRNA transcripts that have been shown to be important for autophagic processes as mined from the literature. mRNA transcripts of the macrophages that were incubated with hHDL, hLDL, JRS4 cells, LPS, and LNPs revealed that traditional indicators of autophagy including Atg factors, Becn1 [214], Gabarap, LC3, Ulk1, Rubicon [215], Uvrag, Zfyve1, and many others, had $\log_2$(FC) values that were either not statistically significant or low (Fig. 3.8A).

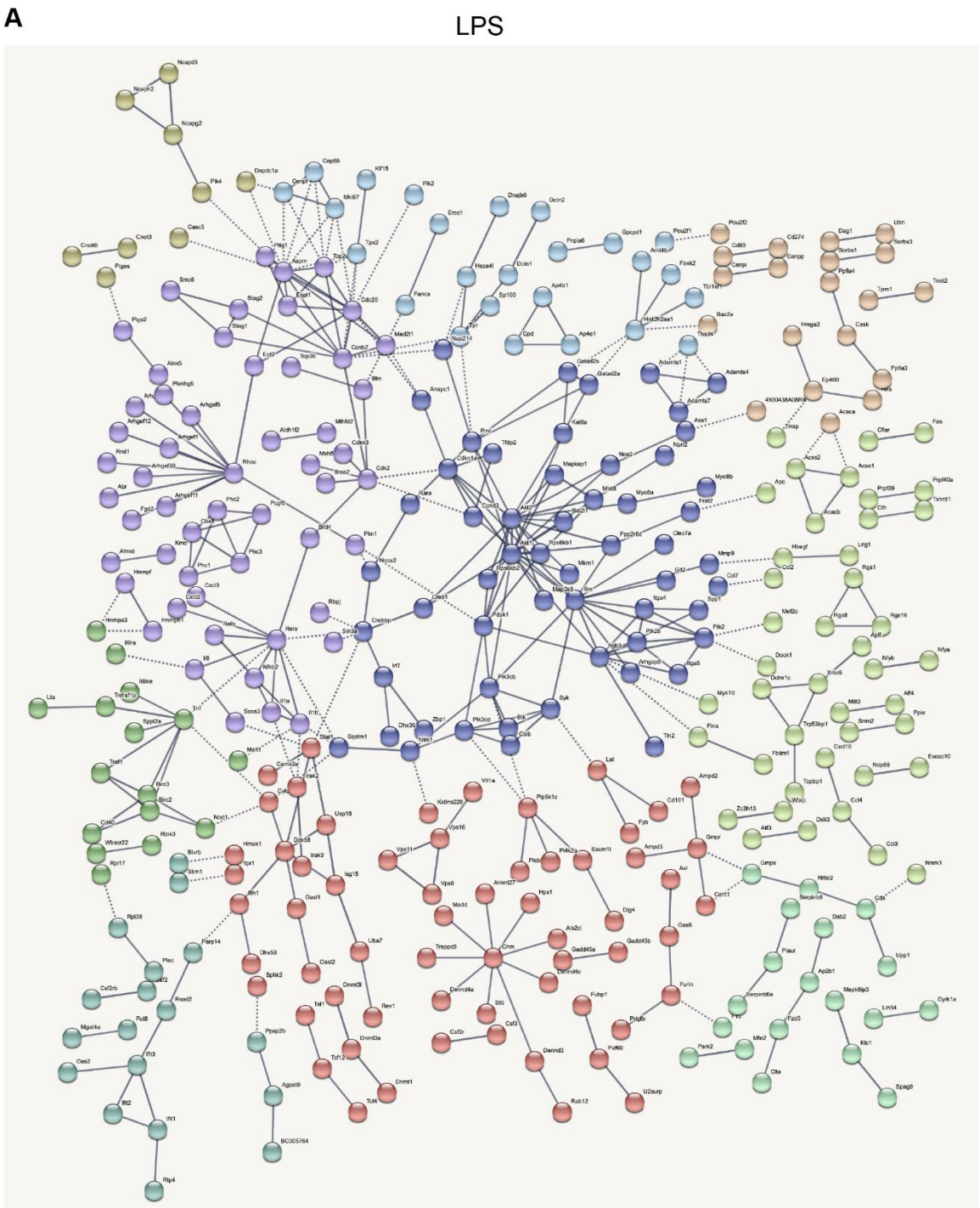

Figure 3.6. STRING database networks of macrophage transcripts after LPS addition. (A) Transcripts with |FC| > 5 vales from PBS controls and Q-values < 0.05 were entered into the STRING database. An interaction score of 0.9 was chosen. Transcripts were grouped into 10 k-means clusters.

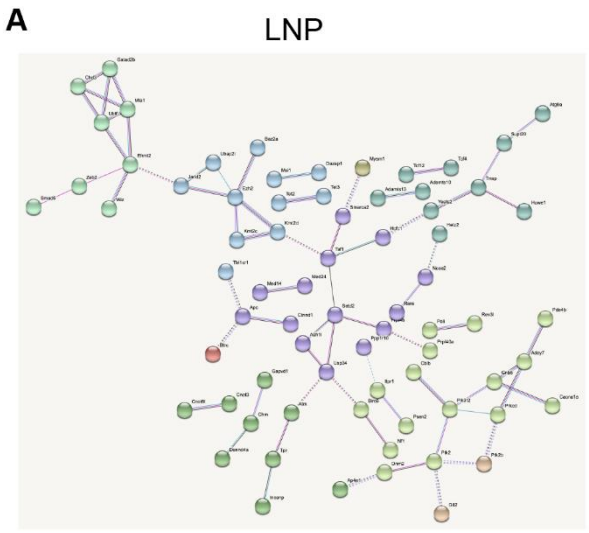

Figure 3.7. STRING database networks of macrophage transcripts after LNP addition. (A) Transcripts with |FC| > 5 vales from PBS controls and Q-values < 0.05 were entered into the STRING database. An interaction score of 0.9 was chosen. Transcripts were grouped into 10 k-means clusters.

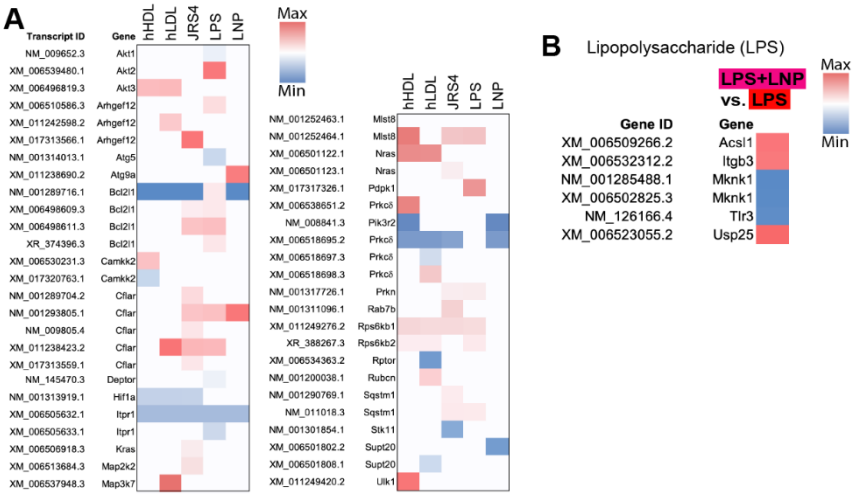

Figure 3.8. hHDL, hLDL, JRS4 cells, LPS, and LNPs autophagy proteins (A) Heat map of transcrips whose proteins are involved in autophagy from macrophages that were incubated in the indicated reagents. **(B))** Heat map of transcrips whose proteins are involved in autophagy from macrophages that were incubated in LPS+LNP versus macrophages that were incubated in LPS.

The exceptions were *Atg9a* for LNPs and *Ulk1* for hHDL. hHDL and hLDL raised Akt3 levels, which inhibits autophagy by activating mTORC2 [206,216,217]; LNPs raised transcripts of the Casp8 homolog, Cflar, which inhibits autophagy [218]. LNPs lowered the $\log_2$(FC) values of *Itpr1* (-21.5), *Pik3r2* (-25), *Prkcζ* (-22), and *Supt20* (-21). Itpr1 is a receptor that mediates calcium release from the ER. It was lowered by all reagents; its role is the context of these reagents is unclear. Reduction of the phosphatidylinositol 3-kinase regulatory subunit beta (Pik3r2) would reduce the amount of macrophage PIP3. This too does not have a clear cause-effect relationship to NP uptake. The effects of the reduction of Prkcζ are widespread and depend on macrophage environment. Prkcζ can function as either a pro-apoptotic or anti-apoptotic protein. Interestingly, it can trigger apoptosis by activating Mapk11 or Mapk14. Neither factor is increased by LNP addition (not shown). Prkcζ can promote the interaction of Card9 and Bcl10, which activates NfκB and MAP kinase p38 pathways [219]. It follows that LNPs have little effect on these pathways as seen throughout this work. Supt20 is required for starvation-induced Atg9a trafficking during autophagy. Thus, we see a potential offset in the Atg9a mechanism.

JRS4 cells and LPS triggered selective autophagy through Sqstm1, as expected [156]. The increase in Rps6kb1/2 by all reagents except LNPs is noteworthy. mTOR1 should activate Rps6kb1/2 leading to IFNγ inhibition and protein synthesis [220]. We also analyzed mRNA from macrophages that were incubated simultaneously with LPS and LNP for 24 hours. An increase or decrease in $\log_2$(FC) values should indicate an effect of LNPs on macrophages in the presence of LPS versus LPS alone. Only six genes showed statistically significant changes (Q-value < 0.05). The combination of LPS+LNP increased *Acsl1* (fatty acid oxidation), Itgb3 (phagosome formation), and *Usp25* (deubiquitinase) transcripts; the LPS+LNP combination decreased *Mknk1* (HIF-1

signaling), and *Tlr3* (dsRNA recognition) (Fig. 3.8B). An increase in Acsl1 should activate mTORC1 and thus reduce autophagy [221]. Usp25 is a negative regulator of IL17 signaling [222]. Its increase should decrease inflammation and thus also decrease autophagy [223]. Downregulation of Mknk1 should reduce the response to cytokines and also should reduce autophagy [224]. Tlr3 reduction should inhibit autophagy [225]. Therefore, we see agreement between fluorescence microscopy, flow cytometry, and RNA-seq data that LNPs lower macrophage autophagy. It should be noted that LPS has a much more powerful effect than LNPs on macrophages.

LNPs trigger few changes in M1-derived macrophage surface markers compared to hHDL, hLDL, JRS4 cells, and LPS

We analyzed ~250 antibodies in the LEGENDscreen panel to determine changes caused by our reagents after our standard incubation times. JRS4 cells caused significant increases in *CD49e*, *CD51*, *CD63*, *CD83*, *CD85k*, complement receptors, *CD98*, *CD100*, *CD120b*, *CD262*, *CD265*, *CD339*, *CD366*, and *CD371* mRNA transcripts (Fig. 3.9A). LPS caused significant increases in *CD9*, *CD14*, *CD49e*, *CD59a*, *CD66a*, *CD85k*, *CD98*, *CD120b*, *CD229/Ly9*, *CD255*, *Galectin-9*, *Gl7*, and *Podoplanin* mRNA transcripts (Fig. 3.9A). LNPs did not cause an increase in a single member of this panel. It is crucial to note that if LNPs triggered significant immune response changes, we should see these changes in this panel over 24-hour timescales. As a comparison, larger, non-degradable, micron-sized particles trigger the increase of *CD80*, *CD86*, and cytokine transcript expression in macrophages after uptake [226].

Figure 3.9. hHDL, hLDL, JRS4 cells, LPS, and LNPs trigger different responses in monocyte cell surface markers (LEGENDscreen). (A) Heat map of the mRNA transcripts of macrophages incubated in DMEM + 10% FBS and either PBS, hHDL, hLDL, JRS4 cells, LPS, or LNPs.

LNPs trigger phenotypes similar to murine primary macrophages and stromal cells

We used the ImmGen database to determine how LNPs affected the phenotype of macrophages compared to available transcript data for ten categories of mouse immune cells [[204]]. This database is a repository of scRNA data for murine immune cells harvested from mice of varying genetic backgrounds. We compared 172 macrophage transcripts with mRNA FC > 5 and Q-value < 0.05 after LNP addition to the FC values of 95 immune cell populations (6 stem cell, 18 B-cell, 37 T-cell, 11 innate lymphocytes, 3 dendritic cell, 9 macrophage, 2 monocyte, 3 granulocyte, 1 mast cell, 5 stromal). Stem cells, macrophages, and stromal cells had the strongest correlations in increases in the same genes (Fig. 3.10A, Fig 3.11A). Interestingly, most of the FC values that increased in our macrophages after LNP addition decreased in the 95 immune cell populations. Yet, several of the genes increased across the lineages including *Sirpα* and *Tlr3*. Several of these genes form a network around the actions of the Ras activator, Nf1; however; a cohesive map is elusive. We next compared 151 macrophage transcripts with mRNA FC < 5 and Q-values < 0.05 after LNP addition to the FC values of 95 immune cell populations. This data set has significant gene identities among the 95 cell conditions (Fig. 3.10B, Fig 3.11B). This means that although these cells perform distinct tasks in the body, the FC values for this set of genes are remarkably conserved.

Discussion

General transcript changes

LNPs increased transcript levels of macrophage genes (dark red boxes in Fig. 3.3, far right column) that span biological processes of chromatin organization, regulation of transcription, regulation of

Figure 3.10. Comparison of the changes in transcript levels of macrophages incubated with LNP versus the changes of the same transcripts in ninety-six separate murine immune cells from the ImmGen database. (A) Box plot of the FC > 5 values of the transcripts shown in Fig. 3.3 in each of the ninety-six data sets in the ImmGen database. Stem cells (light blue), B cells (dark blue), T cells (purple and tan), natural killer cells (light purple), dendritic cells (lime), macrophages (green), monocytes (salmon), granulocytes (red brick), mast cell (cyan), stromal cells (orange). **(B)** Box plot of the FC < 5 values of the transcripts shown in Fig. 3.3 in each of the ninety-six data sets in the ImmGen database.

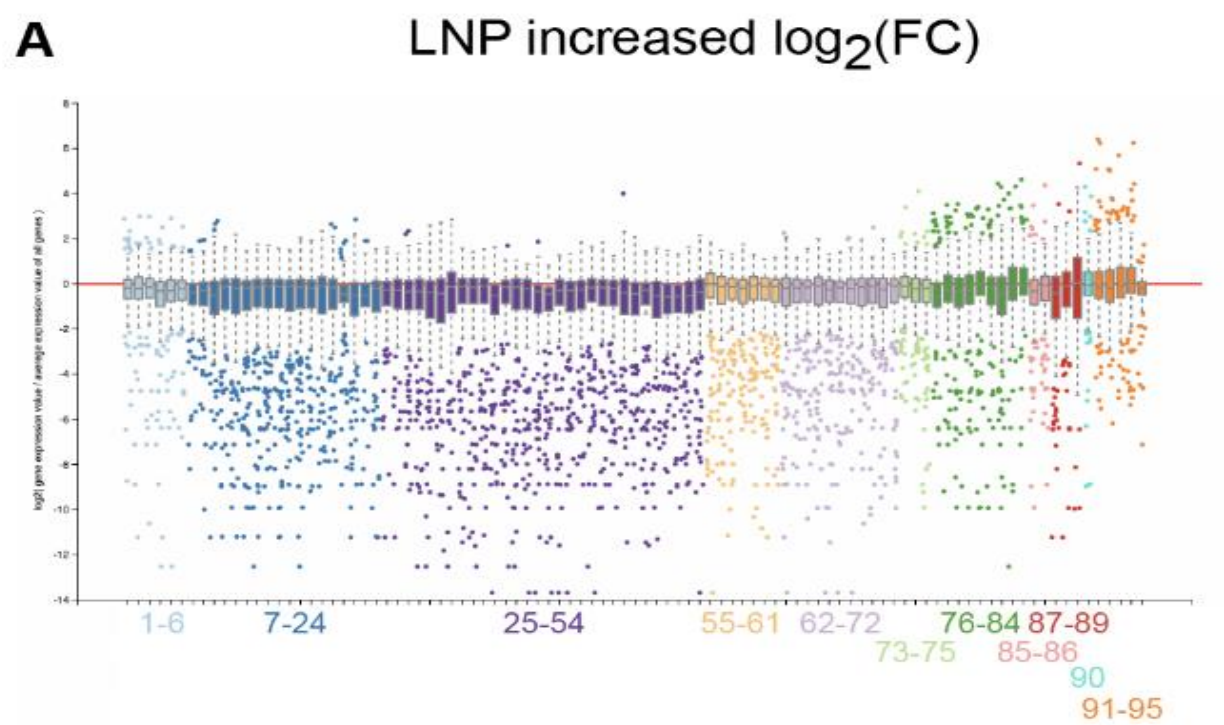
A
LNP increased log2(FC)
1-6
7-24
25-54
55-61
62-72
73-75
76-84
85-86
87-89
90
91-95

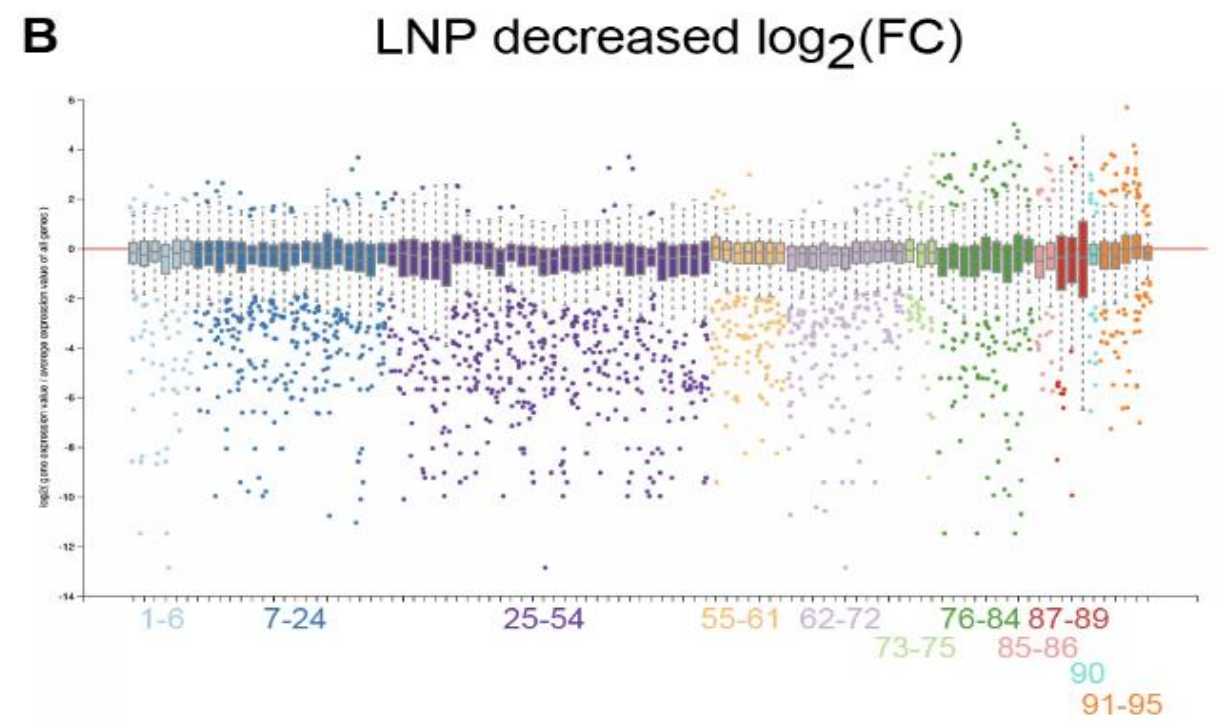
B
LNP decreased log2(FC)
1-6
7-24
25-54
55-61
62-72
73-75
76-84
85-86
87-89
90
91-95

Figure 3.11. Correlated changed transcript with LNP-traeted macrophages incubated with LNP. (A). The gene names that were identified across the ninety-six data sets where the transcript FC values also increased. Boxed inset lists the ninety-six data sets. Stem cells (light blue), B cells (dark blue), T cells (purple and tan), natural killer cells (light purple), dendritic cells (lime), macrophages (green), monocytes (salmon), granulocytes (red brick), mast cell (cyan), stromal cells (orange). **(B)** The gene names that were identified across the ninety-six data sets where the transcript FC values also decreased.

A

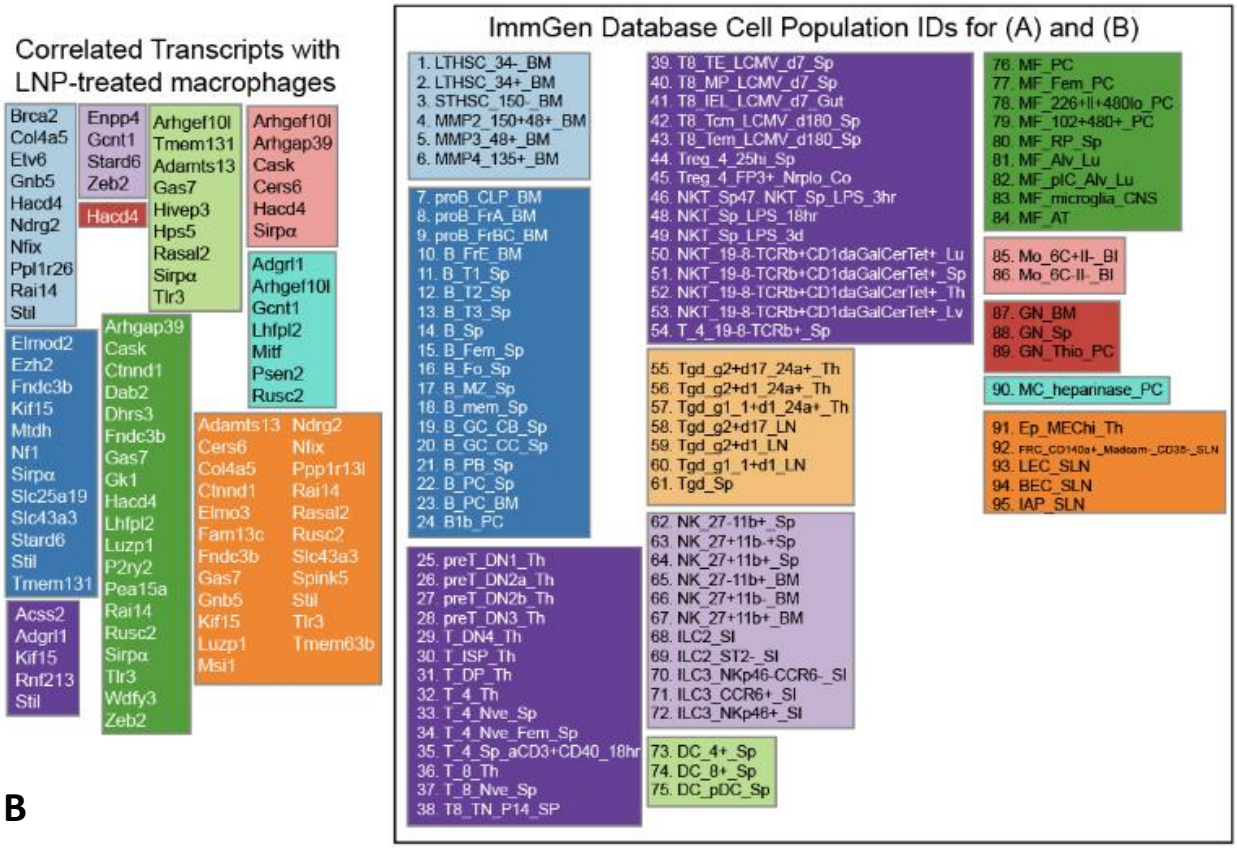
Correlated Transcripts with LNP-treated macrophages
Brca2 Col4a5 Etv6 Gnb5 Hacd4 Ndrg2 Nfix Ppl1r26 Rai14 Stil
Enpp4 Gcnt1 Stard6 Zeb2
Hacd4
Arhgef10l Tmem131 Adamts13 Gas7 Hivep3 Hps5 Rasal2 Sirpα Tlr3
Arhgef10l Arhgap39 Cask Cers6 Hacd4 Sirpα
Adgrl1 Arhgef10l Gcnt1 Lhfpl2 Mitf Psen2 Rusc2
Elmod2 Ezh2 Fndc3b Kif15 Mtdh Nf1 Sirpα Slc25a19 Slc43a3 Stard6 Stil Tmem131
Arhgap39 Cask Ctnnd1 Dab2 Dhrs3 Fndc3b Gas7 Gk1 Hacd4 Lhfpl2 Luzp1 P2ry2 Pea15a Rai14 Rusc2 Sirpα Tlr3 Wdfy3 Zeb2
Adamts13 Cers6 Col4a5 Ctnnd1 Elmo3 Fam13c Fndc3b Gas7 Gnb5 Kif15 Luzp1 Msi1
Ndrg2 Nfix Ppp1r13l Rai14 Rasal2 Rusc2 Slc43a3 Spink5 Stil Tlr3 Tmem63b
Acss2 Adgrl1 Kif15 Rnf213 Stil
ImmGen Database Cell Population IDs for (A) and (B)
1. LTHSC_34-_BM
2. LTHSC_34+_BM
3. STHSC_150-_BM
4. MMP2_150+48+_BM
5. MMP3_48+_BM
6. MMP4_135+_BM
7. proB_CLP_BM
8. proB_FrA_BM
9. proB_FrBC_BM
10. B_FrE_BM
11. B_T1_Sp
12. B_T2_Sp
13. B_T3_Sp
14. B_Sp
15. B_Fem_Sp
16. B_Fo_Sp
17. B_MZ_Sp
18. B_mem_Sp
19. B_GC_CB_Sp
20. B_GC_CC_Sp
21. B_PB_Sp
22. B_PC_Sp
23. B_PC_BM
24. B1b_PC
25. preT_DN1_Th
26. preT_DN2a_Th
27. preT_DN2b_Th
28. preT_DN3_Th
29. T_DN4_Th
30. T_ISP_Th
31. T_DP_Th
32. T_4_Th
33. T_4_Nve_Sp
34. T_4_Nve_Fem_Sp
35. T_4_Sp_aCD3+CD40_18hr
36. T_8_Th
37. T_8_Nve_Sp
38. T8_TN_P14_SP
39. T8_TE_LCMV_d7_Sp
40. T8_MP_LCMV_d7_Sp
41. T8_IEL_LCMV_d7_Gut
42. T8_Tcm_LCMV_d180_Sp
43. T8_Tem_LCMV_d180_Sp
44. Treg_4_25hi_Sp
45. Treg_4_FP3+_Nrplo_Co
46. NKT_Sp47_NKT_Sp_LPS_3hr
48. NKT_Sp_LPS_18hr
49. NKT_Sp_LPS_3d
50. NKT_19-8-TCRb+CD1daGalCerTet+_Lu
51. NKT_19-8-TCRb+CD1daGalCerTet+_Sp
52. NKT_19-8-TCRb+CD1daGalCerTet+_Th
53. NKT_19-8-TCRb+CD1daGalCerTet+_Lv
54. T_4_19-8-TCRb+_Sp
55. Tgd_g2+d17_24a+_Th
56. Tgd_g2+d1_24a+_Th
57. Tgd_g1_1+d1_24a+_Th
58. Tgd_g2+d17_LN
59. Tgd_g2+d1_LN
60. Tgd_g1_1+d1_LN
61. Tgd_Sp
62. NK_27-11b+_Sp
63. NK_27+11b-+Sp
64. NK_27+11b+_Sp
65. NK_27-11b+_BM
66. NK_27+11b-_BM
67. NK_27+11b+_BM
68. ILC2_SI
69. ILC2_ST2-_SI
70. ILC3_NKp46-CCR6-_SI
71. ILC3_CCR6+_SI
72. ILC3_NKp46+_SI
73. DC_4+_Sp
74. DC_8+_Sp
75. DC_pDC_Sp
76. MF_PC
77. MF_Fem_PC
78. MF_226+II+480lo_PC
79. MF_102+480+_PC
80. MF_RP_Sp
81. MF_Alv_Lu
82. MF_pIC_Alv_Lu
83. MF_microglia_CNS
84. MF_AT
85. Mo_6C+II-_BI
86. Mo_6C-II-_BI
87. GN_BM
88. GN_Sp
89. GN_Thio_PC
90. MC_heparinase_PC
91. Ep_MEChi_Th
92. FRC_CD140a+_Madcam-_CD35-_SLN
93. LEC_SLN
94. BEC_SLN
95. IAP_SLN

B

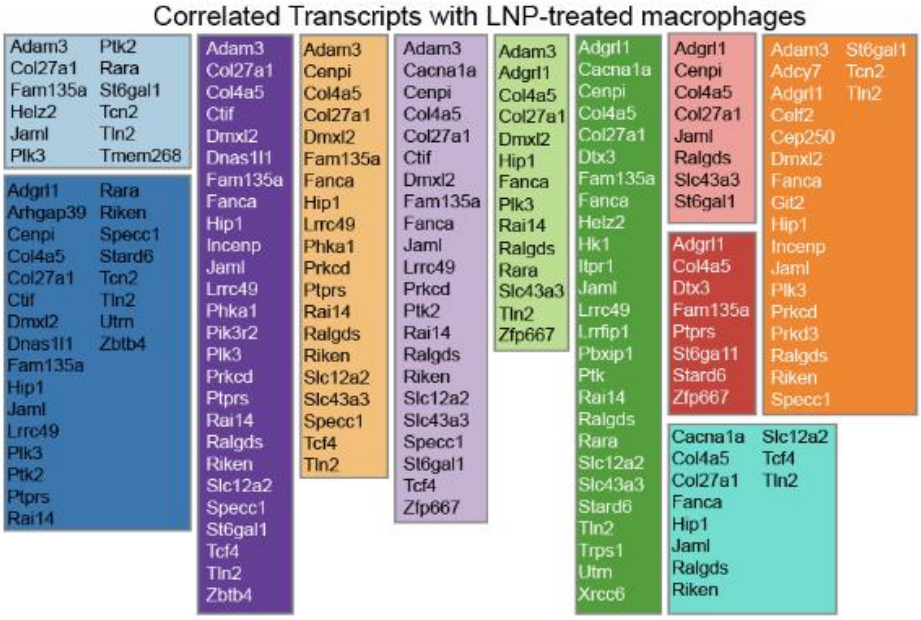
Correlated Transcripts with LNP-treated macrophages
Adam3 Col27a1 Fam135a Helz2 Jaml Plk3
Ptk2 Rara St6gal1 Tcn2 Tln2 Tmem268
Adgrl1 Arhgap39 Cenpi Col4a5 Col27a1 Ctif Dmxl2 Dnas1l1 Fam135a Hip1 Jaml Lrrc49 Ptk3 Ptk2 Ptprs Rai14
Rara Riken Specc1 Stard6 Tcn2 Tln2 Utrn Zbtb4
Adam3 Col27a1 Col4a5 Ctif Dmxl2 Dnas1l1 Fam135a Fanca Hip1 Incenp Jaml Lrrc49 Phka1 Pik3r2 Plk3 Prkcd Ptprs Rai14 Ralgds Riken Slc12a2 Specc1 St6gal1 Tcf4 Tln2 Zbtb4
Adam3 Cenpi Col4a5 Col27a1 Dmxl2 Fam135a Fanca Hip1 Lrrc49 Phka1 Prkcd Ptprs Rai14 Ralgds Riken Slc12a2 Slc43a3 Specc1 Tcf4 Tln2
Adam3 Cacna1a Cenpi Col4a5 Col27a1 Ctif Dmxl2 Fam135a Fanca Jaml Lrrc49 Prkcd Ptk2 Rai14 Ralgds Riken Slc12a2 Slc43a3 Specc1 St6gal1 Tcf4 Zfp667
Adam3 Adgrl1 Col4a5 Col27a1 Dmxl2 Hip1 Fanca Plk3 Rai14 Ralgds Rara Slc43a3 Tln2 Zfp667
Adgrl1 Cacna1a Cenpi Col4a5 Col27a1 Dtx3 Fam135a Fanca Helz2 Hk1 Itpr1 Jaml Lrrc49 Lrrfip1 Pbxip1 Ptk Rai14 Ralgds Rara Slc12a2 Slc43a3 Stard6 Tln2 Trps1 Utrn Xrcc6
Adgrl1 Cenpi Col4a5 Col27a1 Jaml Ralgds Slc43a3 St6gal1
Adgrl1 Col4a5 Dtx3 Fam135a Ptprs St6ga11 Stard6 Zfp667
Cacna1a Col4a5 Col27a1 Fanca Hip1 Jaml Ralgds Riken
Slc12a2 Tcf4 Tln2
Adam3 Adcy7 Adgrl1 Celf2 Cep250 Dmxl2 Fanca Git2 Hip1 Incenp Jaml Plk3 Prkcd Prkd3 Ralgds Riken Specc1
St6gal1 Tcn2 Tln2

macromolecule biosynthesis, and regulation of RNA metabolic processes (*Baza1, Brca2, Btrc, Cnot3, Ctcf, Dab2, Ehmt2, Foxp1, Gatad2b, Gon4l, Mbd1, Mitf, Mysm1, Ncoa2, Nfix, Pax6, Pphln1, Setd2, Sfmbt1, Smad5, Smarca2, Taf1, Tcf25, Tet3, Ubtf,* and *Zeb2*). The functions of these transcripts are largely connected by *Chd3*, a component of the NuRD complex required for spindle organization and centrosome integrity [227]. This indicates that LNPs tend to cause macrophages proliferation. The vast majority of the protein products of the transcripts having strongly LNP-increased $\log_2$(FC) values (Fig. 3.7) are associated with organelles. Only, Arhgef101, Cep295, Cflar, Fyttd1, Hps5, Plec, Prrc2c, and Stil are strictly cytosolic. The LNP-induced increase of *Sirpα* transcripts was unexpected. Sirpα is known to interact with the marker-of-self protein CD47 [228]. This interaction stops phagocytes such as granulocytes and macrophages from engulfing endogenous cells. Sirpα also limits the respiratory burst in phagocytes [229]. This would reduce ROS and Cybb levels. Only LPS increased *Cybb* transcripts (+21.3). Taken in sum, if decreased Sirpα levels lead to increased phagocytosis, increased Sirpα levels may lead to decreased phagocytosis.

LNPs decreased transcript levels of macrophage genes (dark blue boxes in Fig. 3.3, far right column) that span biological processes of transepithelial transport, maintenance of cell polarity, histone modification, and regulation to external stimuli (*Adcy7, Apc, Ash1l, Clasp2, Clock, Fbf1, Incenp, Itpr1, Jmjd1c, Kdm5c, Macf1, Mapkbp1, Mark2, Med24, Mta1, Numa1, Prkcζ, Ptprs, Setd3, Slc12a2, Slc23a2, St6gal1,* and *Tet2*). Prkcζ acts downstream of the Par1, Par4, and Cd36/Gp4 receptors, which are responsible for thrombin binding (Par1, Par2) and free fatty acid and oxLDL transport (CD36). Prkcζ can promote the interaction of Card9 and Bcl10, which activates NFκB and MAP kinase p38 pathways [219]. It follows that LNPs have little effect on these

pathways as seen throughout this work. Polo-like kinase (Plk3) reduction by LNPs (-21.5) should reduce the phosphorylation of Atf2, Bcl2l1, Hif-1a, and p53 – all factors involved in cell cycle regulation. Plk3 is also activated in response to ROS production. Adenylate cyclase type 7 (Adcy7) positively regulates LPS-induced Tnfα production. Thus, LNPs should lower Tnfα levels. Indeed, Tnf (NM_001278601.1, NM_013693.3) levels were lower in LNP-treated macrophages versus both JRS4- and LPS-treated macrophages (-6 vs. ~7 and 0 vs. ~5 for the two isoforms, respectively). LNPs' decrease of macrophage Rara levels should limit inflammatory response [230]. Reduction of the phosphatidylinositol 3-kinase regulatory subunit beta (Pik3r2) would reduce the amount of macrophage PIP3. Both hHDL (-25) and LNPs (-25) reduce Pik3r2. The analog Pik3r3 promotes autophagy [231232]. Therefore, Pik3r2 reduction by hHDL and LNPs could partially explain why these two reagents reduce autophagy. LNPs decreased Agpat1 levels, which converts lysophosphatidic acid (LPA) to phosphatidic acid (PA). This is one of the first steps in DAG and TAG synthesis in the ER. The mechanism for the slight decrease in Creb1 transcripts is unclear.

LNPs and LPS downregulates Cblb, Fcγr1, and epidermal growth factor receptor (Egfr) [232]. All five treatments reduced the transcripts of *Birc6*, *Clasp2*, *Fanca*, *Fbf1*, *Hk1*, *Itpr1*, *Jaml*, *Mark2*, *Rbmx*, *Setd3*, *Slc23a2*, *Tcn2*, *Tet2*, and *Utrn*. Birc6 inhibits apoptosis [233]. Birc6/BRUCE partially modulates the closure of the autophagosome-lysosome by interacting with Stx17 [234]. Rbmx promotes Il1β cleavage of Tnfr1 and the release of exosomes. (*Exosc10*, a component of the exosome, transcripts go up in all categories except LNP). Hk1 phosphorylates glucose and activates the Nlrp3 inflammasome [235]. Setd3 is a methyltransferase of actin His73 [236].

Entry

To elucidate how lipoproteins, JRS4 cells, LPS, and LNPs bind and potentially enter cells, we determined the mRNA $\log_2$(FC) values of ~220 transcripts that are associated with cellular entry including C-type lectin, Fcγr, Rig-I-like, and TLR pathways. hHDL increased Tlr7 levels (Fig. 3.3). Tlr7 is an endosomal receptor, which is typically associated with binding ssRNA molecules. Tlr7 interacts with Myd88 causing the activation of Irak1, Irak4, Traf3, Traf6, which in turn activate NFκB and Irf7 [237,238]. None of these factors had significant FC values after hHDL incubation with macrophages. This shows that *Tlr7* transcript levels may be increased by reasons different from hHDL binding.

hHDL binds CD36, SR-BI, and LIMP-2. *Cd36* levels increased only after LPS treatment. *Scarb1/Srb1* and *Limp-2* transcript levels were statistically constant among treatments. These results were surprising. We expected an increase in these cholesterol and fatty acid transports after lipoprotein addition. Because PEG binds the CD36 super-family of proteins such as LIMP-2 [160,239] and SR-BI [161], we anticipated the transcripts of these genes would potentially increase after LNP treatment, but this was not observed. This is slightly at odds with previous studies showing that PEG NPs interact with SR-BI both *in vitro* and *in vivo* – although the amount of surface-exposed PEG on the NPs in those studies – CNPs and SNPs (100% by mole) - was much higher than on LNPs (2% by mole).

None of the reagents increased Arp2/3-Scar/WAVE complex transcripts [240]. This complex is involved in several uptake processes from endocytosis in yeast to phagocytosis in macrophages [241–243]. Furthermore, none of the reagents increased the transcripts of *Nckap1l*, which was recently discovered to be involved in a variety of immune cell processes including phagocytosis

and migration [242,243]. Interestingly, the hematopoietic-specific HEM1 protein encoded by *Nckap1l* controls cytokine equipoise [244]. It is interesting that neither JRS4 cells nor LPS raised *Nckap1l* levels. HEM1 loss also blocks mTORC2-dependent Akt phosphorylation, which is a critical step in insulin/fed response [206]. Blocking this phosphorylation would most likely trigger autophagy. By not affecting *Nckap1l*, our reagents should not trigger autophagy by this mechanism.

Autophagy, innate immunity, and inflammation

LNPs did not increase the number of transcripts of *Atg5* [245], *Atg12*, *Atg16l1*, cytokines, chemokines, map kinases, *Erk*, *Ikk* [246], *NFκB* factors, *Nod1/2* [171] or *Tax1bp* [247] versus controls (Fig. 3.3, Fig. 3.7). In this regard, the macrophage response to LNPs most resembles the macrophage response to hHDL and hLDL. hHDL and hLDL increased *Akt3* (protein kinase B□) transcript levels. Akt activates mTOR, which inhibits autophagy. Activated mTOR1 should activate p70s6k and Rps6 leading to protein synthesis. Indeed, *Rps6k* isoforms increased (+6) after hHDL and hLDL treatments. Akt inhibits Foxo by phosphorylation; this action should increase cell survival and proliferation. Akt should also increase glucose influx into the macrophage, thus increasing glycolysis. Activated macrophages favor glycolysis over oxidative respiration. JRS4 and LPS increased Tnf and Traf3 (JRS4) levels but not Fadd levels, meaning that macrophages seem to favor inflammation over apoptosis after being exposed to JRS4 and LPS. The Traf pathway should activate Nfκb, but of this protein family only *Nfκbiα* was increased by JRS4 in our data.

Macrophage activation

Macrophage activation can be grouped into four categories with certain degrees of overlap: alternative activation (e.g., CD36, Clec10a, Mrc1), antigen presentation (e.g., H2-Aa, H2-Eb1, He-

Ab1), complement cascade (e.g., C1qc, C1qb), and extracellular matrix receptor-interactions (e.g., CD44, Sdc1, Pfn1, Fn1) including cytoskeletal rearrangement and regulation (e.g., Actγ1, Pfn1, Tmsb4x) [248–250]. Recently, these categories have been found to be subsets of nine stages of macrophage status post murine infection with *Listeria monocytogenes* and *Heligmosomoides polygyrus* [251]. The nine temporal stages were reduced to four end-point categories: phagocytic path (e.g., Fcγr1, Fcγr3, Ncf4), oxidative stress path (e.g., Gsr, Prdx5, Txn1), inflammatory path (e.g., Fcγr1, Ifitm3, Isg20), and remodeling path (e.g., Col1a1, Col3a1, Ddr2). Of these factors, only Actγ1 and extracellular matrix genes of the Col family were present in our statistically screened FC data. Additional key signatures of the four macrophage end-point states were increases in *Apoe, Cxcl13, Ctsb,* and *Pf4*, respectively. *Apoe* was increased by both hHDL and hLDL and is constant for the other three treatments (Fig. 3.2A). Cxc motif chemokine ligand transcripts were consistently increased in our data by JRS4 cells and by LPS, but not by hHDL, hLDL, or LNPs. Ctsb and Pf4 did not appear in our data. Hif1α, Il1α, and Il6 show cyclical expression patterns over the 24 hours post injections [251]. hHDL, hLDL, and JRS4 cells decreased Hif1α levels. This would indicate that these three reagents trigger the 'phagocytic path' response [357].

These results show that NPs do not seem to trigger a phagocytic gene regulation response. Further investigation will involve determining which pathways LNPs and and NPs in general trigger since we show here that macrophages take up significant quantities of them.

Methods

Cell Culture

RAW264.7 macrophages were purchased from ATCC (#TIB-71) and cultured according to the manufacturer's instructions. Macrophages were polarized to an M1 phenotype by adding IFNγ. We used either DMEM + 10% FBS or DMEM (starve) as media for the macrophages for all experiments.

Lipoprotein, JRS4 cells, and nanoparticles

Human high-density lipoprotein (hHDL) and human low-density lipoprotein (hLDL) were obtained from Lee Biosolutions (#361-25, #360-10). Samples were diluted to 10 mg/ml in PBS before administration to macrophages. JRS4 cells were a gift from Dr. Michael Caparon (Washington University, St. Louis). They were cultured in Todd Hewitt broth (Millipore; #T1438). PEO_{56}-PBD_{46} diblock copolymers (filomicelles/CNPs) were synthesized according to the methods of Ref. [201]. PEO_{132}-PBD_{69} diblock copolymers (spheres/SNPs) were a gift from Dr. Frank S. Bates (Minnesota). NPs were formed at 10 mg/ml copolymer using film rehydration with phosphate buffered saline (PBS) as the aqueous buffer as described previously [202]. Nanoparticles were stained with near-infrared (NIR) dye (Thermo; #D12731) and dialyzed overnight into 1 liter of PBS at 4°C [202]. LNPs were obtained from Formumax Scientific Inc. (#F30204BD22) is a PEGylated liposome. They are the structural shell of the anti-cancer NP DOXIL [203].

RNA sequencing and analysis

Macrophages were cultured in 6-well plates. At confluence, each well had enough mRNA for sequencing. Media with or without reagents was removed, macrophages were washed with PBS, and trypsin digested. The macrophages in trypsin-EDTA (~1 ml) were added to 3 ml of DMEM

and pelleted at 300 x *g* for 5 minutes at 4°C. Supernatant was removed, and the mRNA was extracted (Zymo; #R2050). mRNA was shipped on dry ice to BGI for sequencing. Reads were analyzed using the BGI suite. Each of the five conditions were compared to PBS (control). The largest changes in $\log_2$(FC) in each category were combined into one list. This list was used as the basis for Fig. 2E. Additional genes that fell under specific cellular functions such as autophagy were searched for on the BGI website.

Statistics

P-values were determined using the Excel t.test() function.

REFERENCES

1. Mansoori, B., Mohammadi, A., Davudian, S., Shirjang, S. & Baradaran, B. The Different Mechanisms of Cancer Drug Resistance: A Brief Review. *Advanced Pharmaceutical Bulletin* **7**, 339–348 (2017).
2. Hourdequin, K. C., Schpero, W. L., McKenna, D. R., Piazik, B. L. & Larson, R. J. Toxic effect of chemotherapy dosing using actual body weight in obese versus normal-weight patients: a systematic review and meta-analysis. *Annals of Oncology* **24**, 2952–2962 (2013).
3. Klionsky, D. J. *et al.* Guidelines for the use and interpretation of assays for monitoring autophagy (3rd edition). *Autophagy* **12**, 1–222 (2016).
4. Melia, T. J., Lystad, A. H. & Simonsen, A. Autophagosome biogenesis: From membrane growth to closure. *Journal of Cell Biology* **219**, (2020).
5. Mauvezin, C. *et al.* Coordination of autophagosome-lysosome fusion and transport by a Klp98A-Rab14 complex. *Journal of Cell Science* (2016) doi:10.1242/jcs.175224.
6. Jackson, M. P. & Hewitt, E. W. Cellular proteostasis: degradation of misfolded proteins by lysosomes. *Essays in Biochemistry* **60**, 173–180 (2016).
7. Hurley, J. H. & Young, L. N. Mechanisms of Autophagy Initiation. *Annual Review of Biochemistry* **86**, 225–244 (2017).
8. Desantis, V. *et al.* Autophagy: A New Mechanism of Prosurvival and Drug Resistance in Multiple Myeloma. *Translational Oncology* **11**, 1350–1357 (2018).
9. Anozie, U. C. & Dalhaimer, P. Molecular links among non-biodegradable nanoparticles, reactive oxygen species, and autophagy. *Advanced Drug Delivery Reviews* **122**, 65–73 (2017).
10. Li, X. *et al.* Autophagy: A novel mechanism of chemoresistance in cancers. *Biomedicine & Pharmacotherapy* **119**, 109415 (2019).
11. Chen, Y., McMillan-Ward, E., Kong, J., Israels, S. J. & Gibson, S. B. Oxidative stress induces autophagic cell death independent of apoptosis in transformed and cancer cells. *Cell Death & Differentiation* **15**, 171–182 (2008).
12. Rea, S. L., Walsh, J. P., Layfield, R., Ratajczak, T. & Xu, J. New Insights Into the Role of Sequestosome 1/p62 Mutant Proteins in the Pathogenesis of Paget's Disease of Bone. *Endocrine Reviews* **34**, 501–524 (2013).

13. Kirkin, V., Lamark, T., Johansen, T. & Dikic, I. NBR1 co-operates with p62 in selective autophagy of ubiquitinated targets. *Autophagy* **5**, 732–733 (2009).
14. Kirkin, V. *et al.* A Role for NBR1 in Autophagosomal Degradation of Ubiquitinated Substrates. *Molecular Cell* **33**, 505–516 (2009).
15. Lamark, T., Kirkin, V., Dikic, I. & Johansen, T. NBR1 and p62 as cargo receptors for selective autophagy of ubiquitinated targets. *Cell Cycle* **8**, 1986–1990 (2009).
16. Hibshman, J. D. *et al.* Nonselective autophagy reduces mitochondrial content during starvation in *Caenorhabditis elegans*. *American Journal of Physiology-Cell Physiology* **315**, C781–C792 (2018).
17. Traverso, N. *et al.* Role of Glutathione in Cancer Progression and Chemoresistance. *Oxidative Medicine and Cellular Longevity* **2013**, 1–10 (2013).
18. Vatansever, F. *et al.* Antimicrobial strategies centered around reactive oxygen species – bactericidal antibiotics, photodynamic therapy, and beyond. *FEMS Microbiology Reviews* **37**, 955–989 (2013).
19. Snezhkina, A. v. *et al.* ROS Generation and Antioxidant Defense Systems in Normal and Malignant Cells. *Oxidative Medicine and Cellular Longevity* **2019**, 1–17 (2019).
20. Fürstenberger, G., Krieg, P., Müller-Decker, K. & Habenicht, A. J. R. What are cyclooxygenases and lipoxygenases doing in the driver's seat of carcinogenesis? *International Journal of Cancer* **119**, 2247–2254 (2006).
21. Poillet-Perez, L., Despouy, G., Delage-Mourroux, R. & Boyer-Guittaut, M. Interplay between ROS and autophagy in cancer cells, from tumor initiation to cancer therapy. *Redox Biology* **4**, 184–192 (2015).
22. Kim, J., Kundu, M., Viollet, B. & Guan, K.-L. AMPK and mTOR regulate autophagy through direct phosphorylation of Ulk1. *Nature Cell Biology* **13**, 132–141 (2011).
23. Egan, D. F. *et al.* Phosphorylation of ULK1 (hATG1) by AMP-Activated Protein Kinase Connects Energy Sensing to Mitophagy. *Science (1979)* **331**, 456–461 (2011).
24. Egan, D., Kim, J., Shaw, R. J. & Guan, K.-L. The autophagy initiating kinase ULK1 is regulated via opposing phosphorylation by AMPK and mTOR. *Autophagy* **7**, 643–644 (2011).

25. Djavaheri-Mergny, M. *et al.* NF-κB Activation Represses Tumor Necrosis Factor-α-induced Autophagy. *Journal of Biological Chemistry* **281**, 30373–30382 (2006).
26. Boyer-Guittaut, M. *et al.* The role of GABARAPL1/GEC1 in autophagic flux and mitochondrial quality control in MDA-MB-436 breast cancer cells. *Autophagy* **10**, 986–1003 (2014).
27. Kauffman, K. J. *et al.* Delipidation of mammalian Atg8-family proteins by each of the four ATG4 proteases. *Autophagy* 1–19 (2018) doi:10.1080/15548627.2018.1437341.
28. Scherz-Shouval, R. *et al.* Reactive oxygen species are essential for autophagy and specifically regulate the activity of Atg4. *The EMBO Journal* **26**, 1749–1760 (2007).
29. de Gaetano, A. *et al.* Mitophagy and Oxidative Stress: The Role of Aging. *Antioxidants* **10**, 794 (2021).
30. Yoo, S.-M. & Jung, Y.-K. A Molecular Approach to Mitophagy and Mitochondrial Dynamics. *Mol Cells* **41**, 18–26 (2018).
31. Shally, A. & McDonagh, B. The redox environment and mitochondrial dysfunction in age-related skeletal muscle atrophy. *Biogerontology* **21**, 461–473 (2020).
32. Chen, Y. & Dorn, G. W. PINK1-Phosphorylated Mitofusin 2 Is a Parkin Receptor for Culling Damaged Mitochondria. *Science (1979)* **340**, 471–475 (2013).
33. Padman, B. S. *et al.* LC3/GABARAPs drive ubiquitin-independent recruitment of Optineurin and NDP52 to amplify mitophagy. *Nature Communications* **10**, 408 (2019).
34. Lazarou, M. *et al.* The ubiquitin kinase PINK1 recruits autophagy receptors to induce mitophagy. *Nature* **524**, 309–314 (2015).
35. Chen, M. *et al.* Mitophagy receptor FUNDC1 regulates mitochondrial dynamics and mitophagy. *Autophagy* **12**, 689–702 (2016).
36. Zhang, T. *et al.* BNIP3 Protein Suppresses PINK1 Kinase Proteolytic Cleavage to Promote Mitophagy. *Journal of Biological Chemistry* **291**, 21616–21629 (2016).
37. Novak, I. *et al.* Nix is a selective autophagy receptor for mitochondrial clearance. *EMBO Rep* **11**, 45–51 (2010).
38. Bhujabal, Z. *et al.* FKBP8 recruits LC3A to mediate Parkin-independent mitophagy. *EMBO Rep* **18**, 947–961 (2017).

39. Otsu, K., Murakawa, T. & Yamaguchi, O. BCL2L13 is a mammalian homolog of the yeast mitophagy receptor Atg32. *Autophagy* **11**, 1932–1933 (2015).
40. Yamaguchi, O., Murakawa, T., Nishida, K. & Otsu, K. Receptor-mediated mitophagy. *Journal of Molecular and Cellular Cardiology* **95**, 50–56 (2016).
41. van Humbeeck, C., Cornelissen, T. & Vandenberghe, W. Ambra1. *Autophagy* **7**, 1555–1556 (2011).
42. Wei, Y., Chiang, W.-C., Sumpter, R., Mishra, P. & Levine, B. Prohibitin 2 Is an Inner Mitochondrial Membrane Mitophagy Receptor. *Cell* **168**, 224-238.e10 (2017).
43. Zhang, Y. *et al.* Listeria hijacks host mitophagy through a novel mitophagy receptor to evade killing. *Nature Immunology* **20**, 433–446 (2019).
44. Kim, J., Kim, J. & Bae, J.-S. ROS homeostasis and metabolism: a critical liaison for cancer therapy. *Experimental & Molecular Medicine* **48**, e269–e269 (2016).
45. Storz, P. Reactive oxygen species in tumor progression. *Frontiers in Bioscience* **10**, 1881 (2005).
46. Rohrmann, S. *et al.* Meat consumption and mortality - results from the European Prospective Investigation into Cancer and Nutrition. *BMC Medicine* **11**, 63 (2013).
47. del Río, L. A., Sandalio, L. M., Palma, JoséM., Bueno, P. & Corpas, F. J. Metabolism of oxygen radicals in peroxisomes and cellular implications. *Free Radical Biology and Medicine* **13**, 557–580 (1992).
48. Tang, Y., Wang, S., Jiang, J. & Liang, X. Links between cancer stem cells and epithelial– mesenchymal transition. *OncoTargets and Therapy* 2973 (2015) doi:10.2147/OTT.S91863.
49. de Sá Junior, P. L. *et al.* The Roles of ROS in Cancer Heterogeneity and Therapy. *Oxidative Medicine and Cellular Longevity* **2017**, 1–12 (2017).
50. Shi, X., Zhang, Y., Zheng, J. & Pan, J. Reactive Oxygen Species in Cancer Stem Cells. *Antioxidants & Redox Signaling* **16**, 1215–1228 (2012).
51. Vafa, O. *et al.* c-Myc Can Induce DNA Damage, Increase Reactive Oxygen Species, and Mitigate p53 Function. *Molecular Cell* **9**, 1031–1044 (2002).
52. Thorgeirsson, S. S., Factor, V. M. & Snyderwine, E. G. Transgenic mouse models in carcinogenesis research and testing. *Toxicology Letters* **112–113**, 553–555 (2000).

53. Yun, C. W. & Lee, S. H. The Roles of Autophagy in Cancer. *Int J Mol Sci* **19**, (2018).
54. Kenific, C. M., Thorburn, A. & Debnath, J. Autophagy and metastasis: another double-edged sword. *Current Opinion in Cell Biology* **22**, 241–245 (2010).
55. Singh, S. S. *et al.* Dual role of autophagy in hallmarks of cancer. *Oncogene* **37**, 1142–1158 (2018).
56. Mariño, G., Niso-Santano, M., Baehrecke, E. H. & Kroemer, G. Self-consumption: the interplay of autophagy and apoptosis. *Nature Reviews Molecular Cell Biology* **15**, 81–94 (2014).
57. Yang, Z. J., Chee, C. E., Huang, S. & Sinicrope, F. A. The Role of Autophagy in Cancer: Therapeutic Implications. *Molecular Cancer Therapeutics* **10**, 1533–1541 (2011).
58. Gump, J. M. & Thorburn, A. Autophagy and apoptosis: what is the connection? *Trends in Cell Biology* **21**, 387–392 (2011).
59. Li, X., He, S. & Ma, B. Autophagy and autophagy-related proteins in cancer. *Molecular Cancer* **19**, 12 (2020).
60. Liou, G.-Y. & Storz, P. Reactive oxygen species in cancer. *Free Radical Research* **44**, 479–496 (2010).
61. Sullivan, L. B. & Chandel, N. S. Mitochondrial reactive oxygen species and cancer. *Cancer & Metabolism* **2**, 17 (2014).
62. Dadali, T. *et al.* Elevated levels of mitochondrial CoQ10 induce ROS-mediated apoptosis in pancreatic cancer. *Scientific Reports* **11**, 5749 (2021).
63. Yang, H. *et al.* The role of cellular reactive oxygen species in cancer chemotherapy. *Journal of Experimental & Clinical Cancer Research* **37**, 266 (2018).
64. Wang, H. *et al.* NRF2 activation by antioxidant antidiabetic agents accelerates tumor metastasis. *Science Translational Medicine* **8**, (2016).
65. Piskounova, E. *et al.* Oxidative stress inhibits distant metastasis by human melanoma cells. *Nature* **527**, 186–191 (2015).
66. Sznarkowska, A., Kostecka, A., Meller, K. & Bielawski, K. P. Inhibition of cancer antioxidant defense by natural compounds. *Oncotarget* **8**, 15996–16016 (2017).
67. Sayin, V. I. *et al.* Antioxidants Accelerate Lung Cancer Progression in Mice. *Science Translational Medicine* **6**, (2014).

68. Letai, A. G. Diagnosing and exploiting cancer's addiction to blocks in apoptosis. *Nat Rev Cancer* **8**, 121–32 (2008).
69. Levine, B., Sinha, S. & Kroemer, G. Bcl-2 family members: dual regulators of apoptosis and autophagy. *Autophagy* **4**, 600–6 (2008).
70. Zhou, Y.-Y., Li, Y., Jiang, W.-Q. & Zhou, L.-F. MAPK/JNK signalling: a potential autophagy regulation pathway. *Biosci Rep* **35**, (2015).
71. Suhaili, S. H., Karimian, H., Stellato, M., Lee, T.-H. & Aguilar, M.-I. Mitochondrial outer membrane permeabilization: a focus on the role of mitochondrial membrane structural organization. *Biophys Rev* **9**, 443–457 (2017).
72. Tripathi, S. K. & Biswal, B. K. Piperlongumine, a potent anticancer phytotherapeutic: Perspectives on contemporary status and future possibilities as an anticancer agent. *Pharmacological Research* **156**, 104772 (2020).
73. Wang, H. *et al.* Piperlongumine induces apoptosis and autophagy in leukemic cells through targeting the PI3K/Akt/mTOR and p38 signaling pathways. *Oncol Lett* **15**, 1423–1428 (2018).
74. Makhov, P. *et al.* Piperlongumine promotes autophagy via inhibition of Akt/mTOR signalling and mediates cancer cell death. *Br J Cancer* **110**, 899–907 (2014).
75. Rodríguez-Hernández, M. A. *et al.* Dose-dependent regulation of mitochondrial function and cell death pathway by sorafenib in liver cancer cells. *Biochemical Pharmacology* **176**, 113902 (2020).
76. Shen, Q., Xu, Z. & Xu, S. Long non-coding RNA LUCAT1 contributes to cisplatin resistance by regulating the miR-514a-3p/ULK1 axis in human non-small cell lung cancer. *International Journal of Oncology* (2020) doi:10.3892/ijo.2020.5106.
77. Zhang, W. *et al.* Long non-coding RNA LINC00160 functions as a decoy of microRNA-132 to mediate autophagy and drug resistance in hepatocellular carcinoma via inhibition of PIK3R3. *Cancer Letters* **478**, 22–33 (2020).
78. Xiao, F. *et al.* Trim14 promotes autophagy and chemotherapy resistance of gastric cancer cells by regulating AMPK/mTOR pathway. *Drug Development Research* **81**, 544–550 (2020).

79. Condello, M., Mancini, G. & Meschini, S. The Exploitation of Liposomes in the Inhibition of Autophagy to Defeat Drug Resistance. *Frontiers in Pharmacology* **11**, (2020).
80. Hu, Y.-J. *et al.* Nanostructured Dihydroartemisinin Plus Epirubicin Liposomes Enhance Treatment Efficacy of Breast Cancer by Inducing Autophagy and Apoptosis. *Nanomaterials* **8**, 804 (2018).
81. Inokuchi-Shimizu, S. *et al.* TAK1-mediated autophagy and fatty acid oxidation prevent hepatosteatosis and tumorigenesis. *Journal of Clinical Investigation* **124**, 3566–3578 (2014).
82. Loibl, S. & Gianni, L. HER2-positive breast cancer. *The Lancet* **389**, 2415–2429 (2017).
83. Barceló, C. *et al.* T-Type Calcium Channels as Potential Therapeutic Targets in Vemurafenib-Resistant BRAFV600E Melanoma. *Journal of Investigative Dermatology* **140**, 1253–1265 (2020).
84. Wilhelm, S. M. *et al.* Preclinical overview of sorafenib, a multikinase inhibitor that targets both Raf and VEGF and PDGF receptor tyrosine kinase signaling. *Mol Cancer Ther* **7**, 3129–40 (2008).
85. Martin, A. P. *et al.* BCL-2 family inhibitors enhance histone deacetylase inhibitor and sorafenib lethality via autophagy and overcome blockade of the extrinsic pathway to facilitate killing. *Mol Pharmacol* **76**, 327–41 (2009).
86. SAI, K. *et al.* A1 adenosine receptor signal and AMPK involving caspase-9/-3 activation are responsible for adenosine-induced RCR-1 astrocytoma cell death. *NeuroToxicology* **27**, 458–467 (2006).
87. Fasano, C., Disciglio, V., Bertora, S., Lepore Signorile, M. & Simone, C. FOXO3a from the Nucleus to the Mitochondria: A Round Trip in Cellular Stress Response. *Cells* **8**, 1110 (2019).
88. Zhai, B. *et al.* Inhibition of Akt Reverses the Acquired Resistance to Sorafenib by Switching Protective Autophagy to Autophagic Cell Death in Hepatocellular Carcinoma. *Molecular Cancer Therapeutics* **13**, 1589–1598 (2014).
89. Liang, C. *et al.* Hypoxia induces sorafenib resistance mediated by autophagy via activating FOXO3a in hepatocellular carcinoma. *Cell Death & Disease* **11**, 1017 (2020).

90. Wu, Q. *et al.* Blocking Triggering Receptor Expressed on Myeloid Cells-1-Positive Tumor-Associated Macrophages Induced by Hypoxia Reverses Immunosuppression and Anti-Programmed Cell Death Ligand 1 Resistance in Liver Cancer. *Hepatology* **70**, 198–214 (2019).
91. Li, D. *et al.* MicroRNA-375 represses tumor angiogenesis and reverses resistance to sorafenib in hepatocarcinoma. *Cancer Gene Therapy* **28**, 126–140 (2021).
92. Ucar, A. *et al.* The miRNA-212/132 family regulates both cardiac hypertrophy and cardiomyocyte autophagy. *Nature Communications* **3**, 1078 (2012).
93. Xie, M. *et al.* MicroRNA-132 and microRNA-212 mediate doxorubicin resistance by down-regulating the PTEN-AKT/NF-κB signaling pathway in breast cancer. *Biomedicine & Pharmacotherapy* **102**, 286–294 (2018).
94. Yang, Y. *et al.* Silencing of LncRNA-HOTAIR decreases drug resistance of Non-Small Cell Lung Cancer cells by inactivating autophagy via suppressing the phosphorylation of ULK1. *Biochemical and Biophysical Research Communications* **497**, 1003–1010 (2018).
95. Pan, B. *et al.* Mir-24-3p downregulation contributes to VP16-DDP resistance in small-cell lung cancer by targeting *ATG4A*. *Oncotarget* **6**, 317–331 (2015).
96. Wang, H. *et al.* MiR-223 regulates autophagy associated with cisplatin resistance by targeting FBXW7 in human non-small cell lung cancer. *Cancer Cell International* **20**, 258 (2020).
97. Wang, P. *et al.* Roles of microRNA-22 in Suppressing Proliferation and Promoting Sensitivity of Osteosarcoma Cells *via* Metadherin-mediated Autophagy. *Orthopaedic Surgery* **11**, 285–293 (2019).
98. Meng, C. *et al.* MicroRNA-22 regulates autophagy and apoptosis in cisplatin resistance of osteosarcoma. *Molecular Medicine Reports* (2020) doi:10.3892/mmr.2020.11447.
99. Ma, K. *et al.* Exploring the mechanism of cisplatin resistance by transcriptome sequencing and reversing the chemoresistance by autophagy inhibition in small cell lung cancer. *Biochemical and Biophysical Research Communications* **533**, 474–480 (2020).
100. Comincini, S. *et al.* microRNA-17 regulates the expression of ATG7 and modulates the autophagy process, improving the sensitivity to temozolomide and low-dose ionizing

radiation treatments in human glioblastoma cells. *Cancer Biology & Therapy* **14**, 574–586 (2013).

101. Zhou, H. *et al.* The functional role of long non-coding RNAs and their underlying mechanisms in drug resistance of non-small cell lung cancer. *Life Sciences* **261**, 118362 (2020).
102. Kanzawa, T. *et al.* Role of autophagy in temozolomide-induced cytotoxicity for malignant glioma cells. *Cell Death & Differentiation* **11**, 448–457 (2004).
103. Qu, Y. *et al.* The functional role of long noncoding RNA in resistance to anticancer treatment. *Therapeutic Advances in Medical Oncology* **12**, 175883592092785 (2020).
104. Pan, B. *et al.* MiR-200b regulates autophagy associated with chemoresistance in human lung adenocarcinoma. *Oncotarget* **6**, 32805–32820 (2015).
105. Hua, Y.-T., Xu, W.-X., Li, H. & Xia, M. Emerging roles of MiR-133a in human cancers. *J Cancer* **12**, 198–206 (2021).
106. Yuan, Y., Yao, Y. F., Hu, S. N., Gao, J. & Zhang, L.-L. MiR-133a Is Functionally Involved in Doxorubicin-Resistance in Breast Cancer Cells MCF-7 via Its Regulation of the Expression of Uncoupling Protein 2. *PLOS ONE* **10**, e0129843 (2015).
107. WANG, X., ZHU, W., ZHAO, X. & WANG, P. RmiR-133a enhances the sensitivity of Hep-2 cells and vincristine-resistant Hep-2v cells to cisplatin by downregulating ATP7B expression. *International Journal of Molecular Medicine* **37**, 1636–1642 (2016).
108. Li, J. *et al.* miR-133a-3p/FOXP3 axis regulates cell proliferation and autophagy in gastric cancer. *Journal of Cellular Biochemistry* **121**, 3392–3405 (2020).
109. Zhang, L. *et al.* MARCKS inhibition cooperates with autophagy antagonists to potentiate the effect of standard therapy against drug-resistant multiple myeloma. *Cancer Letters* **480**, 29–38 (2020).
110. Peng, R. *et al.* Resistance to FGFR1-targeted therapy leads to autophagy via TAK1/AMPK activation in gastric cancer. *Gastric Cancer* **23**, 988–1002 (2020).
111. Zhou, H. *et al.* The functional role of long non-coding RNAs and their underlying mechanisms in drug resistance of non-small cell lung cancer. *Life Sciences* **261**, 118362 (2020).

112. Huang, F. *et al.* LncRNA BLACAT1 is involved in chemoresistance of non-small cell lung cancer cells by regulating autophagy. *International Journal of Oncology* (2018) doi:10.3892/ijo.2018.4614.
113. Sun, W., Zu, Y., Fu, X. & Deng, Y. Knockdown of lncRNA-XIST enhances the chemosensitivity of NSCLC cells via suppression of autophagy. *Oncology Reports* (2017) doi:10.3892/or.2017.6056.
114. Xiong, H. *et al.* LncRNA HULC triggers autophagy via stabilizing Sirt1 and attenuates the chemosensitivity of HCC cells. *Oncogene* **36**, 3528–3540 (2017).
115. Lin, Z. *et al.* <scp>RNA</scp> m ^{6} A methylation regulates sorafenib resistance in liver cancer through <scp>FOXO</scp> 3-mediated autophagy. *The EMBO Journal* **39**, (2020).
116. Zhai, B. *et al.* Inhibition of Akt Reverses the Acquired Resistance to Sorafenib by Switching Protective Autophagy to Autophagic Cell Death in Hepatocellular Carcinoma. *Molecular Cancer Therapeutics* **13**, 1589–1598 (2014).
117. Zhang, Y. *et al.* HMGB1-mediated autophagy confers resistance to gemcitabine in hormone-independent prostate cancer cells. *Oncology Letters* (2017) doi:10.3892/ol.2017.6965.
118. van den Berg, H. Asparaginase revisited. *Leukemia & Lymphoma* **52**, 168–178 (2011).
119. Wang, L. *et al.* LncRNA BCYRN1-induced autophagy enhances asparaginase resistance in extranodal NK/T-cell lymphoma. *Theranostics* **11**, 925–940 (2021).
120. Ying, S. *et al.* Synthesis, biological evaluation, QSAR and molecular dynamics simulation studies of potential fibroblast growth factor receptor 1 inhibitors for the treatment of gastric cancer. *European Journal of Medicinal Chemistry* **127**, 885–899 (2017).
121. Carter, E. P., Fearon, A. E. & Grose, R. P. Careless talk costs lives: fibroblast growth factor receptor signalling and the consequences of pathway malfunction. *Trends in Cell Biology* **25**, 221–233 (2015).
122. Ajibade, A. A., Wang, H. Y. & Wang, R.-F. Cell type-specific function of TAK1 in innate immune signaling. *Trends in Immunology* **34**, 307–316 (2013).
123. Seki, E. TAK1-dependent autophagy: A suppressor of fatty liver disease and hepatic oncogenesis. *Molecular & Cellular Oncology* **1**, e968507 (2014).

124. Zhu, Y. *et al.* SOX2 promotes chemoresistance, cancer stem cells properties, and epithelial–mesenchymal transition by β-catenin and Beclin1/autophagy signaling in colorectal cancer. *Cell Death & Disease* **12**, 449 (2021).
125. Tian, T. Sox2 enhances the tumorigenicity and chemoresistance of cancer stem-like cells derived from gastric cancer. *Journal of Biomedical Research* **26**, 336–345 (2012).
126. Zamame Ramirez, J. A. *et al.* Blocking drug-induced autophagy with chloroquine in HCT-116 colon cancer cells enhances DC maturation and T cell responses induced by tumor cell lysate. *International Immunopharmacology* **84**, 106495 (2020).
127. MHAIDAT, N. M., BOUKLIHACENE, M. & THORNE, R. F. 5-Fluorouracil-induced apoptosis in colorectal cancer cells is caspase-9-dependent and mediated by activation of protein kinase C-δ. *Oncology Letters* **8**, 699–704 (2014).
128. Zhang, Y. *et al.* HMGB1-mediated autophagy confers resistance to gemcitabine in hormone-independent prostate cancer cells. *Oncology Letters* (2017) doi:10.3892/ol.2017.6965.
129. Chen, H. *et al.* Growth inhibitory effects of dihydroartemisinin on pancreatic cancer cells: involvement of cell cycle arrest and inactivation of nuclear factor-κB. *Journal of Cancer Research and Clinical Oncology* **136**, 897–903 (2010).
130. Ontikatze, T., Rudner, J., Handrick, R., Belka, C. & Jendrossek, V. Dihydroartemisinin is a Hypoxia-Active Anti-Cancer Drug in Colorectal Carcinoma Cells. *Frontiers in Oncology* **4**, (2014).
131. Hu, C., Zhou, L. & Cai, Y. Dihydroartemisinin induces apoptosis of cervical cancer cells via upregulation of RKIP and downregulation of bcl-2. *Cancer Biology & Therapy* **15**, 279–288 (2014).
132. Kang, X. *et al.* Codelivery of dihydroartemisinin and doxorubicin in mannosylated liposomes for drug-resistant colon cancer therapy. *Acta Pharmacologica Sinica* **38**, 885–896 (2017).
133. Kobayashi, S. *et al.* Transcription Factor GATA4 Inhibits Doxorubicin-induced Autophagy and Cardiomyocyte Death. *Journal of Biological Chemistry* **285**, 793–804 (2010).
134. Liu, P. *et al.* The role of autophagy in the cytotoxicity induced by trastuzumab emtansine (T-DM1) in HER2-positive breast cancer cells. *AMB Express* **10**, 107 (2020).

135. Peng, Y. *et al.* Long non-coding RNA: A recently accentuated molecule in chemoresistance in cancer. *Cancer and Metastasis Reviews* **39**, 825–835 (2020).
136. Zinnah, K., Seol, J. & Park, S. Inhibition of autophagy flux by sertraline attenuates TRAIL resistance in lung cancer via death receptor 5 upregulation. *International Journal of Molecular Medicine* **46**, 795–805 (2020).
137. Lin, Y.-H., Lin, K.-H. & Yeh, C.-T. Thyroid Hormone in Hepatocellular Carcinoma: Cancer Risk, Growth Regulation, and Anticancer Drug Resistance. *Frontiers in Medicine* **7**, (2020).
138. Chi, H.-C. *et al.* Thyroid hormone suppresses hepatocarcinogenesis via DAPK2 and SQSTM1-dependent selective autophagy. *Autophagy* **12**, 2271–2285 (2016).
139. Wu, J. *et al.* SZC015, a synthetic oleanolic acid derivative, induces both apoptosis and autophagy in MCF-7 breast cancer cells. *Chemico-Biological Interactions* **244**, 94–104 (2016).
140. LI, L. *et al.* Oleanolic acid inhibits colorectal cancer angiogenesis in vivo and in vitro via suppression of STAT3 and Hedgehog pathways. *Molecular Medicine Reports* **13**, 5276–5282 (2016).
141. Žiberna, L. *et al.* Oleanolic Acid Alters Multiple Cell Signaling Pathways: Implication in Cancer Prevention and Therapy. *International Journal of Molecular Sciences* **18**, 643 (2017).
142. Shi, Y. *et al.* Oleanolic acid induced autophagic cell death in hepatocellular carcinoma cells via PI3K/Akt/mTOR and ROS-dependent pathway. *The Korean Journal of Physiology & Pharmacology* **20**, 237 (2016).
143. Zhou, W., Zeng, X. & Wu, X. Effect of Oleanolic Acid on Apoptosis and Autophagy of SMMC-7721 Hepatoma Cells. *Medical Science Monitor* **26**, (2020).
144. O'Leary, L. *et al.* Decoy receptors block TRAIL sensitivity at a supracellular level: the role of stromal cells in controlling tumour TRAIL sensitivity. *Oncogene* **35**, 1261–1270 (2016).
145. Xia, D. *et al.* Sertraline exerts its antitumor functions through both apoptosis and autophagy pathways in acute myeloid leukemia cells. *Leukemia & Lymphoma* **58**, 2208–2217 (2017).
146. Amit, B. H. *et al.* Proapoptotic and chemosensitizing effects of selective serotonin reuptake inhibitors on T cell lymphoma/leukemia (Jurkat) in vitro. *European Neuropsychopharmacology* **19**, 726–734 (2009).

147. Wei, Y., Pattingre, S., Sinha, S., Bassik, M. & Levine, B. JNK1-Mediated Phosphorylation of Bcl-2 Regulates Starvation-Induced Autophagy. *Molecular Cell* **30**, 678–688 (2008).
148. Clarke, A. J. & Simon, A. K. Autophagy in the renewal, differentiation and homeostasis of immune cells. *Nature Reviews Immunology* **19**, 170–183 (2019).
149. Shibutani, S. T., Saitoh, T., Nowag, H., Münz, C. & Yoshimori, T. Autophagy and autophagy-related proteins in the immune system. *Nature Immunology* **16**, 1014–1024 (2015).
150. Wu, M.-Y. & Lu, J.-H. Autophagy and Macrophage Functions: Inflammatory Response and Phagocytosis. *Cells* **9**, 70 (2019).
151. Qie, Y. *et al.* Surface modification of nanoparticles enables selective evasion of phagocytic clearance by distinct macrophage phenotypes. *Scientific Reports* **6**, 26269 (2016).
152. You, D. J., Lee, H. Y. & Bonner, J. C. Macrophages: First Innate Immune Responders to Nanomaterials. in 15–34 (2020). doi:10.1007/978-3-030-33962-3_2.
153. Song, W. *et al.* The autophagic response to polystyrene nanoparticles is mediated by transcription factor EB and depends on surface charge. *Journal of Nanobiotechnology* **13**, 87 (2015).
154. Settembre, C. *et al.* TFEB Links Autophagy to Lysosomal Biogenesis. *Science (1979)* **332**, 1429–1433 (2011).
155. Rusmini, P. *et al.* Trehalose induces autophagy via lysosomal-mediated TFEB activation in models of motoneuron degeneration. *Autophagy* **15**, 631–651 (2019).
156. Nakagawa, I. *et al.* Autophagy Defends Cells Against Invading Group A *Streptococcus*. *Science (1979)* **306**, 1037–1040 (2004).
157. Hadjidemetriou, M., Al-Ahmady, Z. & Kostarelos, K. Time-evolution of in vivo protein corona onto blood-circulating PEGylated liposomal doxorubicin (DOXIL) nanoparticles. *Nanoscale* **8**, 6948–6957 (2016).
158. Kristensen, K., Engel, T. B., Stensballe, A., Simonsen, J. B. & Andresen, T. L. The hard protein corona of stealth liposomes is sparse. *Journal of Controlled Release* **307**, 1–15 (2019).

159. FOGELMAN, A. M., van LENTEN, B. J., WARDEN, C., HABERLAND, M. E. & EDWARDS, P. A. Macrophage lipoprotein receptors. *Journal of Cell Science* **1988**, 135–149 (1988).
160. Neculai, D. *et al.* Structure of LIMP-2 provides functional insights with implications for SR-BI and CD36. *Nature* **504**, 172–176 (2013).
161. Raith, M. *et al.* Elongated PEO-based nanoparticles bind the high-density lipoprotein (HDL) receptor scavenger receptor class B I (SR-BI). *Journal of Controlled Release* **337**, 448–457 (2021).
162. Gustafson, H. H., Holt-Casper, D., Grainger, D. W. & Ghandehari, H. Nanoparticle uptake: The phagocyte problem. *Nano Today* **10**, 487–510 (2015).
163. Roberts, R. *et al.* Autophagy and formation of tubulovesicular autophagosomes provide a barrier against nonviral gene delivery. *Autophagy* **9**, 667–682 (2013).
164. Daniel J Klionsky *et al.* Guidelines for the use and interpretation of assays for monitoring autophagy (4th edition). *Autophagy* **17**, 1–382 (2021).
165. Luo, O. J. *et al.* Multidimensional single-cell analysis of human peripheral blood reveals characteristic features of the immune system landscape in aging and frailty. *Nature Aging* **2**, 348–364 (2022).
166. Shi, C.-S. & Kehrl, J. H. TRAF6 and A20 regulate lysine 63-linked ubiquitination of Beclin-1 to control TLR4-induced autophagy. *Sci Signal* **3**, ra42 (2010).
167. Xu, Y. *et al.* Toll-like Receptor 4 Is a Sensor for Autophagy Associated with Innate Immunity. *Immunity* **27**, 135–144 (2007).
168. Nazio, F. *et al.* mTOR inhibits autophagy by controlling ULK1 ubiquitylation, self-association and function through AMBRA1 and TRAF6. *Nat Cell Biol* **15**, 406–16 (2013).
169. Xu, Y., Liu, X.-D., Gong, X. & Eissa, N. T. Signaling pathway of autophagy associated with innate immunity. *Autophagy* **4**, 110–2 (2008).
170. Franco, L. H. *et al.* Autophagy downstream of endosomal Toll-like receptor signaling in macrophages is a key mechanism for resistance to Leishmania major infection. *Journal of Biological Chemistry* **292**, 13087–13096 (2017).
171. Travassos, L. H. *et al.* Nod1 and Nod2 direct autophagy by recruiting ATG16L1 to the plasma membrane at the site of bacterial entry. *Nat Immunol* **11**, 55–62 (2010).

172. Hsu, H.-Y. & Wen, M.-H. Lipopolysaccharide-mediated Reactive Oxygen Species and Signal Transduction in the Regulation of Interleukin-1 Gene Expression. *Journal of Biological Chemistry* **277**, 22131–22139 (2002).
173. Anozie, U. C. & Dalhaimer, P. Molecular links among non-biodegradable nanoparticles, reactive oxygen species, and autophagy. *Advanced Drug Delivery Reviews* **122**, 65–73 (2017).
174. Jia, L., Hao, S.-L. & Yang, W.-X. Nanoparticles induce autophagy via mTOR pathway inhibition and reactive oxygen species generation. *Nanomedicine* **15**, 1419–1435 (2020).
175. Raj, E. N., Lin, Y., Chen, C., Liu, K. & Chao, J. Selective Autophagy Pathway of Nanoparticles and Nanodrugs: Drug Delivery and Pathophysiological Effects. *Advanced Therapeutics* **3**, 2000085 (2020).
176. Gao, J. *et al.* PEG-Ceramide Nanomicelles Induce Autophagy and Degrade Tau Proteins in N2a Cells . *International Journal of Nanomedicine* **Volume 15**, 6779–6789 (2020).
177. Quan, H., Park, H. C., Kim, Y. & Yang, H.-C. Modulation of the anti-inflammatory effects of phosphatidylserine-containing liposomes by PEGylation. *Journal of Biomedical Materials Research Part A* **105**, 1479–1486 (2017).
178. Gerlach, B. D. *et al.* Efferocytosis induces macrophage proliferation to help resolve tissue injury. *Cell Metabolism* **33**, 2445-2463.e8 (2021).
179. Tattoli, I. *et al.* Amino Acid Starvation Induced by Invasive Bacterial Pathogens Triggers an Innate Host Defense Program. *Cell Host & Microbe* **11**, 563–575 (2012).
180. Sabatini, D. M., Erdjument-Bromage, H., Lui, M., Tempst, P. & Snyder, S. H. RAFT1: A mammalian protein that binds to FKBP12 in a rapamycin-dependent fashion and is homologous to yeast TORs. *Cell* **78**, 35–43 (1994).
181. Li, M., Wang, Z., Wang, P., Li, H. & Yang, L. TFEB: A Emerging Regulator in Lipid Homeostasis for Atherosclerosis. *Frontiers in Physiology* **12**, (2021).
182. Liu, L. *et al.* Chloroquine inhibits cell growth in human A549 lung cancer cells by blocking autophagy and inducing mitochondrial-mediated apoptosis. *Oncology Reports* (2018) doi:10.3892/or.2018.6363.

183. Jarai, B. M. & Fromen, C. A. Nanoparticle Internalization Promotes the Survival of Primary Macrophages. *Advanced NanoBiomed Research* **2**, 2100127 (2022).
184. Wang, F. *et al.* Time resolved study of cell death mechanisms induced by amine-modified polystyrene nanoparticles. *Nanoscale* **5**, 10868 (2013).
185. Paiva, C. N. & Bozza, M. T. Are Reactive Oxygen Species Always Detrimental to Pathogens? *Antioxidants & Redox Signaling* **20**, 1000–1037 (2014).
186. Scherz-Shouval, R. *et al.* Reactive oxygen species are essential for autophagy and specifically regulate the activity of Atg4. *The EMBO Journal* **26**, 1749–1760 (2007).
187. Shin, Y. J. *et al.* Rapamycin Reduces Reactive Oxygen Species in Cultured Human Corneal Endothelial Cells. *Current Eye Research* **36**, 1116–1122 (2011).
188. Martinez, J. *et al.* Molecular characterization of LC3-associated phagocytosis reveals distinct roles for Rubicon, NOX2 and autophagy proteins. *Nature Cell Biology* **17**, 893–906 (2015).
189. Bime, C. *et al.* Reactive Oxygen Species–Associated Molecular Signature Predicts Survival in Patients with Sepsis. *Pulmonary Circulation* **6**, 196–201 (2016).
190. Cui, J., Guo, A.-X., Wang, L.-Y. & Yin, J.-Y. Abstract 1289: CSDE1 mediated translation reprogramming under stress. *Cancer Research* **80**, 1289–1289 (2020).
191. Wang, J. *et al.* iNOS Interacts with Autophagy Receptor p62 and is Degraded by Autophagy in Macrophages. *Cells* **8**, 1255 (2019).
192. Gillmore, J. D. *et al.* CRISPR-Cas9 In Vivo Gene Editing for Transthyretin Amyloidosis. *New England Journal of Medicine* **385**, 493–502 (2021).
193. Subramanian, S. *et al.* Long-term culture-expanded alveolar macrophages restore their full epigenetic identity after transfer in vivo. *Nature Immunology* **23**, 458–468 (2022).
194. Liu, C.-L. *et al.* Toll-like receptor 7 deficiency protects apolipoprotein E-deficient mice from diet-induced atherosclerosis. *Scientific Reports* **7**, 847 (2017).
195. Matsui, T., Itoh, T. & Fukuda, M. Small GTPase Rab12 regulates constitutive degradation of transferrin receptor. *Traffic* **12**, 1432–43 (2011).
196. Chen, P., Kanehira, K. & Taniguchi, A. Role of toll-like receptors 3, 4 and 7 in cellular uptake and response to titanium dioxide nanoparticles. *Science and Technology of Advanced Materials* **14**, 015008 (2013).

197. Gerster, R. *et al.* Anti-inflammatory Function of High-Density Lipoproteins via Autophagy of IκB Kinase. *Cellular and Molecular Gastroenterology and Hepatology* **1**, 171-187.e1 (2015).
198. Fotakis, P. *et al.* Anti-Inflammatory Effects of HDL (High-Density Lipoprotein) in Macrophages Predominate Over Proinflammatory Effects in Atherosclerotic Plaques. *Arteriosclerosis, Thrombosis, and Vascular Biology* **39**, (2019).
199. Cai, L., Wang, Z., Meyer, J. M., Ji, A. & van der Westhuyzen, D. R. Macrophage SR-BI regulates LPS-induced pro-inflammatory signaling in mice and isolated macrophages. *Journal of Lipid Research* **53**, 1472–1481 (2012).
200. Wilhelm, S. *et al.* Analysis of nanoparticle delivery to tumours. *Nature Reviews Materials* **1**, 16014 (2016).
201. Won, Y.-Y., Davis, H. T. & Bates, F. S. Giant Wormlike Rubber Micelles. *Science (1979)* **283**, 960–963 (1999).
202. Dalhaimer, P., Bates, F. S. & Discher, D. E. Single Molecule Visualization of Stable, Stiffness-Tunable, Flow-Conforming Worm Micelles. *Macromolecules* **36**, 6873–6877 (2003).
203. Hu, Y., Haynes, M. T., Wang, Y., Liu, F. & Huang, L. A Highly Efficient Synthetic Vector: Nonhydrodynamic Delivery of DNA to Hepatocyte Nuclei *in Vivo*. *ACS Nano* **7**, 5376–5384 (2013).
204. Open-source ImmGen: mononuclear phagocytes. *Nature Immunology* **17**, 741–741 (2016).
205. Szklarczyk, D. *et al.* The STRING database in 2021: customizable protein-protein networks, and functional characterization of user-uploaded gene/measurement sets. *Nucleic Acids Res* **49**, D605–D612 (2021).
206. Humphrey, S. J. *et al.* Dynamic Adipocyte Phosphoproteome Reveals that Akt Directly Regulates mTORC2. *Cell Metabolism* **17**, 1009–1020 (2013).
207. Cheng, Z. *et al.* Focal Adhesion Kinase-mediated Phosphorylation of Beclin1 Protein Suppresses Cardiomyocyte Autophagy and Initiates Hypertrophic Growth. *Journal of Biological Chemistry* **292**, 2065–2079 (2017).
208. Zhu, L. *et al.* Low density lipoprotein mimics insulin action on autophagy and glucose uptake in endothelial cells. *Scientific Reports* **9**, 3020 (2019).

209. Ding, L., Zhang, L., Kim, M., Byzova, T. & Podrez, E. Akt3 kinase suppresses pinocytosis of low-density lipoprotein by macrophages via a novel WNK/SGK1/Cdc42 protein pathway. *Journal of Biological Chemistry* **292**, 9283–9293 (2017).
210. Kanerva, K. *et al.* LDL Cholesterol Recycles to the Plasma Membrane via a Rab8a-Myosin5b-Actin-Dependent Membrane Transport Route. *Developmental Cell* **27**, 249–262 (2013).
211. Lee, Y. *et al.* Coactivation of the CLOCK–BMAL1 complex by CBP mediates resetting of the circadian clock. *Journal of Cell Science* **123**, 3547–3557 (2010).
212. Blacher, E. *et al.* Aging disrupts circadian gene regulation and function in macrophages. *Nature Immunology* **23**, 229–236 (2022).
213. Sarek, G. *et al.* CDK phosphorylation of TRF2 controls t-loop dynamics during the cell cycle. *Nature* **575**, 523–527 (2019).
214. Copetti, T., Bertoli, C., Dalla, E., Demarchi, F. & Schneider, C. p65/RelA Modulates *BECN1* Transcription and Autophagy. *Molecular and Cellular Biology* **29**, 2594–2608 (2009).
215. Zhong, Y. *et al.* Distinct regulation of autophagic activity by Atg14L and Rubicon associated with Beclin 1–phosphatidylinositol-3-kinase complex. *Nature Cell Biology* **11**, 468–476 (2009).
216. Karin, M. Nuclear factor-κB in cancer development and progression. *Nature* **441**, 431–436 (2006).
217. Miao, L. *et al.* mTORC1 is necessary but mTORC2 and GSK3β are inhibitory for AKT3-induced axon regeneration in the central nervous system. *Elife* **5**, (2016).
218. Lee, J.-S. *et al.* FLIP-mediated autophagy regulation in cell death control. *Nature Cell Biology* **11**, 1355–1362 (2009).
219. Strasser, D. *et al.* Syk kinase-coupled C-type lectin receptors engage protein kinase C-δ to elicit Card9 adaptor-mediated innate immunity. *Immunity* **36**, 32–42 (2012).
220. Arif, A. *et al.* EPRS is a critical mTORC1-S6K1 effector that influences adiposity in mice. *Nature* **542**, 357–361 (2017).
221. Grevengoed, T. J., Cooper, D. E., Young, P. A., Ellis, J. M. & Coleman, R. A. Loss of long-chain acyl-CoA synthetase isoform 1 impairs cardiac autophagy and mitochondrial structure

through mechanistic target of rapamycin complex 1 activation. *The FASEB Journal* **29**, 4641–4653 (2015).

222. Zhong, B. *et al.* Negative regulation of IL-17-mediated signaling and inflammation by the ubiquitin-specific protease USP25. *Nature Immunology* **13**, 1110–1117 (2012).
223. Ramakrishnan, R. K. *et al.* IL-17 Induced Autophagy Regulates Mitochondrial Dysfunction and Fibrosis in Severe Asthmatic Bronchial Fibroblasts. *Frontiers in Immunology* **11**, (2020).
224. Li, J. *et al.* Identification of potential autophagy-associated lncRNA in prostate cancer. *Aging* **13**, 13153–13165 (2021).
225. Gao, T. *et al.* TLR3 contributes to persistent autophagy and heart failure in mice after myocardial infarction. *Journal of Cellular and Molecular Medicine* **22**, 395–408 (2018).
226. Merkley, S. D. *et al.* Polystyrene microplastics induce an immunometabolic active state in macrophages. *Cell Biology and Toxicology* **38**, 31–41 (2022).
227. Sillibourne, J. E., Delaval, B., Redick, S., Sinha, M. & Doxsey, S. J. Chromatin remodeling proteins interact with pericentrin to regulate centrosome integrity. *Mol Biol Cell* **18**, 3667–80 (2007).
228. Oldenborg, P.-A. *et al.* Role of CD47 as a Marker of Self on Red Blood Cells. *Science (1979)* **288**, 2051–2054 (2000).
229. van Beek, E. M. *et al.* SIRPα Controls the Activity of the Phagocyte NADPH Oxidase by Restricting the Expression of gp91phox. *Cell Reports* **2**, 748–755 (2012).
230. Lee, D.-Y. *et al.* MicroRNA-10a is crucial for endothelial response to different flow patterns via interaction of retinoid acid receptors and histone deacetylases. *Proc Natl Acad Sci U S A* **114**, 2072–2077 (2017).
231. Xu, W., Yu, M., Qin, J., Luo, Y. & Zhong, M. LACTB Regulates PIK3R3 to Promote Autophagy and Inhibit EMT and Proliferation Through the PI3K/AKT/mTOR Signaling Pathway in Colorectal Cancer . *Cancer Management and Research* **Volume 12**, 5181–5200 (2020).
232. Pennock, S. & Wang, Z. A Tale of Two Cbls: Interplay of c-Cbl and Cbl-b in Epidermal Growth Factor Receptor Downregulation. *Molecular and Cellular Biology* **28**, 3020–3037 (2008).

233. Lamers, F. *et al.* Identification of BIRC6 as a novel intervention target for neuroblastoma therapy. *BMC Cancer* **12**, 285 (2012).
234. Ebner, P. *et al.* The IAP family member BRUCE regulates autophagosome–lysosome fusion. *Nature Communications* **9**, 599 (2018).
235. Wolf, A. J. *et al.* Hexokinase Is an Innate Immune Receptor for the Detection of Bacterial Peptidoglycan. *Cell* **166**, 624–636 (2016).
236. Wilkinson, A. W. *et al.* SETD3 is an actin histidine methyltransferase that prevents primary dystocia. *Nature* **565**, 372–376 (2019).
237. Zhang, Z. *et al.* Structural Analysis Reveals that Toll-like Receptor 7 Is a Dual Receptor for Guanosine and Single-Stranded RNA. *Immunity* **45**, 737–748 (2016).
238. van der Made, C. I. *et al.* Presence of Genetic Variants Among Young Men With Severe COVID-19. *JAMA* **324**, 663–673 (2020).
239. Dalhaimer, P. & Blankenship, K. R. All-Atom Molecular Dynamics Simulations of Polyethylene Glycol (PEG) and LIMP-2 Reveal That PEG Penetrates Deep into the Proposed CD36 Cholesterol-Transport Tunnel. *ACS Omega* **7**, 15728–15738 (2022).
240. Haney, M. S. *et al.* Identification of phagocytosis regulators using magnetic genome-wide CRISPR screens. *Nature Genetics* **50**, 1716–1727 (2018).
241. Sirotkin, V., Beltzner, C. C., Marchand, J.-B. & Pollard, T. D. Interactions of WASp, myosin-I, and verprolin with Arp2/3 complex during actin patch assembly in fission yeast. *Journal of Cell Biology* **170**, 637–648 (2005).
242. Weiner, O. D. *et al.* Hem-1 complexes are essential for Rac activation, actin polymerization, and myosin regulation during neutrophil chemotaxis. *PLoS Biol* **4**, e38 (2006).
243. Weiner, O. D., Marganski, W. A., Wu, L. F., Altschuler, S. J. & Kirschner, M. W. An actin-based wave generator organizes cell motility. *PLoS Biol* **5**, e221 (2007).
244. Cook, S. A. *et al.* HEM1 deficiency disrupts mTORC2 and F-actin control in inherited immunodysregulatory disease. *Science (1979)* **369**, 202–207 (2020).
245. Kimmey, J. M. *et al.* Unique role for ATG5 in neutrophil-mediated immunopathology during M. tuberculosis infection. *Nature* **528**, 565–569 (2015).

246. Hayashi, K., Taura, M. & Iwasaki, A. The interaction between IKKα and LC3 promotes type I interferon production through the TLR9-containing LAPosome. *Science Signaling* **11**, (2018).
247. Lin, C. *et al.* LAMTOR2/LAMTOR1 complex is required for TAX1BP1-mediated xenophagy. *Cellular Microbiology* **21**, (2019).
248. Ydens, E. *et al.* Profiling peripheral nerve macrophages reveals two macrophage subsets with distinct localization, transcriptome and response to injury. *Nature Neuroscience* **23**, 676–689 (2020).
249. Lin, J.-D. *et al.* Single-cell analysis of fate-mapped macrophages reveals heterogeneity, including stem-like properties, during atherosclerosis progression and regression. *JCI Insight* **4**, (2019).
250. King, K. R. *et al.* IRF3 and type I interferons fuel a fatal response to myocardial infarction. *Nature Medicine* **23**, 1481–1487 (2017).
251. Sanin, D. E. *et al.* Predictive framework of macrophage activation. *bioRxiv* 2021.08.02.454825 (2021) doi:10.1101/2021.08.02.454825.

Vita

Tehran, Iran is where Monireh Asoudeh was raised. She attended Sharif University of Technology after high school, where she earned a Bachelor of Science in Chemical Engineering. The next step she decided to take was graduate school, so she enrolled at the University of Tennessee in Knoxville to go toward a Doctor of Philosophy in Chemical and Biomolecular Engineering. Her area of interest is the study of nanoparticles and how they enter cells to deliver drugs more effectively. She is looking for employment prospects in the pharmaceutical industries after graduation.